UNIVERSIDADE FEDERAL DO RIO GRANDE DO SUL
FACULDADE DE AGRONOMIA
PROGRAMA DE PÓS-GRADUAÇÃO EM FITOTECNIA

FENOTIPAGEM DE ALTO RENDIMENTO PARA A PREDIÇÃO DE PARÂMETROS DE SOJA SUBMETIDA AO ALAGAMENTO E MILHO UTILIZANDO SENSOR MULTIESPECTRAL

Charleston dos Santos Lima
Engenheiro Agrônomo/ UNIJUI
Mestre em Agrobiologia/ UFSM

Tese apresentada como um dos requisitos para a obtenção do Grau de Doutor em Fitotecnia
Área de concentração em Produção Vegetal

Porto Alegre (RS), Brasil
Outubro de 2025

CIP - Catalogação na Publicação

Lima, Charleston dos Santos
FENOTIPAGEM DE ALTO RENDIMENTO PARA A PREDIÇÃO DE PARÂMETROS DE SOJA SUBMETIDA AO ALAGAMENTO E MILHO UTILIZANDO SENSOR MULTIESPECTRAL / Charleston dos Santos Lima. -- 2025.
79 f.
Orientador: Christian Bredemeier.

Coorientador: Ivan Ricardo Carvalho.

Tese (Doutorado) -- Universidade Federal do Rio Grande do Sul, Faculdade de Agronomia, Programa de Pós-Graduação em Fitotecnia, Porto Alegre, BR-RS, 2025.

1. Fenotipagem. 2. Espectral. 3. Alagamento. 4. Sensoriamento remoto. 5. Índices espectrais. I. Bredemeier, Christian, orient. II. Carvalho, Ivan Ricardo, coorient. III. Título.

Elaborada pelo Sistema de Geração Automática de Ficha Catalográfica da UFRGS com os dados fornecidos pelo(a) autor(a).

CHARLESTON DOS SANTOS LIMA
Engenheiro Agrônomo - UNIJUI
Mestre em Agrobiologia - UFSM

TESE

Submetida como parte dos requisitos
para obtenção do Grau de

DOUTOR EM FITOTECNIA

Programa de Pós-Graduação em Fitotecnia
Faculdade de Agronomia
Universidade Federal do Rio Grande do Sul
Porto Alegre (RS), Brasil

Aprovado em: 24/10/2025
Pela Banca Examinadora

CHRISTIAN BREDEMEIER
Orientador
UFRGS

IVAN RICARDO CARVALHO
Coorientador
UNIJUI

SIMONE MUNDSTOCK JAHNKE
Coordenadora do Programa de Pós-Graduação em Fitotecnia

CLAUDIO WILSON MENDES JR.
UFRGS – PPG GEOCIÊNCIAS

LÚCIO AMARAL
UFSM – PPG AGRICULTURA DE PRECISÃO

ANDRÉ LUIS VIAN
UFRGS – PPG FITOTECNIA

PAULO VITOR DUTRA DE SOUZA
Diretor da Faculdade de Agronomia

AGRADECIMENTOS

Agradeço primeiramente a Deus pela oportunidade de ter chegado até aqui.

Agradeço aos meus pais Antonio Eloir de Jesus Lima e Rosane de Fátima dos Santos Lima pelo incentivo, esforço e apoio durante toda essa trajetória. Dedico essa tese a vocês, com certeza isso não seria possível sem o alicerce chamado família. Adicionalmente, meu agradecimento especial aos melhores irmãos do mundo: Chawana dos Santos Lima e Cleverson dos Santos Lima, desconheço pessoas mais amorosas e legais. Amo vocês.

Agradeço a minha namorada, Jacqueline Flores Schmitz, por suportar um namorado por vezes nervoso, estressado e muito ansioso. Aprendo com você todos os dias e espero que sigamos juntos nessa jornada da vida e do conhecimento por muitos anos.

Muito obrigado também ao meu orientador Christian Bredemeier, que me ensinou e pilotar um drone e acima de tudo, foi um parceiro durante os anos de doutorado. Jamais esquecerei o seu esforço para me ajudar!

Obrigado ao meu coorientador Ivan Ricardo Carvalho, por todos os ensinamentos e paciência com o aluno, a estatística tornou-se fascinante com a sua orientação.

Obrigado a todos os amigos que a “Salinha 01 – UFRGS” me trouxe, especialmente a Vanessa, Daniel, Inácio, Luiza e Estéfani, que participaram em algum momento dessa caminhada.

Obrigado aos professores André Vian, André Thomas, Marcelo Pacheco e Itamar, os quais sempre trouxeram bons conselhos e foram parceiros na roda de chimarrão. Isso também fez toda a diferença.

Meus agradecimentos ao PPG Fitotecnia e ao CNPq, pela bolsa de estudos.

E muito obrigada também aos membros da banca examinadora, pelas contribuições e ensinamentos.

“A mente que se abre para uma nova ideia
Jamais retorna ao seu tamanho original.”
Albert Einstein

FENOTIPAGEM DE ALTO RENDIMENTO PARA A PREDIÇÃO DE PARÂMETROS DE SOJA SUBMETIDA AO ALAGAMENTO E MILHO UTILIZANDO SENSOR MULTIESPECTRAL.[1]

Autor: Charleston dos Santos Lima
Orientador: Christian Bredemeier
Coorientador: Ivan Ricardo Carvalho

RESUMO

A utilização de dados espectrais para a análise de plantas em diferentes condições de manejo e estimativa de parâmetros agronômicos constitui uma importante alternativa para a aumentar a velocidade na avaliação de genótipos mais produtivos e tolerantes a fatores promotores de estresse. Neste sentido, o presente estudo foi desenvolvido com o objetivo de I) avaliar a tolerância ao alagamento de 48 genótipos de soja e II) realizar a predição de variáveis de campo em plantas de milho submetidas a diferentes cenários (Doses de N, momento de voo e safras), a partir de sensores espectrais proximais e embarcados em aeronave remotamente pilotada (RPA) com base na metodologia de modelos mistos. Em ambos os estudos se utilizou a RPA DJI Phantom 4 multiespectral para a coleta de imagens em diferentes bandas espectrais, seguido da aquisição de dados com sensores proximais e mensuração de variáveis de campo. Adicionalmente, os dados foram submetidos a análise de componentes da variância e parâmetros genéticos/fenotípicos estimados (RELM-BLUP), com a aplicação de regressão por stepwise para cada variável de interesse agronômico. Para a cultura da soja submetida ao alagamento, os índices espectrais MSAVI, NDVI, OSAVI, SAVI, VEG, MGRVI, EVI2, NDRE, GRVI, BNDVI e RGBindex demonstraram maior estabilidade e confiabilidade, permitindo a predição de variáveis com elevado coeficiente de determinação (>0,90). Além disso, quando se analisou os dados de parcelas de milho com base nos diferentes momentos de voo (estádios fenológicos), doses de nitrogênio e safras, constatou-se que os índices com maior confiabilidade foram EXGRaw, TGI, GNDVI, NDRE, CIRE, GVI, CVI, BNDVI, PanNDVI, SRNIRRe, SFDVI, RGBindex, NDVI, SAVI, MSAVI e OSAVI, obtendo-se um agrupamento conforme a condição de safra e estádio fenológico analisado. Finalmente, as variáveis de campo preditas com base na metodologia apresentaram coeficiente de determinação acima de 0,80, exceto para a biomassa e peso de cem grãos. Concluiu-se que os dados espectrais coletados a partir de VANT's podem ser utilizados para a análise de plantas com base na utilização de modelos mistos, o que permite a correta dedução dos efeitos fixos e aleatórios em cada índice de vegetação e a utilização de modelo multivariado simples para a predição de variáveis de campo.

[1]Tese de Doutorado em Fitotecnia, Faculdade de Agronomia, Universidade Federal do Rio Grande do Sul, Porto Alegre, RS, Brasil. (79f.) Outubro, 2025.

HIGH-THROUGHPUT PHENOTYPING FOR PREDICTING PARAMETERS OF FLOODED SOYBEAN AND CORN USING MULTISPECTRAL SENSOR [1].

Author: Charleston dos Santos Lima
Adviser: Christian Bredemeier
Coadviser: Ivan Ricardo Carvalho

ABSTRACT

The use of spectral data for the analysis of plants under different management conditions and estimation of agronomic parameters constitutes an important alternative to increase the speed in the evaluation of more productive genotypes that are tolerant to stress-promoting factors. Therefore, the present study was developed with the objective of I) evaluating the flooding tolerance of 48 soybean genotypes and II) predicting field variables in corn plants subjected to different scenarios (N doses, flight moment and season), from proximal spectral sensors and those embedded in an remotely piloted aircraft based on the mixed model methodology. The research used the DJI Phantom 4 multispectral RPA to collect images in different spectral bands, followed by data acquisition with proximal sensors and measurement of field variables. Additionally, the data were subjected to variance component analysis and estimated genetic/phenotypic parameters (RELM-BLUP), with the application of stepwise regression for each variable of agronomic interest. For soybean crops subjected to flooding, the spectral index MSAVI, NDVI, OSAVI, SAVI, VEG, MGRVI, EVI2, NDRE, GRVI, BNDVI and RGBindex demonstrated greater stability and reliability, allowing the prediction of variables with a high coefficient of determination (>0.90). Furthermore, when analyzing the data from corn plots based on the different flight moment (phenological stages), nitrogen doses and season, it was found that the most reliable indexes were EXGRaw, TGI, GNDVI, NDRE, CIRE, GVI, CVI, BNDVI, PanNDVI, SRNIRRe, SFDVI, RGBindex, NDVI, SAVI, MSAVI and OSAVI, obtaining a grouping according to the season condition and phenological stage analyzed. Finally, the field variables predicted based on the methodology presented a coefficient of determination above 0.80, except for biomass and hundred-grain weight. Therefore, it was concluded that spectral data collected from UAVs can be used for plant analysis based on the use of mixed models, which allows the correct deduction of fixed and random effects in each vegetation index and the use of a simple multivariate model for the prediction of field variables.

[1]Doctoral Thesis in Plant Science, Faculdade de Agronomia, Universidade Federal do Rio Grande do Sul, Porto Alegre, RS, Brazil. (79p.) October, 2025.

SUMÁRIO

Página
1 INTRODUÇÃO 1

2 REVISÃO BIBLIOGRÁFICA 4
2.1 A cultura da soja 4
2.2 A cultura do milho e a importância da avaliação nutricional 5
2.3 Estresse por alagamento na cultura da soja 6
2.4 Fundamentos de imagens digitais 8
2.5 Sensoriamento remoto na agricultura 12
2.6 Fenotipagem de plantas e o uso de RPA's 15
2.7 Modelos mistos aplicados a dados espectrais 16
2.8 Referências bibliográficas 18

3 ARTIGO I 28
3.1 Abstract 29
3.2 Introduction 29
3.3 Materials and Methods 30
3.3 Results 35
3.4 Discussion 42
3.5 Conclusions 44
3.6 References 44

4 ARTIGO II 48
4.1 Abstract 49
4.2 Introduction 49
4.3 Materials and Methods 50
4.4 Results 54
4.5 Discussion 60
4.6 Conclusions 62
4.7 References 63

5 CONSIDERAÇÕES FINAIS 70

RELAÇÃO DE TABELAS

Página

REVISÃO BIBLIOGRÁFICA

Tabela 1. Regiões do espectro eletromagnético. 12

ARTIGO I

Table 1. Vegetation indices (VIs) used to analyze soybean cultivars. 33
Table 2. Deviance analysis ($p < 0.05$) using the restricted maximum likelihood method (RELM) in 48 36
Table 3. Analysis of variance components and estimated genetic parameters. 36
Table 4. Variable prediction from multiple linear models (stepwise).....42

ARTIGO II

Table 1. List of spectral vegetation indices calculated in out study. 53
Table 2. Deviance analysis by maximum likelihood test (RLT) $p<0.05$. 55
Table 3. Estimates of variance components by restricted maximum likelihood (REML) for the vegetation indices and field variables analyzed in different phenological stages and two growing seasons in maize. 56
Table 4. Multivariate models for each field variable from vegetation indices in maize. 59

RELAÇÃO DE FIGURAS

Página

REVISÃO BIBLIOGRÁFICA

Figura 1. Espectro eletromagnético e elementos de imagem (pixel).....8

ARTIGO I

Figure 1. Location and experimental design used to evaluate 48 soybean genotypes subjected to two environments (flooded or non-flooded), during the 2022/23 growing season. 31
Figure 2. Visual rating scale referring to the flooding tolerance scores (FTS). 1: no symptoms of injury and 9: death of all plants in the plot. 32
Figure 3. Platforms and sensors used to collect spectral data. 32
Figure 4. Workflow diagram of the procedures used in the present study.....35
Figure 5. BLUP analysis with predicted genetic data for the MSAVI index. 38
Figure 6. BLUP analysis with predicted genetic data for the MGRVI index. 38
Figure 7. BLUP with the predicted genetic data for the RGB index. 39
Figure 8. BLUP with the predicted genetic data for the EXG index. 39
Figure 9. BLUP with estimated genetic data for plant height (cm).....40
Figure 10. BLUP with genetic data estimated for shoot biomass (kg ha^{-1}). 40
Figure 11. BLUP with predicted genetic data for grain yield (kg ha^{-1}). 41
Figure 12. Relationship between observed and predicted genetic data (RELM-BLUP analysis) using linear models for flooding tolerance score—FTS (a), shoot biomass (b), and grain yield (c). 42

ARTIGO II

Figure 1. Localization of the experimental area (A and B), experimental design (C) and remote sensing platforms used (D). 51

Página

Figure 2. Temperature and precipitation data during the 2022/23 (A) and 2023/24 (B) growth seasons. 52
Figure 3. Workflow for data acquisition and analysis during the growing season maize 2022/2023 (S1) and 2023/2024 (S2) in different phenological stages. 53
Figure 4. Principal components analysis of the BLUP values for each vegetation indices. 58
Figure 5. BLUP of maize yield data subjected to nitrogen doses and different phenological stages in the season growing 2022/2023 (A) and 2023/2024 (B).....58
Figure 6. Map with the frequency and number of predictor indices for each field variable in maize. *Yellow and green rectangles represent the absence or presence of the vegetation index in the prediction model for each field variable, respectively. 60

1 INTRODUÇÃO

Seleção rápida de genótipos adaptados a diferentes ambientes de cultivo e fatores promotores de estresse é uma das demandas da agricultura atualmente. Contudo, métodos tradicionais de fenotipagem são caros e apresentam baixo rendimento operacional para avaliações em grande escala, o que representa um gargalo na capacidade do setor agrícola em atender a demanda mundial por alimentos até 2050 (Hein et al., 2021; Xiao et al., 2022). Logo, ferramentas que proporcionem aumento na velocidade de seleção de genótipos com alta adaptabilidade e estabilidade em diferentes sistemas de produção torna-se imprescindível.

Nos últimos dez anos, o sistema de rotação soja – arroz aumentou significativamente no Brasil, ocupando 30% da área destinada a produção de arroz no estado do Rio Grande do Sul, devido aos benefícios associados ao controle de plantas daninhas e incremento na produtividade do arroz irrigado (Ribas et al., 2021). Entretanto, a produtividade média da soja nessas áreas é inferior a 1,8 Mg ha^{-1}, devido a condição de solo com pouca drenagem natural e suscetibilidade a períodos de alagamento, após a ocorrência de chuvas intensas durante o ciclo da cultura (Sartori et al. 2016; Ye et al., 2018). Existe recentemente uma alta demanda por estudos e cultivares mais adaptadas a essa condição específica (Goergen et al., 2023).

Atualmente, a maior parte da fenotipagem de linhagens de soja submetidas ao alagamento é realizada de forma subjetiva, com a aplicação de notas de tolerância baseadas nos sintomas visuais e experiência do avaliador. Sendo uma metodologia que apresenta elevado tempo de coleta e erros de observação (FOYER et al., 2016; WU et al., 2017). Isso torna a fenotipagem de alto rendimento, baseada na utilização de sensores proximais ou embarcados em aeronaves remotamente pilotadas (RPA), uma estratégia para coletar informações de plantas de maneira rápida e de baixo custo (ARAUS et al., 2018).

Além da análise morfológica de genótipos no campo, a avaliação nutricional de forma rápida e de baixo custo torna-se indispensável para verificar a resposta a diferentes estratégias de adubação, principalmente para culturas exigentes em adubação nitrogenada como o milho. Principalmente em estádios fenológicos anteriores ao florescimento, o que permite a intervenção em casos de deficiência de nitrogênio (Fernandez et al., 2020; Deng et al., 2023).

Sensores espectrais podem capturar a reflectância do dossel em diferentes comprimentos de onda do espectro eletromagnético ou faixas de comprimento (bandas espectrais), abrangendo desde o visível (400 – 700 nm) ao infravermelho próximo (700 – 1200 nm), o que possibilita o cálculo de diferentes índices espectrais e estimativa de caracteres agronômicos (JIN et al., 2020). Recentemente, Santana et al. (2022) evidenciaram que os índices espectrais diferença normalizada do verde (GNDVI), diferença normalizada da borda do vermelho (NDRE) e índice de vegetação por diferença normalizada (NDVI), possibilitaram a caracterização de genótipos quanto ao ciclo e produtividade de grãos. Adicionalmente, Oliveira et al. (2023) evidenciaram que variáveis espectrais como o índice de vegetação ajustado ao solo (SAVI) e índice melhorado (EVI), podem ser utilizados como critério de seleção para a obtenção de genótipos de soja mais produtivos. Contudo, ainda existem poucos estudos sobre a caracterização e seleção de genótipos de soja submetidos ao alagamento com base em características espectrais, bem como a remoção dos efeitos do ambiente na análise (tratamento x estádio fenológico x safra), para a correta seleção de índices preditores, o que tende a dificultar a seleção das variáveis espectrais para cada momento avaliado.

Considerando os fatores que podem afetar a predição de variáveis na cultura do milho, a resposta das plantas a doses de nitrogênio (N) torna-se imprescindível, ocorrendo variabilidade espacial e temporal em decorrência da diferença nutricional entre plantas e estádio fenológico amostrado e safra (SHRESTHA et al., 2023). Desta forma, os modelos tendem a sofrer alterações quanto ao melhor preditor de variáveis dependendo do cenário avaliado (Doses, estádio fenológico e safras). Além disso, observa-se alta influência da temperatura, luminosidade, incremento de biomassa e discrepância de tratamentos, o que tende a reduzir o coeficiente de determinação das predições abaixo de 70% (CHEN et al., 2018; Li et al., 2023). Isso demanda a aplicação de metodologias estatísticas que permitam a dedução do efeito ambiental presente nos dados e melhorar a predição de caracteres de importância agronômica na cultura do milho (CARVALHO et al., 2018).

O presente estudo foi desenvolvido com o objetivo geral de avaliar a tolerância ao alagamento de 48 genótipos de soja e predição de variáveis de campo em plantas de milho submetidas a diferentes cenários (Doses de N, momento de voo e safras), a partir de sensores espectrais proximais e embarcados em ARP's. Os objetivos específicos foram: (1) Decompor os componentes de variância e parâmetros genéticos estimados para os índices espectrais via RELM-BLUP e identificar variáveis mais confiáveis para a seleção de cultivares submetidas ao alagamento. (2) Testar o modelo linear na predição do escore de tolerância, biomassa e produtividade de grãos, a partir de dados fenotípicos e valores genéticos estimados. (3) Aplicar a metodologia RELM-BLUP para a remoção dos fatores associados ao momento de voo (estádio fenológico) e safras em índices espectrais. (4) Realizar a predição de todas as variáveis de campo com o uso de dados espectrais analisados pela metodologia na cultura do milho.

2 REVISÃO BIBLIOGRÁFICA

2.1 A cultura da soja

A produção da cultura da soja (Glycine max L. – Família: Fabaceae), aumentou cerca de 9,4 vezes nos últimos 50 anos no Brasil, em resposta ao aumento do consumo mundial de soja devido ao seu alto valor proteico e teor de óleo (Messina, 2022). Neste sentido, a expansão da fronteira agrícola é um dos fatores de maior relevância para este aumento, com incremento médio de 2% ao ano (Zalles *et al*., 2019; Silva et al., 2023). Possuí área cultivada de 47,4 milhões de hectares e produção estimada de 169 milhões de toneladas (USDA, 2025).

Atualmente, o cultivo de soja é realizado em praticamente todas as regiões produtoras do Brasil, principalmente no Sul e Centro-Oeste, os quais detém a maior área cultivada e rendimento potencial (Greschuk *et al*., 2023). Neste sentido, o melhoramento genético de cultivares contribuiu fortemente para a expansão da área cultiva, a partir da seleção de genótipos com menor mortalidade a campo, maior índice de colheita, redução de acamamento, período vegetativo menor e adaptabilidade a diferentes ambientes de produção (Finoto *et al*., 2021; Umburanas *et al*., 2022). Dentre tais alterações morfo-fisiológicas, genótipos com menor grupo de maturidade e maior taxa fotossintética foram algumas das principais modificações observadas (Todeschini *et al*., 2019; Campos *et al*., 2023). Desta forma, foi possível obter um incremento médio de até 30 kg ha^{-1} ano^{-1}.

O cenário de mudanças climáticas exigiu do melhoramento de plantas genótipos de soja mais tolerantes a múltiplos estresses ambientais como déficit hídrico ou excesso hídrico, altas temperaturas, ondas de calor e distribuição irregular de precipitação. Neste sentido, plantas tolerantes a essas condições tendem a manter elevada taxa de sobrevivência, transpiração e fotossíntese, a partir de folhas com maior número de estômatos com diâmetro reduzido (Lin *et al*., 2019; Jumrani *et al*., 2022; Demicheli *et al*., 2023). Obtendo-se menores perdas de biomassa, eficiência reprodutiva e produtividade de grãos. Entretanto, a seleção de

tais genótipos ainda se baseia nos métodos tradicionais de observação e avaliação a campo, resultando num atraso significativo na homologação e certificação de cultivares mais tolerantes a tais estresses para o mercado.

2.2 A cultura do milho e a importância da avaliação nutricional

O milho (Zea mays L.) é o terceiro cereal mais importante no mundo, o qual, juntamente com trigo e arroz, fornecem cerca de 30% da demanda energética das pessoas em países em desenvolvimento, sendo o cereal mais produzido e o segundo mais consumido (Shah *et al*., 2016). Atualmente, o milho é semeado em praticamente todas as regiões do mundo, em uma área de 22,6 milhões de hectares, e tem produção de 131 bilhões de toneladas, das quais 9,5% são produzidas pelo Brasil, o que o torna o terceiro maior produtor mundial deste cereal (USDA, 2025).

Os grãos de milho se constituem um dos alimentos base dentro da cadeia do agronegócio, dado a sua importância na composição de rações, produção de fármacos e alimentação humana, possuindo aproximadamente 72% de amido, 10% de proteína, 4% de gordura e fonte de vitaminas B12 e C, sendo considerado um dos alimentos estratégicos no combate a anemia em países subdesenvolvidos (Nuss; Tanumihardjo, 2010; Rocha; Marin, 2011).

Estima-se que eventos climáticos adversos e deficiência nutricional promovem perdas de produtividade de 10 a 45% na cultura do milho, devido à redução no crescimento, número de grãos por planta e peso dos grãos (Hussain *et al*., 2019; Torres-Rodríguez *et al*., 2021; Waqas *et al*., 2021), o que impacta diretamente na economia nacional, a qual depende desta commoditie para vários setores.

A cultura do milho apresenta alta demanda por fertilizantes nitrogenados, variando entre 16,4 a 22,3 kg de nitrogênio por tonelada de grãos produzidos, sendo o nutriente que frequentemente limita a obtenção de altas produtividades (Setiyono *et al*., 2010; Morris *et al*., 2018). Logo, ferramentas de fenotipagem que aceleram o processo de caracterização nutricional de plantas é fundamental para avaliar a resposta vegetal a diferentes manejos de adubação antes do período crítico de florescimento (Fernandez *et al*., 2020). Neste sentido, pesquisas já têm evidenciado que sensores ópticos ativos apresentam melhores métricas para a predição do conteúdo nutricional em plantas comparado a dados espectrais obtidos

com o uso de sensores passivos embarcados em ARP's (Song *et al*., 2022; Rehman *et al*., 2022). Entretanto, nenhum estudo abordou a dedução do fator ambiental associado ao momento da aquisição dos dados (voo ARP) e estádio fenológico, o que pode melhorar a acurácia dos dados obtidos com sensores embarcados em ARP's.

2.3 Estresse por alagamento na cultura da soja

A produção agrícola é uma atividade frequentemente exposta a diferentes tipos de estresses durante o desenvolvimento das plantas. Tais estresses podem impactar negativamente no rendimento e qualidade das culturas (Bashir *et al*., 2019), o que exige da comunidade científica a pesquisa e desenvolvimento de genótipos cada vez mais resilientes e adaptados a condições ambientais extremas (Razzaq *et al*., 2021).

O excesso hídrico é o segundo maior estresse abiótico, responsável por causar prejuízos bilionários principalmente no setor agrícola, estradas e transportes (Shirzaei *et al*., 2021). Com perdas globais devido a condições de alagamento de 4, 3, 2 e 1% na cultura da soja, arroz, trigo e milho, respectivamente (Kim *et al*., 2023). Ainda tem-se que a região Sul do Brasil é uma das mais afetadas pela alteração do regime de precipitação

A ocorrência do estresse por alagamento promove a redução dos níveis ótimos de oxigênio molecular (O_2) no solo. Levando a um estado de hipóxia quando o nível de O_2 limita a respiração aeróbica da rizosfera (1 a 5%), ou anoxia na ausência total de O_2 (Sasidharan *et al*., 2017). Com variações quanto ao nível da água durante o estresse, obtendo-se o alagamento parcial quando a lâmina de água cobre apenas o solo ou submergência total da parte aérea da planta (Sasidharan *et al*., 2017). Ambos promovem a redução da fosforilação oxidativa e consequentemente, uma crise energética pela menor produção de adenosina trifosfato (ATP) e moléculas redutoras (Fukao *et al*., 2019; Pan *et al*., 2021).

A cultura da soja tem sido utilizada como estratégia de rotação em áreas de terras baixas no Sul do Brasil, contribuindo para a recuperação do solo e ganhos de produtividade no sistema arroz – soja (Goulart; Reichert; Rodrigues, 2020). Contudo, devido a condição natural de solos hidromórficos nessas áreas, períodos de alagamento parcial durante a primavera – verão podem ocorrer com frequência, principalmente no início do desenvolvimento da cultura (Tagliapietra *et al*., 2021).

Com redução de 50, 80 e 90% na produtividade de grãos quando o alagamento ocorre durante os estádios fenológicos de plântula, vegetativo e no florescimento, respectivamente (YE *et al*., 2018; Shen *et al*., 2023). Contudo, a duração do estresse e condições meteorológicas durante o alagamento podem alterar o nível de tolerância das plantas. Verificando-se menor mortalidade e redução de crescimento em anos com temperatura média do ar abaixo de 35 ºC (Goergen *et al*., 2023; Shen *et al*., 2023).

Em condições de alagamento, plantas de soja tendem a restringir o crescimento e consumo de carboidratos para suportar o período de estresse, denominado de resposta quiescente (Tamang *et al*., 2021). Além da produção de aerênquima para aumentar a oxigenação das raízes submersas (Thomas *et al*., 2005). Modificações a nível fisiológico e metabólico também podem ser observadas, como estratégia para manter a produção de energia mesmo em baixas concentrações de O_2. Tal alteração metabólica pode ser realizada a partir de hemoglobinas não simbióticas (GLB), as quais têm a capacidade de transportar oxigênio da parte aérea até as raízes via complexo GLB-O_2 (Dordas, 2009).

Recentemente, Koltum *et al*. (2022) evidenciaram que genótipos de soja sob alagamento aumentaram a expressão de genes GLB1, álcool desidrogenase (ADH), nitrato redutase (NR) e oxidase alternativa (AOX). Isso indica a tentativa de manter o metabolismo aeróbico, aumento da fermentação alcólica para regenerar adenosina difosfato (ADP^+) na célula e consumo de óxido nítrico a partir da produção de nitrato (Nakayama *et al*., 2017; Casarotto *et al*., 2019). Além disso, AOX e enzimas antioxidantes destacam-se durante a recuperação, devido ao aumento de radicais livres e estresse oxidativo após a reoxigenação do solo (Tamang *et al*., 2014).

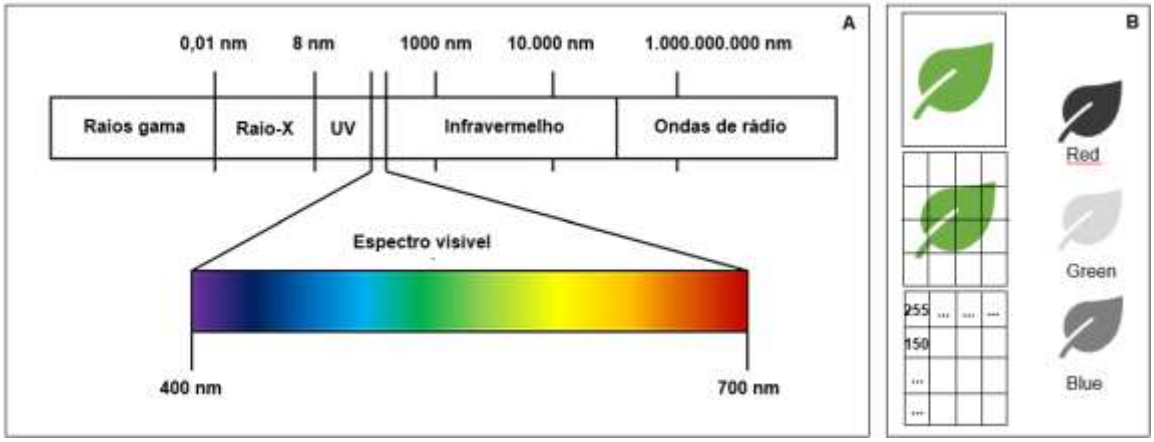
Em condições de campo, genótipos tolerantes ao alagamento tendem a apresentar maior taxa de germinação (>80%), menor dano foliar visual e menor percentual de perda de biomassa e produtividade (Fletcher *et al*., 2023). Obtendo-se materiais mais adaptados e estáveis nessas condições a partir do método de seleção baseado na avaliação da escala de tolerância no campo, também conhecido como escore de tolerância ao alagamento (ETA) (Wu *et al*., 2017), pela qual se tem a escala aqui representada por seus valores extremos definidos como: 1: nenhum sintoma de injúria e 9: morte de todas as plantas da parcela.

Embora a condição de hipóxia seja o primeiro estresse observado em plantas, outro ponto a ser considerado é a toxicidade pelo excesso de ferro, devido

a alteração do potencial hidrogeniônico (pH) e potencial redox do solo (Gotoh, Patrick, 1974). Esta condição permite a maior disponibilidade de íon ferroso (Fe^{2+}) na solução do solo, alteração do estado redox da célula e aumento significativo de estresse oxidativo via radical hidroxil ($HO^{\bullet}$) (Hell *et al*., 2003; Muller *et al*., 2017). Neste sentido, Lapaz *et al* (2020) observaram que plantas de soja sob alagamento apresentam maior toxicidade pelo excesso de ferro, com redução de 90, 50 e 90% na taxa fotossintética, biomassa e produtividade, respectivamente, seguido da inibição do transporte de amido das folhas para os órgãos dreno e aumento significativo de peróxido de hidrogênio (H_2O_2) e malondialdeído (MDA).

2.4 Fundamentos de imagens digitais

A aquisição de uma imagem é o processo pelo qual obtém-se a representação da realidade espacial em duas dimensões: X e Y (2D). Em resposta a captura da energia luminosa por sensores analógicos e armazenamento de tal informação em elementos de imagem (pixels), os quais são arranjados em linhas e colunas compondo uma matriz de dados (Figura 1) (Zhang *et al*., 2015).



Fonte: Lima (2024)

Figura 1. Espectro eletromagnético e elementos de imagem (pixel).

Qualquer sensor de imagem requer energia para produzir uma imagem. Logo, a energia do sol torna-se a mais comum, a qual viaja no espaço a 300.000 km/s na forma de comprimento de onda, também conhecida como espectro eletromagnético (Figura 1) (Kim, Chung, 2021). Tais comprimentos de onda só podem ser detectados quando interagem com a matéria: poeira, umidade, gases e aerossóis, o que permite a detecção da energia refletida a partir de sensores ópticos (Abbasi-Moghadam *et al*., 2016).

O registro digital é realizado por detectores de estado sólido como “Charge-Coupled Device” (CCD) ou “Complementary Metal-Oxide-Semiconductor” (CMOS), os quais captam fótons de energia em comprimentos de onda de 400 a 750 nm, convertem os mesmos em corrente elétrica e posteriormente em sinal digital, com diferenças significativas quanto a forma de captura e processamento do sinal (Li *et al*., 2014). Dispositivo CCD converte os fótons capturados em sinal elétrico, transporta para fora do sensor, é amplificado, passa por um conversor analógico-digital e finalmente é transformado em valor digital. Por outro lado, CMOS tem um amplificador de sinal acoplado a cada pixel, passando diretamente por um conversor analógico digital e geração do valor digital, o que permite a fabricação de câmeras mais leves. Atualmente, sensores de imagem (RGB-NIR) possuem detectores do tipo CCD e CMOS, com bons resultados para estimativa do teor de clorofilas e conteúdo nutricional de plantas (Chung *et al*., 2018; Zhou *et al*., 2019; Souza *et al*., 2022). Tais sensores permitem a adequada conversão da energia luminosa e em escala distinta (número digital), conforme o brilho ou intensidade registrada para cada pixel, os “bits” da imagem – resolução radiométrica (Riba, 2022).

A nível de pixel, a quantidade de informação armazenada depende da configuração da câmera quanto ao número de bits disponíveis (Lee *et al*., 2017), em resposta aos valores distintos (intensidade) que um pixel pode discriminar um objeto quanto a sua cor em cada região do espectro eletromagnético. Neste sentido, uma imagem binária (1 bit), pode apresentar apenas dois valores de intensidade possíveis, onde: 0 indica o brilho mínimo (preto) e 1 o máximo (branco). Contudo, a maioria das câmeras digitais atualmente fornecem imagens em escala de cinza com 16 bits (2^{16} valores), obtendo-se uma escala de nível de intensidade variando de 0 a 65.536 tons de cinza, com ganho de informação espectral a medida que aumenta-se os bits da imagem (Liao *et al*., 2023).

Imagens coloridas são compostas pelo arranjo de canais nos comprimentos de onda de cores primárias como o vermelho (*red*: R), verde (*green*: G) e azul (*blue*: B) – resolução espectral. Tais canais combinados dentro de cada pixel podem formar todas as cores que o olho humano pode identificar. Entretanto, algumas câmeras podem captar outras porções do espectro não visível como o infravermelho próximo, aumentando a quantidade de informação armazenada por cada pixel.

A configuração do dispositivo para aquisição de imagens determina a qualidade quanto a resolução espacial da imagem. Desta forma, quanto maior o número de pixels de menor tamanho, maior o nível de detalhamento – resolução espacial. Logo, um maior número de pixels por metro na realidade pode proporcionar maior nível de definição quanto às formas e cores na imagem (Yamamoto *et al*., 2017). Adicionalmente, a distância focal também determina a escala na aquisição de imagens, pois refere-se a distância entre a lente e os detectores de energia luminosa, com a resolução espacial sendo também proporcional à distância focal da câmera (Yang; Fang, 2014). Adicionalmente, distância (altura) da câmera ao alvo, sistema de lentes e resolução radiométrica dos detectores de estado sólido também podem influenciar na qualidade da imagem gerada.

Algumas correções podem ser efetuadas para garantir a melhor qualidade da imagem. Correção radiométrica refere-se a redução de distorções da energia eletromagnética registrada pelo detector com o auxílio de painéis de reflectância ou sensor de radiação acoplado à câmera, obtendo-se maior estabilidade espectral de um objeto em diferentes condições de luminosidade (Xue *et al*., 2023). Além disso, a correção geométrica visa reduzir erros de posicionamento geográfico e altimetria, a qual pode ser realizada a partir de “Pontos de controle de solo” (PCS) ou “Ground control points” (GCP’s), com coordenadas conhecidas (x, y, z), atreladas a um sistema de referência geodésico (Datum horizontal ou planimétrico) conhecidos, (ex. World Geodetic System 1984 - WGS 84 ou Sistema de Referência Geocêntrico para as Américas 2000 - SIRGAS 2000), obtendo-se erros abaixo de seis centímetros a partir de oito PCS e distribuição homogênea no ângulo de visão do sensor (Ulvi, 2021). Contudo, a precisão também pode ser afetada pela exatidão de posicionamento dos pontos de controle e do método de correção utilizado, o que exige o adequado levantamento das coordenadas de cada ponto, processamento e inserção das informações no ortomosaico.

Embora imagens RGB representem a realidade em duas dimensões (2D), técnicas que utilizam duas câmeras com sensores RGB-D, são comuns para obtenção do modelo tridimensional (3D) de objetos. Estes baseiam-se na reconstrução estereoscópica, com pontos homólogos da cena observada por diferentes ângulos, ou o cálculo do tempo que um feixe de luz leva para entrar em contato com o objeto e retornar até o sensor, estimando a profundidade dos

elementos na imagem (Zhang *et al*., 2015; Gené-Mola *et al*., 2020). Contudo, a quantidade de radiação e distância do alvo podem reduzir a qualidade da imagem, com baixa aplicabilidade em condições de campo.

Com base na técnica de fotogrametria, imagens obtidas por sensores embarcados em aeronaves remotamente pilotadas permitem a mensuração e modelagem 3D de objetos, a partir de parâmetros como: coordenadas, orientação e distância focal da câmera (Tavani *et al*., 2014). Além disso, elementos de orientação interna da câmera como distância focal, coordenadas (x, y) e coeficiente de distorção da lente são necessários para a calibração do equipamento, bem como os elementos de orientação externa como coordenadas x, y, z e ângulos de rotação (Ômega, phi, Kappa), os quais definem a inclinação e direção da câmera (Ethrog, 1984). Desta forma, torna-se possível a obtenção dos coeficientes de distorções tangencial e radial da imagem, para minimizar distorções e construção do ortomosaico com coerência a cena real.

Após a obtenção das fotos georreferenciadas via sistema global de navegação por satélite – GNSS, algoritmos de concatenação de imagens detectam pontos em comum em cada par de imagens sobrepostas durante o voo, o que permite a extração das coordenadas x, y, z dos elementos e criação de uma nuvem de pontos aleatórios representando a superfície dos objetos na imagem em 3 dimensões (Verhoeven, 2011). Adicionalmente, antes do alinhamento definitivo das imagens, a remoção de erros presentes na nuvem esparsa via projeção de erros, reconstrução de incertezas e acurácia de projeção é fundamental para reduzir as distorções da imagem, além da inserção das coordenadas de cada ponto de controle com intuito de corrigir erros de posicionamento e exclusão de fotos com baixa qualidade ou falhas no georreferenciamento (Ludwig et al., 2020).

A partir da nuvem esparsa de pontos homólogos, os softwares de processamento podem criar uma nuvem densa de pontos, de modo que, cada objeto presente na imagem seja precisamente detalhado via pontuações relacionadas as coordenadas x, y, z de cada pixel correlacionado. A partir disso, o modelo digital de superfície pode ser gerado com base na pré definição das formas presentes na imagem e consequentemente o ortomosaico, ou seja, uma única imagem obtida a partir da junção de várias fotos sobrepostas.

2.5 Sensoriamento remoto na agricultura

Sensoriamento remoto é um ramo da geofísica que busca compreender métodos e aplicações dessa ciência para adquirir informações de um objeto sem entrar em contato direto com o elemento analisado, a partir da resposta acústica, ondas gravitacionais e eletromagnéticas específicas de cada alvo (Kundu *et al*., 2021; Inoue, 2020). Tal resposta eletromagnética baseia-se no fluxo de energia constante em diferentes frequências (f), medido em hertz (Hz), comprimentos de onda (λ), expresso em nanômetros (nm) ou micrômetros (μm) e energia do fóton (E= f / λ) (Omia *et al*., 2023). A frequência é inversamente proporcional ao comprimento de onda, o que permite agrupar todos os comprimentos de onda existentes em um espectro eletromagnético, além de classificar os mesmos em regiões de acordo com sua frequência (Zwinkels, 2015; Zhang *et al*., 2019) (Tabela 1). Quanto maior o comprimento de onda, menor será a sua frequência e o seu nível energético (energia da radiação).

Tabela 1. Regiões do espectro eletromagnético.

Comprimento de onda (nm)	**Frequência** (Hz)	**Descrição**
<0,1 nm	$>10^{22}$	Raios gama
0,1 – 10 nm	10^{18}	Raio X
10 – 380 nm	10^{16}	Raio ultravioleta
400 – 700 nm	10^{15}	Visível red: 660; green: 550; blue: 400 nm
680 - 750 nm	10^{14}	Red Edge
765 – 1250 nm	10^{14}	Infravermelho próximo (NIR)
1300 nm - 2600 nm	10^{13}	Infravermelho médio (MIR)
3000 - 1.000.000 nm	10^{12}	Infravermelho de onda longa (FIR)
1 mm - 1 metro	10^{10}	Microondas
> 1 metro	10^{3}	Ondas de rádio

Considerando toda a radiação solar que atinge a superfície terrestre, a mesma apresenta porções do espectro de alta energia como raios ultravioleta (290 – 400 nm), luz visível (400 – 700 nm) e ondas maiores como o infravermelho próximo (765 – 1100 nm), sendo as regiões comumente estudadas no sensoriamento remoto, incluindo estudos sobre plantas (Sishodia *et al*., 2020) – Janela atmosférica. Infravermelho de onda longa, microondas e ondas de rádio, também podem interagir com o dossel de plantas, contudo, a avaliação de tais comprimentos de onda normalmente é realizada a partir de plataformas orbitais e em maior escala (Bi *et al*., 2024).

Frações da radiação eletromagnética no visível (RGB) e infravermelho que atingem a vegetação podem sofrer interações específicas como transmissão,

reflexão e absorção (Segarra *et al*., 2020). Sendo tais interações afetadas pela capacidade de absorção e difusão da luz no interior da folha, devido ao conteúdo de clorofilas, espessura e camadas de parênquima paliçádico e lacunoso (Xu; Ye, 2023).

Durante o processo de fotossíntese, a clorofila (a) absorve preferencialmente comprimentos de onda no laranja- vermelho (600 - 680 nm) e clorofila (b) na região violeta-azul (380 - 450 nm), com fraca absorção da luz verde (550 nm), o que resulta na aparência verde das folhas na maioria das plantas devido a maior reflectância (McCree, 1971; Zhen *et al*., 2019). Logo, isso facilita a penetração da luz verde no interior do dossel, ativação de fotossistemas em células mais profundas e pode reduzi o estresse por intensidade luminosa em horários de maior radiação (Kume *et al*., 2016; Liu; Lersel, 2021). Adicionalmente, carotenoides são pigmentos acessórios que podem atuar na captação de luz (400 nm) ou na dissipação do excesso de energia na forma de calor, a partir de alterações na conformação da proteína do complexo antena (Liguori *et al*., 2017). Desta forma, clorofilas e carotenoides são os pigmentos responsáveis pela capacidade do vegetal absorver radiação solar.

Considerando que a reflectância das plantas é inversamente proporcional à absortância, as mesmas podem ser caracterizadas quanto à capacidade de absorver ou transmitir radiação incidente sob condições específicas, também conhecido como assinatura espectral da vegetação (Estrada *et al*., 2023). A qual é gerada a partir da interação de ondas eletromagnéticas com corpos da superfície, devido a transição de elétrons, vibração e rotação molecular (Li *et al*., 2013), o que tende a afetar a absortância, transmitância e reflectância dos materiais em diferentes comprimentos de onda. Desta forma, torna-se possível a identificação de plantas a nível de espécie, correlação de respostas espectrais com caracteres quantitativos e avaliação dos efeitos da interação genótipo x ambiente com o uso de ferramentas do sensoriamento remoto, principalmente na região do visível e red edge (Lqbal *et al*., 2021; Li *et al*., 2023).

Sensores ópticos responsáveis pela coleta de informações referente a reflectância da radiação em plantas são classificados em duas categorias, ativo ou passivo. O sensor óptico ativo emite radiação em direção ao alvo e captura a energia refletida dos mesmos. Por outro lado, o sensor óptico passivo captura a energia refletida pela superfície dos alvos. Ambos têm a capacidade medir a reflectância nas regiões do espectro visível e infravermelho próximo. Contudo,

atualmente, grande parte dos sensores utilizados no monitoramento de plantas é de natureza passiva, com foco nas regiões do visível para avaliações morfológicas e de coloração, além de informações do infravermelho para estimativa do conteúdo de água e ocorrência de estresses em plantas (Zhang; Zhou, 2019; Jafarbiglu; Pourreza, 2022; Berger *et al*., 2022).

Técnicas de espectroscopia por imagem baseiam-se na construção de um espaço tridimensional, duas dimensões espaciais (x,y) e uma espectral (λ), criando camadas de imagem em diferentes comprimentos de onda para cada pixel registrado (Omia *et al*., 2023), possuindo variações de detalhamento dependendo do sensor utilizado. Neste sentido, sensores multiespectrais embarcados em RPA's têm a capacidade de captar a reflectância da vegetação em porções específicas do espectro eletromagnético, obtendo-se de 3 a 5 camadas ou bandas espectrais discretas para cada pixel da imagem (Sara *et al*., 2021). Por outro lado, sensores hiperespectrais podem captar a resposta espectral em dezenas bandas estreitas do espectro (5 nm cada banda), o que permite a criação de curvas de reflectância e detalhamento a nível de químico e físico do objeto estudado (Adão *et al*., 2017). Contudo, embora sensores hiperespectrais possuam alta resolução espectral, o investimento inicial com plataforma de ancoragem, baterias e software de processamento é dez vezes maior comparado a utilização de sensores multiespectrais, resultando em menor utilização dos mesmos em estudos de campo (Olivetti *et al*., 2023).

Sensores multiespectrais têm sido amplamente utilizados na agricultura, principalmente para a predição da produtividade dos principais cereais produtores de grãos, baseado na utilização de dados espectrais e características morfológicas, com coeficiente de determinação (r^2) acima de 0.6 (Nakano *et al*., 2023; Tanabe *et al*., 2023). Contudo, apenas 8% dos estudos têm avaliado a resposta espectral de outras culturas, com foco apenas em avaliações fenotípicas e condições ideais de cultivo, sem considerar variação temporal, espacial e a própria interação genótipo x ambiente (Tao *et al*., 2022). Logo, variações ambientais podem afetar significativamente a resposta espectral das plantas e reduzir a confiabilidade das predições e a ausência desta decomposição analítica em estudos com variáveis espectrais pode influenciar significativamente a resposta espectral das plantas e reduzir a confiabilidade das modelagens.

2.6 Fenotipagem de plantas e o uso de RPA’s

Uma das etapas do processo de melhoramento de plantas é constituído pela fenotipagem, sendo definido como o estudo das características agronômicas de cada linhagem em níveis morfológico e fisiológico durante o desenvolvimento, com auxílio de finos métodos de mensuração ou descrição para caracterizar o fenótipo (Fiorani; Schurr, 2013; Johannsen, 2014).

De modo geral, as características de cada organismo (fenótipo) são geneticamente dependentes, sendo influenciadas pela expressão de genes específicos em determinado momento (Xiao *et al*., 2022). Contudo, fatores ambientais como temperatura, luz, disponibilidade de água e fertilidade do solo modificam a expressão desses genes (Westhues *et al*., 2021), o que leva a demonstração de características morfo-fisiológicas dependentes da interação genótipo x ambiente (Xu, 2016). Logo, tais interações precisam ser avaliadas e quantificadas em programas de melhoramento genético.

A fenotipagem clássica baseia-se na avaliação destrutiva e escore visual para identificar indivíduos superiores quanto ao crescimento vegetal e tolerância a determinado estresse, respectivamente (Maranna *et al*., 2021). Entretanto, esse processo possui baixo rendimento operacional e dificuldade em avaliar de maneira rápida características mais complexas relacionadas à tolerância da planta a condições de estresse (Jiménez *et al*., 2017; Reynolds *et al*., 2020).

Recentemente, a necessidade de evolução do conhecimento sobre técnicas de fenotipagem resultou na criação da “fenômica de plantas”, baseada na utilização de múltiplos protocolos e metodologias para o estudo multidimensional, rápido e preciso de organismos em ampla escala (Yang *et al*., 2020). Este processo originou a fenotipagem de alto rendimento a partir da utilização de ferramentas do sensoriamento remoto e tecnologia da informação para a análise de grande volume de dados, em substituição a métodos manuais (Shen *et al*., 2022).

RPA’s constituem a mais recente tecnologia utilizada dentro do sensoriamento remoto, com a capacidade de realizar um mapeamento preciso e rápido de centenas de parcelas em poucos minutos, além de minimizar os efeitos de alterações ambientais associadas ao consumo de tempo com plataformas de solo ou sensores proximais manuais (Sankaran *et al*., 2015; Araus *et al*., 2018).

Devido à sobreposição de imagens durante o voo e o georreferenciamento das mesmas, cada foto é o produto da sobreposição de várias imagens de um mesmo objeto, constituindo um ortomosaico, o que garante um alto grau de

detalhamento e a capacidade de criação de modelos de elevação de superfície (Nex; Remondino, 2014). Adicionalmente, plataformas aéreas podem carregar diferentes sensores acoplados como câmeras RGB, multiespectrais, termais e hiperespectrais, permitindo coleta de imagens com alta resolução espacial e temporal, devido à possibilidade de monitoramento em qualquer estádio da cultura. Isso torna possível a avaliação contínua de características fenotípicas importantes como biomassa da parte aérea, altura de plantas, área foliar, conteúdo de nitrogênio nos tecidos, incidência de doenças e produtividade (Xie; Yang, 2020; Machwitz *et al*., 2021).

2.7 Modelos mistos aplicados a dados espectrais

Embora a utilização de dados temporais seja de grande relevância na avaliação e predição de parâmetros agronômicos, fatores associados ao ambiente como: locais, anos, estresses e estádios fenológicos distintos podem afetar a avaliação de experimentos. Isso ocorre em situações nas quais são exigidas a caracterização de plantas em diferentes cenários de cultivo, com a necessidade de compreender a natureza deste fenômeno e obter a separação dos componentes que compõem a variância observada a partir dos modelos mistos (Resende *et al*., 2014).

Atualmente, a predição de variáveis agronômicas em estudos de fenotipagem tem utilizado modelos simples como lineares multivariados e modelos complexos não lineares como Random Forest (RF), Suport Vector Machine (SVM), Partial Least Squares regression (PLSR) e redes neurais. Neste sentido, Yang *et al*. (2023) avaliaram a performance dos modelos PLSR, SVM, ANN e RF na predição do conteúdo de nitrogênio de trigo, milho, arroz e batata. Tais autores reportaram que o modelo RF apresentou as melhores métricas quanto ao coeficiente de determinação (>0.80) e erro médio (<0.3), o que pode ser explicado pela capacidade de rodar centenas de vezes os dados com cada variável preditora, permitindo-se descartar variáveis sem importância, também conhecido como técnica “Random-forest-recursive” (Darst *et al*., 2018). Contudo, o relatório do processamento não permite a dedução dos efeitos referente a cada fator dentro da análise, bem como o motivo da ocorrência de variáveis menos ou mais importantes.

Embora o modelo misto RELM-BLUP seja considerado preditivo, o mesmo busca estimar os efeitos que estão atuando sobre os valores coletados para cada

variável, de modo que o pesquisador possa verificar quais variáveis apresentam maior confiabilidade na avaliação de plantas em virtude da interferência de fatores associados ao genótipo, ambiente, manejo, erro experimental e a interação entre eles (Carvalho *et al*., 2020). Logo, os efeitos fixos e aleatórios podem ser deduzidos e o valor coletado sofre uma alteração em função da retirada dos efeitos relacionados aos fatores de variação, ou seja, um novo valor é gerado. Tal procedimento é uma nova forma de modelar plantas, pois a sobreposição de variáveis (multicolinearidade), efeito ambiental e erro estão sempre presentes em dados espectrais, o que pode gerar um modelo de predição enviesado e com baixa aplicabilidade sob outras condições de estudo.

Procedimentos estatísticos baseados no teste de máxima verossimilhança/ melhor preditor linear não viesado (RELM-BLUP) via modelos mistos, têm sido eficientes para avaliar os efeitos associados a influência genética e ambiental para cada variável mensurada (Smith *et al*., 2005; Olivoto *et al*., 2018), também chamado de efeitos fixos e aleatórios. Além disso, modelos mistos reduzem ruídos relacionados a dados ausentes e características sem efeito aditivo, o que permite a seleção de parâmetros com maior importância para a caracterização de genótipos (Hu, 2015; Carvalho *et al*., 2020).

Variáveis agronômicas quantitativas como altura de plantas, biomassa, concentração de nutrientes e produtividade são características herdáveis e podem ser selecionadas indiretamente por parâmetros com alta herdabilidade (H^2) (Falconer; Mackay, 1996). Desta forma, parâmetros indiretos avaliados com alta herdabilidade tendem a apresentar correlação com a variável quantitativa, além de contribuir no ganho genético a partir do uso da mesma (Carvalho *et al*., 2018), com menor influência do ambiente e do erro experimental.

Embora a metodologia RELM-BLUP seja mais aplicada em experimentos voltados ao melhoramento de plantas, a avaliação de ensaios com múltiplos ambientes deve considerar a dedução dos efeitos fixos e aleatórios a partir da técnica de modelos mistos. Neste sentido, devido a necessidade de integrar tais análises em diferentes experimentos Olivoto e Lúcio (2020) desenvolveram o pacote “Metan” em linguagem R para a manipulação, visualização e modelagem de dados. Logo, variáveis espectrais podem também ser analisadas a partir da metodologia para a remoção de ruídos associados à mudança espectral pela exposição a diferentes tratamentos ou fatores ligados ao momento da aquisição de aquisição de imagensdusnte o voo da RPA, selecionando índices espectrais mais

estáveis e com adequada herdabilidade para o uso em programas de melhoramento (Adak *et al*., 2021; Oliveira *et al*., 2023). Essa decomposição de dados permite a utilização de modelos de machine learning mais simples e com estrutura mais parcimoniosa, devido a menor quantidade de preditores necessários.

2.8 Referências bibliográficas

ABBASI-MOGHADAM, D. *et al*. Design and implementation of camera CCD readout for a remotesensing LEO satellite. **Optik**, [S.L], v. 127, n. 8, p. 4178-4184, 2016.

ADAK, A. *et al*. Temporal vegetation indices and plant height from remotely sensed imagery can predict grain yield and flowering time breeding value in maize via machine learning regression. **Remote Sensing**, Basel, v. 13, n. 11, p. 1-21, 2021.

ADÃO, T. *et al*. Hyperspectral imaging: a review on uav-based sensors, data processing and applications for agriculture and forestry. **Remote Sensing**, Basel, v. 9, n. 11, p. 1-30, 2017.

ARAUS, J. L. *et al*. Translating high-throughput phenotyping into genetic gain. **Trends in Plant Science**, Amsterdam, v. 23, n. 5, p. 451–466, 2018.

BASHIR, K. *et al*. Recent advances in the characterization of plant transcriptomes in response to drought, salinity, heat, and cold stress. **F1000 Research**, London, v. 14, n. 8, p. 1-8, 2019.

BERGER, K. *et al*. Multi-sensor spectral synergies for crop stress detection and monitoring in the optical domain: A review. **Remote Sensing of Environment**, Amsterdam, v. 280, p. 1-23, 2022.

BI, Y. *et al*. Atmospheric temperature measurements using microwave hyper-spectrum from geostationary satellite: band design, weighting functions and information content. **Remote Sensing**, Basel, v. 16, n. 2, p. 1-16, 2024.

CAMPOS, L. H. R. *et al*. Genetic progress of 18 years of a soybean breeding program for the Brazilian Central-West. **Revista Ciência Agronômica**, Fortaleza, v. 54, n, 16, p. 1-8, 2023.

CARVALHO, I. R. *et al*. Biometric models and maize genetic breeding: A review. **Australian Journal of Crop Science**, Lismore, v. 12, n. 11, p. 1796 – 1805, 2018.

CASAROTTO, G. *et al*. Expression of genes related to soil flooding tolerance in soybeans. **Acta Scientiarum**, Maringá, v. 41, n. 4279, p. 1-11, 2019.

CHUNG, S.; BRESHEARS, L. E.; YOON, J. Y. Smartphone near infrared monitoring of plant stress. **Computers and Electronics in Agriculture**,

Amsterdam, v. 154, n. 49, p. 93-98, 2018.

CUI, J. *et al*. Maize grain yield enhancement in modern hybrids associated with greater stalk lodging resistance at a high planting density: a case study in northeast China. **Scientific Reports**, London, v. 12, n. 14647, p. 1-12, 2022.

DARST, B. F.; MALECKI, K. C.; ENGELMAN, C. D. Using recursive feature elimination in random forest to account for correlated variables in high dimensional data. **BMC Genetics**, London, v. 19, n. 65, p. 1-6, 2018.

DEMICHELI, J. *et al*. Improving drought tolerance in soybean by classical breeding leads to physiological adjustments of photosynthesis and stomata functioning. **Plant Stress**, Amsterdam, v. 10, n. 100275, p. 1-10, 2023.

DENG, T. *et al*. Late split-application with reduced nitrogen fertilizer increases yield by mediating source–sink relations during the grain filling stage in summer maize. **Plants**, Basel, v. 12, n. 625, 2023.

DORDAS, C. Nonsymbiotic hemoglobins and stress tolerance in plants. **Plant Science**, Amsterdam, v. 176, n. 4, p. 433–440, 2009.

ESTRADA, F. *et al*. Exploring plant responses to abiotic stress by contrasting spectral signature changes. **Frontiers in Plant Science**, Lausanne, v. 13, p. 1-17, 2023.

ETHROG, U. Non-metric camera calibration and photo orientation using parallel and perpendicular lines of the photographed objects. **Photogrammetria**, Amsterdam, v. 39, n. 1, p. 13-22, 1984.

FALCONER, D. S.; MACKAY, T. F. C. **Introduction to Quantitative Genetics**. 4. ed. Longmans Green: Harlow, 1996.

FERNANDEZ, J. A. *et al*. Late-season nitrogen fertilization on maize yield: A meta-analysis. **Field Crops Research**, Amsterdam, v. 247, n. 107586, p. 1-11, 2020.

FINOTO, E. L. *et al*. Sowing times in adaptation, stability, productivity, and oil and protein contents of soybean genotypes. **Revista Caatinga**, Mossoró, v. 34, n. 4, p. 799-812, 2021.

FIORANI, F.; SCHURR, U. Future scenarios for plant phenotyping. **Annual Review of Plant Biology**, Palo Alto, v. 64, n. 12, p. 267–291, 2013.

FLETCHER, E. *et al*. Evaluating the effects of flooding stress during multiple growth stages in soybean. **Agronomy**, Basel, v. 13, n. 1243, p. 1-11, 2023.

FOYER, C. H.*et al*. Neglecting legumes has compromised human health and sustainable food production. **Nature Plants**, London, v. 2, n. 8, p. 1–10, 2016.

FUKAO, T. *et al*. Submergence and waterlogging stress in plants: A review highlighting research opportunities and understudied aspects. **Frontiers in Plant Science**, Lausanne, v. 10, n. 16, p. 1-24, 2019.

GENÉ-MOLA, J. *et al*. Assessing the performance of rgb-d sensors for 3d fruit crop canopy characterization under different operating and lighting conditions. **Sensors**, Basel, v. 20, n. 7072, p. 1-21, 2020.

GOERGEN, P. C. H. *et al*. Tolerance of soybean cultivars to flooding stress in vegetative growth stages. **Pesquisa Agropecuária Brasileira**, Brasília, v. 58, n. 21, p. 1-10, 2023.

GOTOH, S.; PATRICK, W. H. Transformation of iron in a waterlogged soil as influenced by redox potential and ph. **Soil Science Society of America Journal**, Madison, v. 38, n. 1, 66-71, 1974.

GOULART, R. Z.; REICHERT, J. M.; RODRIGUES, M. F. Cropping poorly-drained lowland soils: Alternatives to rice monoculture, their challenges and management strategies. **Agricultural Systems**, Amsterdam, v. 177, n. 28, p. 1–7, 2020.

GRESCHUK, L. T. *et al*. A soil productivity system reveals most Brazilian agricultural lands are below their maximum potential. **Scientific Reports**, London, v. 13, n. 1, p. 1-14, 2023.

HEIN, T. N.; CIAMPITTI, I. A.; JAGADISH, S. V. Bottlenecks and opportunities in field-based high-throughput phenotyping for heat and drought stress. **Journal of Experimental Botany**, Oxford, v. 72, n. 14, p. 5102–5116, 2021.

HELL, R.; STEPHAN, U. W. Iron uptake, trafficking and homeostasis in plants. **Planta**, London, v. 216, n. 4, p. 541–551, 2003.

HU, X. A comprehensive comparison between ANOVA and BLUP to valuate location-specific genotype effects for rape cultivar trials with random locations. **Field Crops Research**, Amsterdam, v. 179, n. 18, p. 144-149, 2015.

HUSSAIN, H. A. *et al*. Interactive effects of drought and heat stresses on morpho-physiological attributes, yield, nutrient uptake and oxidative status in maize hybrids. **Scientific Reports**, London, v. 9, n. 3890, p. 1–12, 2019.

INOUE, Y. Satellite and drone based remote sensing of crops and soils for smart farming – a review. **Soil Science and Plant Nutrition**, Tokyo, v. 66, n. 6, p. 798-810, 2020.

JAFARBIGLU, H.; POURREZA, A. A comprehensive review of remote sensing platforms, sensors, and applications in nut crops. **Computers and Electronics in Agriculture**, Amsterdam, v. 197, n. 67, p. 1-23, 2022.

JIMÉNEZ, J. C. *et al*. Non-destructive phenotyping to identify Brachiaria hybrids tolerant to waterlogging stress under field conditions. **Frontiers in Plant Science**, Lusanne, v. 8, n. 34, p. 1–10, 2017.

JIN, X. *et al*. High-throughput estimation of crop traits: A review of ground and aerial phenotyping platforms. **IEEE Geoscience and Remote Sensing Magazine**,

v. 9, n. 1, p. 200–231, 2020.

JOHANNSEN, W. The genotype conception of heredity1. **International Journal of Epidemiology**, Oxford, v. 43, n. 4, p. 989–1000, 2014.

JUMRANI, K. *et al*. Screening soybean genotypes for high-temperature tolerance bymaximin-minimaxmethod based on yield potential and loss. **Agronomy**, Basel, v. 12, n. 11, p. 1-17, 2022.

KIM, J.; CHUNG, Y. S. A short review of RGB sensor applications for accessible high-throughput phenotyping. **Journal of Crop Science and Biotechnology**, Seul, v. 24, n. 5, p. 495-499, 2021.

KIM, W. *et al*. Flood impacts on global crop production: advances and limitations. **Environmental Research Letters**, Bristol, v. 18, n. 5, p. 1-10, 2023.

KOLTUM, A. *et al*. Uncovering the roles of hemoglobins in soybean facing water stress. **Gene**, Amsterdam, v. 810, n. 5, p. 1-12, 2022.

KUME, A.; AKITSU, T.; NASAHARA, K. N. Leaf color is fine-tuned on the solar spectra to avoid strand direct solar radiation. **Journal of Plant Research**, Tokyo, v. 129, n. 4, p. 615-624, 2016.

KUNDU, R. *et al*. Near real time monitoring of potato late blight disease severity using field based hyperspectral observation. **Smart Agricultural Technology**, Amsterdam, v. 1, n. 18, p. 1-9, 2021.

LAPAZ, A. M. *et al*. Response of soybean to soil waterlogging associated with iron excess in the reproductive stage. **Physiology and Molecular Biology of Plants**, New Delhi, v. 26, n. 8, p. 1635–1648, 2020.

LEE, H.*et al*. Pixel-level deep segmentation: artificial intelligence quantifies muscle on computed tomography for body morphometric analysis. **Journal of Digital Imaging**, Nova York, v. 30, n. 4, p. 487-498, 2017.

LI, C. *et al*. Evaluating potential of leaf reflectance spectra to monitor plant genetic variation. **Plant Methods**, London, v. 19, n. 1, p. 1-28, 2023.

LI, L.; ZHANG, Q.; HUANG, D. A review of imaging techniques for plant phenotyping. **Sensors**, Basel, v. 14, n. 11, p. 20078-20111, 2014.

LI, Q. *et al*. Review of spectral imaging technology in biomedical engineering: achievements and challenges. **Journal of Biomedical Optics**, Bellingham, v. 18, n. 10, p. 1-29, 2013.

LIAO, L.; LIU, W.; LIU, S. Effect of bit depth on cloud segmentation of remote-sensing images. **Remote Sensing**, Basel, v. 15, n. 10, p. 1-18, 2023.

LIGUORI, N. *et al*. Different carotenoid conformations have distinct functions in light-harvesting regulation in plants. **Nature Communications**, London, v. 8, n. 1, p. 1-9, 2017.

LIN, Y. *et al*. Identification of genes/proteins related to submergence tolerance by transcriptome and proteome analyses in soybean. **Scientific Reports**, London, v. 9, n. 1, p. 1-16, 2019.

LIU, J.; LERSEL, M. W. V. Photosynthetic physiology of blue, green, and red light: light intensity effects and underlying mechanisms. **Frontiers in Plant Science**, Lausanne, v. 12, n. 163, p. 1-14, 2021.

LQBAL, I. M. *et al*. Identifying the spectral signatures of invasive and native plant species in two protected areas of pakistan through field spectroscopy. **Remote Sensing**, Basel, v. 13, n. 19, p. 1-26, 2021.

LUDWIG, M. *et al*. Quality assessment of photogrammetric methods a workflow for reproducible UAS orthomosaics. **Remote Sensing**, Basel, v. 12, n. 22, p. 1-18, 2020.

MACHWITZ, M. *et al*. Bridging the gap between remote sensing and plant phenotyping challenges and opportunities for the next generation of sustainable agriculture. **Frontiers in Plant Science**, Lausanne, v. 12, n. 108, p. 1-8, 2021.

MARANNA, S. *et al*. Breeding for higher yield, early maturity, wider adaptability and waterlogging tolerance in soybean (*Glycine max* L.): a case study. **Scientific Reports**, London, v. 11, p. 1-16, 2021.

MCCREE, K. J. The action spectrum, absorptance and quantum yield of photosynthesis in crop plants. **Agricultural Meteorology**, Amsterdam, v. 9, p. 191-216, 1971.

MESSINA, M. Perspective: Soybeans can help address the caloric and protein needs of a growing global population. **Frontiers in Nutrition**, Lusanne, v. 9, p. 1-9, 2022.

MORRIS, T. F. *et al*. Strengths and limitations of nitrogen rate recommendations for corn and opportunities for improvement. **Agronomy Journal**, Hoboken, v. 110, n. 1, p. 1–37, 2018.

MULLER, C. *et al*. Ecophysiological responses to excess iron in lowland and upland rice cultivars. **Chemosphere**, Oxford, v. 189, p. 123-133, 2017.

NAKANO, H. *et al*. Predicting rice grain yield using normalized difference vegetation index from UAV and GreenSeeker. **Crop and Environment**, Amsterdam, v. 2, p. 59-65, 2023.

NAKAYAMA, T. J. *et al*. Insights into soybean transcriptome reconfiguration under hypoxic stress: Functional, regulatory, structural, and compositional characterization. **Plos One**, v. 12, n. 11, p. 1-20, 2017.

NEX, F.; REMONDINO, F. UAV for 3D mapping applications: A review. **Applied Geomatics**, Berlin, v. 6, n. 1, p. 1–15, 2014.

NUSS, E. T.; TANUMIHARDJO, S. A. Maize: A paramount staple crop in the context of global nutrition. **Comprehensive Reviews in Food Science and Food Safety**, Chicago, v. 9, n. 4, p. 417–436, 2010.

OLIVEIRA, J. F. *et al*. Spectral variables as criteria for selection of soybean genotypes at different vegetative stages. **Remote Sensing Applications: Society and Environment**, Amsterdam, v. 32, p. 1-8, 2023.

OLIVETTI, D. *et al*. Comparing unmanned aerial multispectral and hyperspectral imagery for harmful algal bloom monitoring in artificial ponds used for fish farming. **Drones**, Basel, v. 7, n. 7, p. 1-26, 2023.

OLIVOTO, T.; LÚCIO, A. D. Metan: An R package for multi-environment trial analysis. **Methods in Ecology and Evolution**, Hoboken, v. 11, p. 783–789, 2020.

OLIVOTO, T. *et al*. REML/BLUP and sequential path analysis in estimating genotypic values and interrelationships among simple maize grain yield-related traits. **Genetics and Molecular Research**, Ribeirão Preto, v. 16, n. 1, p. 1-19, 2018.

OMIA, E. *et al*. Remote sensing in field crop monitoring: a comprehensive review of sensor systems, data analyses and recent advances. **Remote Sensing**, Basel, v. 15, n. 2, p. 1-46, 2023.

PAN, J. *et al*. Mechanisms of waterlogging tolerance in plants: research progress and prospects. **Frontiers in Plant Science**, Lausanne, v. 11, p. 1-16, 2021.

RAZZAQ, A. *et al*. Next-generation breeding strategies for climate-ready crops. **Frontiers in Plant Science**, Lausanne, v. 12, p. 1-27, 2021.

REHMAN, T. H.; LUNDY, M. E.; LINQUIST, B. A. Comparative sensitivity of vegetation indices measured via proximal and aerial sensors for assessing n status and predicting grain yield in rice cropping systems. **Remote Sensing**, Basel, v. 14, n. 12, p. 1-18, 2022.

RESENDE M. D. V.; SILVA, F. F. E.; AZEVEDO, C. F. **Estatística matemática, biométrica e computacional: Modelos Mistos, Multivariados, Categóricos e Generalizados (REML/BLUP), Inferência Bayesiana, Regressão Aleatória, Seleção Genômica, QTL-GWAS, Estatística Espacial e Temporal**. 1. ed. Visconde do Rio Branco: Suprema, 2014.

REYNOLDS, M. *et al*. Breeder friendly phenotyping. **Plant Science**, Amsterdam, v. 295, p. 1-21, 2020.

RIBA, J. R. Application of image sensors to detect and locate electrical discharges: a review. **Sensors**, Basel, v. 22, n. 15, p.1-19, 2022.

RIBAS, G. G. *et al*. Assessing yield and economic impact of introducing soybean to the lowland rice system in southern Brazil. **Agricultural Systems**, Amsterdam, v. 88, p. 1-10, 2021.

ROCHA, D.; MARIN, V. A. Transgênicos-Plantas Produtoras de Fármacos (PPF). **Ciência & Saúde Coletiva**, Rio de Janeiro, v. 16, n. 7, p. 3339–3347, 2011.

SANKARAN, S. et al. Low-altitude, high-resolution aerial imaging systems for row and field crop phenotyping: A review. **European Journal of Agronomy**, Amsterdam, v. 70, p. 112–123, 2015.

SANTANA, D. D. *et al*. High throughput phenotyping allows the selection of soybean genotypes for earliness and high grain yield. **Plant Methods**, London, v. 18, n. 13, p. 1 – 11, 2022.
SARA, D. *et al*. Hyperspectral and multispectral image fusion techniques for high resolution applications: a review. **Earth Science Informatics**, Heidelberg, v. 14, p. 1685–1705, 2021.

SARTORI, G. M. S. *et al*. Sistemas de preparo do solo e de semeadura no rendimento de grãos de soja em área de várzea. **Ciência Rural**, Santa Maria, v. 46, n. 3, p. 492-498, 2016.

SASIDHARAN, R. *et al*. Community recommendations on terminology and procedures used in flooding and low oxygen stress research. **New Phytologist**, Oxford, v. 214, n. 4, p. 1403-1407, 2017.

SEGARRA, J. *et al*. Remote sensing for precision agriculture: sentinel-2 improved features and applications. **Agronomy**, Basel, v. 10, n. 5, p. 1-18, 2020.

SETIYONO, T. D. *et al*. Estimating maize nutrient uptake requirements. **Field Crops Research**, Amsterdam, v. 118, p. 158–168, 2010.

SHAH, R. T.; PRASAD, K.; KUMAR, P. Maize - A potential source of human nutrition and health: A review. **Cogent Food and Agriculture**, London, v. 2, n. 1, p. 1–9, 2016.

SHEN, T. *et al*. Effects of flooding duration and growing stage on soybean growth based on a multi-year experiment. **Sustainability**, Basel, v. 15, n. 1, p. 1-14, 2023.

SHEN, Y. *et al*. Omics-based interdisciplinarity is accelerating plant breeding. **Current Opinion in Plant Biology**, Amsterdam, v. 66, p. 1–7, 2022.

SHIRZAEI, M. *et al*. Persistent impact of spring floods on crop loss in U.S. Midwest. **Weather and Climate Extremes**, Amsterdam, v. 34, p. 1-9, 2021.

SILVA, D. S. *et al*. Temperature effect on Brazilian soybean yields, and farmers' responses. **International Journal of Agricultural Sustainability**, London, v. 21, n. 1, p. 1-16, 2023.

SISHODIA, R.; RAY, R. L.; SINGH, S. K. Applications of remote sensing in precision agriculture: a review. **Remote Sensing**, Basel, v. 12, n. 19, p. 1-31, 2020.

SMITH, A. B.; CULLIS, B. R.; THOMPSON, R. The analysis of crop cultivar breeding and evaluation trials: an overview of current mixed model approaches.

Journal of Agricultural Science, Cambridge, v. 143, p. 449-462, 2005.

SONG, X. *et al*. Winter wheat nitrogen estimation based on ground-level and uav-mounted sensors. **Sensors**, Basel, v. 22, n. 2, p. 1-19, 2022.

SOUZA, J. J. *et al*. UAV-based hyperspectral monitoring using push-broom and snapshot sensors: a multisite assessment for precision viticulture applications. **Sensors**, Basel, v. 22, n. 17, p. 1-30, 2022.

TAGLIAPIETRA, E. L. *et al*. Biophysical and management factors causing yield gap in soybean in the subtropics of Brazil. **Agronomy Journal**, Hoboken, v. 113, p. 1882-1894, 2021.

TAMANG, B. G. *et al*. Overlapping and stress-specific transcriptomic and hormonal responses to flooding and drought in soybean. **The Plant Journal**, Oxford, v. 107, p. 100-117, 2021.

TAMANG, B. G. *et al*. Physiological and transcriptomic characterization of submergence and reoxygenation responses in soybean seedlings. **Plant, Cell and Environment**, Malden, v. 37, p. 2350-2365, 2014.

TANABE, R.; MATSUI, T.; TANAKA, T. S. T. Winter wheat yield prediction using convolutional neural networks and UAV-based multispectral imagery. **Field Crops Research**, Amsterdam, v. 291, p. 1-9, 2023.

TAO, H. *et al*. Proximal and remote sensing in plant phenomics: 20 years of progress, challenges, and perspectives. **Plant Communications**, Cambridge, v. 3, p. 1-39, 2022.

TAVANI, S. *et al*. Building a virtual outcrop, extracting geological information from it, and sharing the results in google earth via open plot and photoscan: an example from the khaviz anticline (Iran). **Computers & Geosciences**, Oxford, v. 63, p. 44–53, 2014.

THOMAS, A. L.; GUERREIRO, S. M. C.; SODEK, L. Aerenchyma formation and recovery from hypoxia of the flooded root system of nodulated soybean. **Annals of Botany**, London, v. 96, p. 1191–1198, 2005.

TODESCHINI, M. H. *et al*. Soybean genetic progress in South Brazil: physiological, phenological and agronomic traits. **Euphytica**, v. 215, p. 1-13, 2019.

TORRES-RODRÍGUEZ, J. V. *et al*. Low nitrogen availability inhibits the phosphorus starvation response in maize (Zea mays ssp. mays L.). **BMC Plant Biology,** London, v. 21, p. 1–18, 2021.

ULVI, A. The effect of the distribution and numbers of ground control points on the precision of producing orthophoto maps with an unmanned aerial vehicle. **Journal of Asian Architecture and Building Engineering**, Tokyo, v. 20, p. 806-817, 2021.

UMBURANAS, R. C. *et al*. Changes in soybean cultivars released over the past 50 years in southern Brazil. **Scientific Reports**, London, v. 12, p. 1-14, 2022.

USDA. United States Department of Agriculture. [**Base de Dados USDA**]. Disponível em:https://apps.fas.usda.gov/psdonline/app/index.html#/app/advQuery, acessado em: 16 de agosto de 2025.

VERHOEVEN, G. Taking computervision aloft – archaeological three-dimensional reconstructions from aerial photographswith photoscan. **Archaeological Prospection**, Chichester, v. 18, p. 67–73, 2011.

WAQAS, M. A. *et al*. Thermal stresses in maize: Effects and management strategies. **Plants**, Basel, v. 10, p. 1–23, 2021.

WESTHUES, C. C. *et al*. Prediction of maize phenotypic traits with genomic and environmental predictors using gradient boosting frameworks. **Frontiers in Plant Science**, Lausanne, v. 12, 2021.

WU, C.; ZENG, A.; CHEN, P.; FLOREZ-PALACIOS, L.; HUMMER, W.; MOKUA, J.; KLEPADLO, M.; YAN, L.; MA, Q.; CHENG, Y. An effective field screening method for flood tolerance in soybean. **Plant Breeding**, Berlin, p. 1-10, 2017.

XIAO, Q. *et al*. Advanced high-throughput plant phenotyping techniques for genomewide association studies: A review. **Journal of Advanced Research**, Amsterdam, v. 35, p. 215–230, 2022.

XIE, C.; YANG, C. A review on plant high-throughput phenotyping traits using UAV-based sensors. **Computers and Electronics in Agriculture**, Amsterdam, v. 178, 2020.

XU, K.; YE, H. Light scattering in stacked mesophyll cells results in similarity characteristic of solar spectral reflectance and transmittance of natural leaves. **Scientific Reports**, London, v. 13, p. 1-15, 2023.

XU, Y. Envirotyping for deciphering environmental impacts on crop plants. **Theoretical and Applied Genetics**, Berlin, v. 129, n. 4, p. 653–673, 2016.

XUE, B. *et al*. Radiometric correction of multispectral field images captured under changing ambient light conditions and applications in crop monitoring. **Drones**, Basel, v. 7, p. 1-15, 2023.

YAMAMOTO, K.; TOGAMI, T.; YAMAGUCHI, N. Super-resolution of plant disease images for the acceleration of image-based phenotyping and vigor diagnosis in agriculture. **Sensors**, Basel, v. 17, p. 1-13, 2017.

YANG, W. *et al*. Crop phenomics and high-throughput phenotyping: Past decades, current challenges, and future perspectives. **Molecular Plant**, Beijing, v. 13, n. 2, p. 187–214, 2020.

YANG, X.; FANG, S. Effect of field of view on the accuracy of camera calibration. **Optik**, [S.L], v. 125, p. 844-849, 2014.

YANG, H. *et al*. Machine learning models fed with optimized spectral indices to advance crop nitrogen monitoring. **Field Crops Research**, Amsterdam, v. 293, p.

1-15, 2023.

YE, H. *et al*. A major natural genetic variation associated with root system architecture and plasticity improves waterlogging tolerance and yield in soybean. **Plant, Cell & Environment**, Oxford, v. 41, p. 2169–2182, 2018.

ZALLES, V. *et al*. Near doubling of Brazil's intensive row crop área since 2000. **PNAS**, Washington, v. 116, p. 428-435, 2019.

ZHANG, F.; ZHOU, G. Estimation of vegetation water contente using hyperspectral vegetation indices: a comparison of crop water indicators in response to water stress treatments for summer maize. **BMC Ecology**, London, v. 19, p. 1-12, 2019.

ZHANG, Y. *et al*. A fast 3D reconstruction system with a low-cost camera accessory. **Scientific Reports**, London, v. 5, p. 1-7, 2015.

ZHANG, Z.; MA, X.; ZHONG, J. Single-pixel imaging by means of Fourier spectrum Acquisition. **Nature communications**, London, v. 6, p. 1-6, 2015.

ZHEN, S.; HAIDEKKER, M.; LERSEL, M. W. V. Far-red light enhances photochemical efficiency in a wavelength-dependent manner**. Physiologia Plantarum**, Malden, v. 167, p. 21-33, 2019.

ZHOU, C. *et al*. Imaging analysis of chlorophyll fluorescence induction for monitoring plant water and nitrogen treatments. **Measurement**, London, v. 136, p. 478-486, 2019.

ZWINKKELS, J. Light, Electromagnetic Spectrum. **Encyclopedia of Color Science and Technology**, New York, 2015.

3 ARTIGO I

Use of Phenomics in the selection of UAV-based vegetation indices and prediction of agronomic traits in soybeans subjected to flooding

* Artigo formatado e publicado conforme as normas da Revista AgriEngineering 2024, 6, 3261–3278. https://doi.org/10.3390/agriengineering6030186

Use of Phenomics in the selection of UAV-based vegetation indices and prediction of agronomic traits in soybeans subjected to flooding*

Charleston dos Santos Lima[1]*, Darci Francisco Uhry Junior [1], Ivan Ricardo Carvalho[2] and Christian Bredemeier[1]

[1]Department of Phytotechnics; Federal University of Rio Grande do Sul (UFRGS), Porto Alegre 91540-000, RS, Brazil; charlescep009@gmail.com, alemaouhry@yahoo.com.br, bredemeier@ufrgs.br
[2]Department of Agriculture; Northwestern Regional University of the State of Rio Grande do Sul (UNIJUI), Ijuí 98700-000, RS, Brazil; Ivan.carvalho@unijui.edu.br
*Correspondence: charlescep009@gmail.com

3.1 Abstract

Flooding is a frequent environmental stress that reduces soybean growth and grain yield in many producing areas in the world, such as, e.g., in the United States, Southeast Asia and Southern Brazil. In these regions, soybean is frequently cultivated in lowland areas in crop rotation with rice, which provides numerous technical, economic and environmental benefits. In this context, the identification of the most important spectral variables for the selection of more flooding-tolerant soybean genotypes is a primary demand within plant phenomics, enabling faster and more reliable results by using multispectral sensors mounted on unmanned aerial vehicles (UAV). Accordingly, this research aimed to identify the optimal UAV-based multiespectral vegetation indices for characterizing the response of soybean genotypes subjected to flooding and to test the best linear model fit in predicting tolerance scores, relative maturity group, biomass, and grain yield based on phenomic analysis. 48 soybean cultivars were sown in two environments (flooded and non-flooded). Ground evaluations and UAV-image acquisition were conducted at 13, 38 and 69 days after flooding and at grain harvest, corresponding to the phenological stages V8, R1, R3 and R8, respectively. Data were subjected to variance component analysis and estimated genetic parameters, with stepwise regression applied for each agronomic variable of interest. Our results showed that vegetation indices behave differently in their suitability for more-tolerant genotype selection. Using this approach, phenomic analysis efficiently identified indices with high heritability, accuracy, and genetic variation (>80%), as observed for MSAVI, NDVI, OSAVI, SAVI, VEG, MGRVI, EVI2, NDRE, GRVI, BNDVI, and RGB-index. Additionally, variables predicted based on estimated genetic data via phenomics had determination coefficients above 0.90, enabling the reduction of important variables within the linear model.

Keywords: Phenotyping, breeding, flood, spectral

3.2 Introduction

Soybean [Glycine max (L.) Merr.] is one of the most relevant commodities on the global market, due to its high oil and protein contents, and is widely used for human and animal nutrition [1,2]. Between 2000 and 2020, global soybean production in-creased by around 50% in response to the expansion of the agricultural frontier to pre-viously uncultivated regions [3]. This was possible due to the genetic improvement of plants, obtaining more productive cultivars adapted to new growing conditions [4].

Genotypes tolerant to flooded environments have been one of the demands of new production systems, as soybeans have been increasingly sown in lowland areas, which have historically been cultivated with rice (Oryza sativa). However, such areas have hydromorphic soils and are subjected to periods of flooding, generating a reduction of up to 56% in grain yield [5,6]. Therefore, the development of genotypes adapted to conditions of water excess is essential to enable cultivation in these areas.

Currently, the identification of soybean genotypes with increased flooding tolerance and productive stability is based on manual and laborious measurements in the field and visual observation [7], resulting in low operational yield and data reliability [8]. One of the alternatives is the use of high-throughput phenotyping procedures, based on the use of multispectral sensors

embedded in unmanned aerial vehicles (UAVs). This process allows the collection of spectral information of the reflected radi-ation by plants at different wavelengths of the electromagnetic spectrum and correla-tion with agronomic traits [9,10].

From the extraction of reflectance data, vegetation indices (VIs) can be calculated using a metric transformation of the data to measure the presence and state of vegeta-tion [11]. Such index values are directly related to the characteristics of the photosyn-thetic response of vegetation to incident light. Therefore, healthy plants have high re-flectance in the near-infrared region (>790 nm) and low reflectance in the red one (660 nm), due to the absorption peak of photosynthetic pigments, resulting in high normal-ized index values [12].

Vegetation indices have been used to monitor crop development due to their rela-tionship with morphological and physiological characteristics of vegetation. Several studies have shown that VIs can adequately estimate variables such as plant height, shoot biomass, and grain yield [13–15]. However, the prediction of parameters from mixed models with multiple variables and growing environments has now become in-dispensable for genotype selection [16,17]. This allows us to understand the relation-ship between vegetation indices and genetic components in breeding programs [18].

Methodologies based on restricted maximum likelihood (RELM) and best linear unbiased predictor (BLUP) have been used to extract the genetic contribution in the evaluated traits and increase the accuracy of predictions [19]. In this way, the values are stratified into genotypic effects (G), environment (E), and G × E interaction effects [20]. However, there are no studies using genetic spectral data for the prediction and selection of soybean genotypes subjected to flooding. Therefore, understanding the as-sociation between variables obtained by multispectral imaging, such as vegetation in-dices (VIs), and agronomic traits of interest for flooding tolerance is crucial for breed-ing programs. This approach can identify easier-to-measure variables to be used in the indirect selection of genotypes for more expensive-to-measure traits, resulting in a faster, labor-saving, and large-scale selection process.

The focus of this study is the possibility of identifying promising spectral variables for the selection of soybean genotypes with increased flooding tolerance using the RELM-BLUP methodology. The objective of this research was to identify the best vegetation indices to be used to characterize these genotypes and to test the best adjustment of the linear model in predicting the tolerance score, relative maturity group, shoot biomass, and grain yield from phenomics analysis.

3.3 Materials and Methods

3.3.1 Experimental design

The field experiment was conducted at the Rice Experimental Station of the Ri-ograndense Rice Institute, located in the municipality of Cachoeirinha/RS, southern Brazil (UTM Coordinates: 490000 Easting, 6690000 Northing, zone 22 S) (Figure 1). The soil of the experimental site is classified as a Haplic gleisol (lowland soil), exhibiting the following physical and chemical characteristics in the 0–20 cm layer: clay = 190 mg dm−3; pH = 5.8; P = 20.6 mg dm−3; K = 74 mg dm−3; and organic matter = 14 g kg−1.

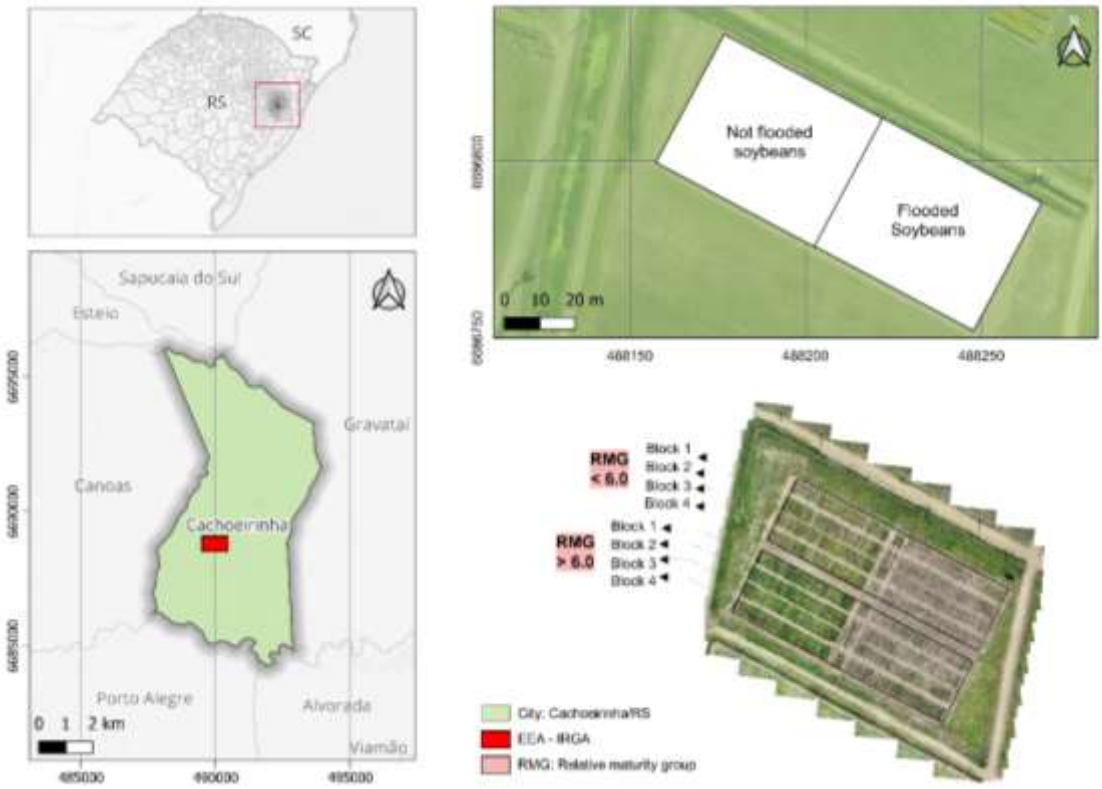


Figure 1. Location and experimental design used to evaluate 48 soybean genotypes subjected to two environments (flooded or non-flooded), during the 2022/23 growing season.

To ensure greater genetic variability among the tested materials, 48 soybean cul-tivars contrasting in terms of relative maturity group (RMG) were sown under rainfed conditions, in a randomized block design in a 48 × 2 factorial scheme (48 cultivars and two environments—flooded or non-flooded), with four repetitions (Figure 1). The experimental units consisted of four rows spaced 0.5 m apart and six meters long, totaling 12 m^2.

The cultivars were sown with a plot seeder in a furrow-ridge system on 18 No-vember 2022, with a density of 36 plants m2, which already had industrial seed treat-ment with fungicide and are listed below: RMG < 6.0: BRMX 57K58, BRMX 57I59, BRMX 57IX60, BRMX 57IX60, DM 54IX57, DM 56I59, DM 60IX64, NEO 510, NEO 560, NEO 560, NEO 580, NEO 590I2X, CZ15B70 IPRO, ST580 I2X, ST592 IPRO, ST 599 IPRO, P95Y02 IPRO, P95R40 IPRO, P95Y42 IPRO, P95R95 IPRO, P95Y95 IPRO, B5560CE, B5595CE, GH2258 IPRO, M5710 I2X, M5710 I2X and M5737 XT; RMG > 6.0: BRMX 64I61, DM 64I63, DM 66I68, DM 70I71, NEO 610, NEO 630, CZ16B17 IPRO, CZ26B12 I2X, ST611 IPRO, ST622 IPRO, TECIRGA6070RR, FTR3868, FTR4664, FTR2266, FTR3165, TMG 2264 IPRO, TMG 2165 IPRO, TMG 22X65 I2X, TMG 7061 PRO, BS IRGA 1642 IPRO, GH5993 IPRO, GH6433 I2X, M6130 I2X, and M6100 XTD. Fertilization consisted of the application of 250 kg ha−1 of triple superphosphate at sowing and 300 kg ha−1 of potassium chloride on topdressing, divided into two appli-cations (at V1 and V4 soybean growth stages), for a yield expectation of 4 Mg ha−1. The other crop management practices were performed according to recommendations for soybean cultivation.

3.2.2. Field Evaluations

The different soybean genotypes were subjected to flooding stress at flowering (phenological stage R1), with a water layer of 5 to 10 cm above ground level. The duration of flooding stress was six days, according to the appearance of injury symptoms in the most sensitive cultivars, and then the area was immediately drained to remove excess water.

After drainage, plant response was assessed at 13, 38, and 69 DAF (days after flooding), based on visual notes according to the flooding tolerance score (FTS). This was based on the

evaluation criteria described by [21], where a score of 1 indicates no apparent injury and a score of 9 indicates death of all plants in the plot (Figure 2).

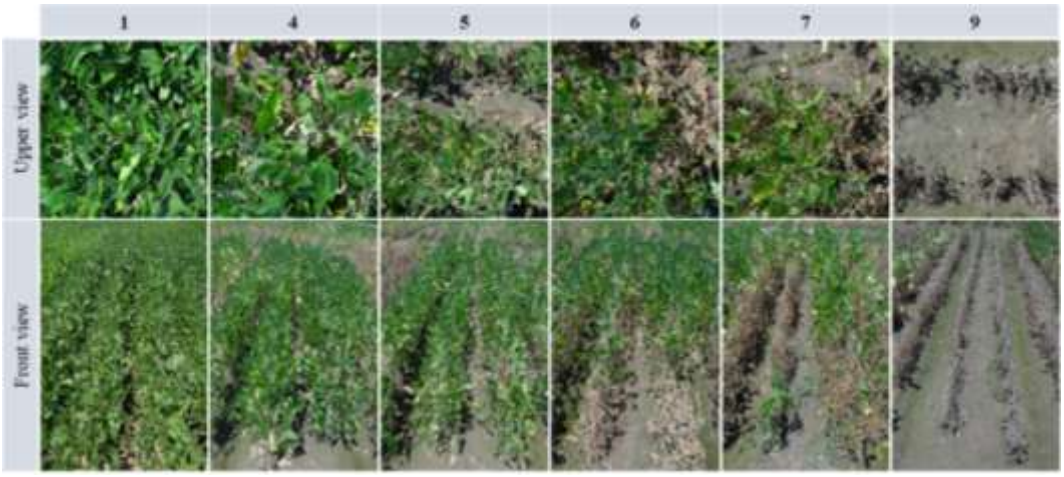


Figure 2. Visual rating scale referring to the flooding tolerance scores (FTS). 1: no symptoms of injury and 9: death of all plants in the plot.

At the same time, the height of 10 representative plants of each plot was measured (ALT_o), with the height determined from the soil surface to the tip of the penultimate trifoliate leaf, with the data expressed in cm plant−1. Additionally, the relative chloro-phyll content was estimated with the aid of a chlorophyll meter (Figure 3), with measurements carried out on 10 completely expanded random trifoliate leaves in each plot, which were also sampled to quantify the percentage of leaf nitrogen. Proximal NDVI was also determined with a spectroradiometer equipped with an active sensor (Greenseeker, Trimble, Figure 3), which emits radiation at wavelengths in the red (660 nm) and near-infrared (790 nm) regions. This procedure is used as a reference param-eter for NDVI data collected from different crops.

Grain yield was determined by harvesting two central rows of each plot having a length of five meters (area of 5 m2), at the R8 phenological stage (grain maturity). Sam-ples were subjected to screening, cleaning, and weighing on a precision scale, with the values adjusted to 13% water content.

PLATAFORM	SENSOR	BANDS	FINALITY
 DJI Phanton 4 Advanced	 Passive sensor	RGB composition (red, green, blue)	Estimate plant height from the digital terrain and surface model
 DJI Phanton 4 Multiespectral	 Passive sensor	R: red G: green B: blue RE: Red-Edge NIR: Near infrared	Collection of canopy reflectance data and calculation of vegetation indices.
 ClorofiLOG - Falker	Active sensor (It emits red and near infrared radiation)	red (650 nm); near infrared (940 nm)	Relative chlorophyll content in SPAD units
 Greenseeker - Trimbal	Active sensor (It emits red and near infrared radiation)	red: 660 nm; near infrared: 790 nm	Proximal NDVI

Figure 3. Platforms and sensors used to collect spectral data.

3.2.3. Image Acquisition Using UAV

The collection of images for spectral evaluation of each genotype was carried out before flooding, at 13, 38, and 69 DAF (days after flooding) and on the day of grain harvest, when the plants were at the phenological stage V8 (eight fully developed nodes), R1 (onset of flowering), R3 (onset of pod formation), R5 (grain filling), and R8 (physiological maturity). The evaluation in both environments (flooded and non-flooded) was carried out on the same day, to avoid changes in flight conditions.

All flights for image collection were carried out with the aid of a multispectral DJI Phantom 4 RTK unmanned aerial vehicle—UAV (Figure 3), with autonomous flight control via the Pix4D application, which allowed the acquisition of the multispectral reflectance of plants in the wavelengths of red (R: 660 nm), green (G: 550 nm), blue (B: 450 nm), red-edge (RE: 730 nm) and near-infrared (NIR: 840 nm) regions of the elec-tromagnetic spectrum, with a resolution of 20 megapixels. The general settings con-sisted of 70% frontal and 70% lateral overlap, a flight height of 30 m above ground lev-el, a camera angle of 90º (nadir), and a flight direction diagonal to the plots. The ground sample distance (GSD) of the processed orthomosaics was 2 cm.

The time for image collection was the same for all flights, which were carried out between 12:00 and 13:00. Additionally, the irradiance sensor (sunshine sensor) attached to the upper end of the UAV was used for radiometric correction of the imag-es.

To estimate soybean plant height, the DJI Phanton 4 Advanced platform was used with a RGB camera with a 12-megapixel resolution. This was used to build the digital surface (DSM) and digital terrain (DTM) models, with a flight height of 20 m above ground level and frontal and lateral image overlap of 75%.

Image processing was carried out using the Agisoft Metashape Professional soft-ware version 2.0 to construct the orthomosaics, one for each flight, which were associ-ated with geographical information from seven ground control points (GCPs) georef-erenced with GNSS-RTK for geometric correction of the photos. To extract spectral in-formation from the orthomosaics, the QGIS software version 3.28 and the "raster calculator" plugin were used to separate the wavelengths (spectral bands) present in each image. From this, the two central lines having a length of four meters of each plot were delimited by adding a shapefile vector layer and then extracting the digital number (reflectance) of each spectral band, to calculate the different vegetation indices (VIs) in the visible and multispectral regions (Table 1).

Table 1. Vegetation indices (VIs) used to analyze soybean cultivars.

Type	Index	Equation
RGB	Excess green	EXG = 2*(G(R + G + B)) − (R/(R + G + B)) − B/(R + G + B))
	Excess raw green	EXGRaw = 2*G − R − B
	Excess red	EXR = (1.4*R − G)/(R + G + B)
	Excess raw red	ExRRaw = 1.4*R − G
	Vegetation extraction color index	CIVE = (0.44*R − 0.81*G + 0.39*B)/(R + G + B) + 18.79
	Normalized green–red index	GRVI = (G − R)/(G + R)
	Excess modified red	ExRM = (2*R − G − B)/(R + G + B)
	Vegetative index	VEG = g/((r^a)*(b^(1 − a))) a = 0.667, r = R/(R + G + B), g = G/(G + R + B), b = B/(R + G + B)
	Excess blue	ExB = (1.4*B − G)/(R + G + B)
	Normalized blue difference	NDB = (G − B)/(G + B)
	Atmospheric resistant index in visible	VARI = (G–R)/(G + R + B)
	Green leaf Index	GLI = ((G − R) + (G − B))/(2*G + R + B)
	Triangular green Index	TGI = (−0.5)*[(190)*(R − G) − (120)*(R − B)]/(R + G + B)
	Red–blue Index	RBI = (R − B)/(R + B)

	Modified green–red index	MGRVI = $(G^2–R^2)/(G^2+R^2)$
	RGB index	RGBindex = $(G^2 - B*R)/ (G^2 + B*R)$
MULTISPECTRAL	Normalized difference	NDVI = (NIR − R)/(NIR + R)
	Edge of red	NDRE = (NIR − RE)/(NIR + RE)
	Soil-adjusted index	SAVI = (1 + 0.5) * [(NIR − R)/(NIR + R + 0.5)]
	Modified soil-adjusted index	MSAVI = (2*NIR + 1−sqrt((2*NIR + 1)*2−8* (NIR−R)))/2
	Optimized soil-adjusted index	OSAVI = (1 + 0.5)*((NIR − R)/(NIR + R + 0.5))
	Improved vegetation index	EVI = 2.5*(NIR − R)/(NIR + 6*R − 7.5*B + 1)
	Normalized difference from green	GNDVI = ((NIR − G)/(NIR + G))
	Chlorophyll-green index	CIG = NIR/G − 1
	Red-edge chlorophyll index	CIRE = NIR/RE − 1
	Simple ratio index	RVI = NIR/R
	Vegetation difference index	DVI = NIR − R
	Green vegetation difference index	GDVI = NIR − G
	Green ratio vegetation index	GVI = NIR/G
	Vegetation-chlorophyll index	CVI = $NIR*(R/G^2)$
	Improved vegetation index 2	EVI2 = 2.5*(NIR − R)/(NIR + 2.4*R + 1)
	Normalized blue difference	BNDVI = (NIR − B)/(NIR + B)
	R-Re normalized difference	NDVIRE = (RE − R)/(RE + R)
	PanNDVI	PanNDVI = NIR − (G + R + B)/ NIR + (G + R + B)
	Simple NIR/RE ratio	SRNIRRe = NIR/RE
	Spectral feature depth	SFDVI = ((NIR + G)/2) − ((R + NIR)/2)

The VIs used in the present study were chosen because they are widely used in highthroughput plant phenotyping procedures and, in general, in remote sensing studies of vegetation [15]. Furthermore, the VIs shown in Table 1 include the most important bands of the electromagnetic spectrum related to vegetation studies, e.g., the visible bands (blue, green, and red) as well as the infrared ones, e.g., red-edge and near-infrared (NIR).

The estimated plant height (HEI_e) followed the same methodological procedure regarding image processing and obtaining orthomosaics. However, in the QGIS software version 2.0, the two central lines of each plot were delimited by the vector layer, and the digital surface model (DSM) was subtracted from the digital terrain model (DTM), generating the plant height raster layer. To reduce the effect of the soil on the image, the orthomosaic was binarized with values of 0 (soil/background) and 1 (vegetation). After that, the plant height raster layer was divided by the binary layer and then the estimated average plant height per plot was obtained. The summarized workflow diagram of the procedures used in the present study is shown below (Figure 4).



Figure 4. Workflow diagram of the procedures used in the present study.

3.2.4. Statistical Analysis

Data were subjected to the assumptions of the statistical model (model additivity, normality, and homogeneity of residual variances). Afterwards, deviance analysis was carried out at a 5% probability using the X2 test. Additionally, the Akaike criterion and the convergence of the restricted maximum likelihood model (RELM) were analyzed.

The model that best represents the nature of the data was $Yij = \mu + Bj + Gi + Ej + \varepsilon ij$, where Yij is the value measured for each variable in each plot; Bj is the (fixed) block effect; Gj indicates the genetic effect attributed to the cultivars (random); Ej represents the (fixed) environment effect; and εij is the effect associated with the experimental error.

The variables that demonstrated significance of the complete model were used for the estimation of the phenotypic variance (σ2P), broad heritability (H2), genotype mean heritability or strict heritability (h2mg), genotype x environment determination coeficiente (GEIr2), accuracy (Ac), genotypic correlation between environments (rgloc), genotypic variation coefficient (Cvg), and experimental error (Cve) for each biometric and spectral variable.

Based on the REML estimates, it was possible to postulate the best unbiased linear predictor (BLUP), which was weighted by the significance of the genotype x environment interaction model (G × E). Therefore, a new average was obtained for each variable analyzed, without the interference of the environment (flooded or non-flooded). Furthermore, in order to verify which variables are the most important for predicting tolerance scores, plant height, shoot biomass, and grain yield, a stepwise (backward) regression model was applied to remove collinear or unimportant variables in the prediction. In this sense, the dependent variables were fixed, with explanatory variables submitted to the multiple linear regression model (y = x1 . . . xn), using the StepWise procedures at 5% by the t-test, according to the methodology proposed by [22]. Additionally, the independence of variables, absence of inflation, and collinearity were postulated.

All statistical analyses were performed in Rstudio software version 4.3, using the LM (Linear model-native), Metan, and ggplot2 packages [23].

3.3 Results

3.3.1 Analysis of Variance Components

The deviance analysis showed a significant effect for the G × E interaction ($p < 0.05$) for most of the variables analyzed (Table 2), except for the indices BNDVI, EVI2, MSAVI, NDVI, NDVI_G,

NDVIRE, OSAVI, RGBindex, SAVI, and grain yield. Therefore, it was evident that some VIs can present stability even in different environments, presenting a genotype-dependent spectral response.

Table 2. Deviance analysis ($p < 0.05$) using the restricted maximum likelihood method (RELM) in 48 soybean genotypes subjected to two environments.

Model	HEI_e	HEI_o	Biomass	BNDVI	CHLT	CIG	CIRE
Gen	0.000	0.000	0.000	0.000	0.249	0.016	0.000
G × E	0.000	0.000	0.009	0.212	0.000	0.000	0.001
Model	**CVI**	**DVI**	**EVI2**	**EXG**	**EXGRaw**	**GDVI**	**GLI**
Gen	0.925	0.000	0.000	0.000	0.000	0.004	0.000
G × E	0.000	0.000	0.999	0.034	0.000	0.000	0.000
Model	**GNDVI**	**GRVI**	**GVI**	**MGRVI**	**MSAVI**	**N_leaf**	**NDB**
Gen	0.000	0.000	0.016	0.000	0.000	0.186	0.000
G × E	0.000	0.003	0.000	0.007	0.984	0.002	0.015
Model	**NDRE**	**NDVI**	**NDVI_G**	**NDVIRE**	**OSAVI**	**PanNDVI**	**Plants_L**
Gen	0.000	0.000	0.000	0.000	0.000	0.000	0.378
G × E	0.025	0.999	1.000	0.155	1.000	0.002	0.000
Model	**Plants_M**	**TGW**	**GY**	**RGBindex**	**RVI**	**SAVI**	**SFDVI**
Gen	1.000	0.000	0.000	0.000	0.000	0.000	0.002
G × E	0.000	0.000	0.161	0.347	0.000	0.999	0.000
Model	**SRNIRRe**	**TGI**	**VARI**	**VEG**			
Gen	0.046	0.000	0.907	0.000			
G × E	0.000	0.000	0.000	0.000			

Gen: genotype effect; G × E: effect of the genotype-environment interaction. HEI_e: estimated height; HEI_o: observed height; N_leaf: nitrogen in leaf tissue; Plants_L: plants with pods at harvest; Plants_M: dead plants; TGW: thousand grain weight; GY: grain yield.

The analysis of variance components and estimated genetic parameters are presented in Table 3. In general, broad sense heritability (H^2) and genotypic correlation between environments (rgloc) presented values lower than 60% for most parameters analyzed. This suggests a greater contribution from the heritability of the average genotype (h^2mg), G × E interaction ($GEIr^2$), genotypic coefficient of variation (CVg), and error coefficient of variation (CVe).

Table 3. Analysis of variance components and estimated genetic parameters.

Parameters	σ^2 P	(H^2)	$GEIr^2$	h^2mg	Ac	rgloc	CVg	CVe	CVg/ CVe
GLI	0.00	0.35	0.23	0.67	0.82	0.36	1.03	1.14	0.91
SRNIRRe	0.00	0.20	0.40	0.44	0.67	0.50	2.15	3.03	0.71
VARI	0.00	0.01	0.65	0.03	0.18	0.65	0.72	3.76	0.19
MSAVI	0.00	0.49	0.00	0.88	0.94	0.00	3.79	3.86	0.98
NDVI	0.00	0.49	0.00	0.88	0.94	0.00	5.54	5.69	0.97
OSAVI	0.00	0.49	0.00	0.88	0.94	0.00	5.54	5.69	0.97
SAVI	0.01	0.49	0.00	0.88	0.94	0.00	5.54	5.69	0.97
VEG	0.02	0.47	0.12	0.81	0.90	0.22	6.33	5.90	1.07
NDVIRe	0.00	0.43	0.05	0.83	0.91	0.08	5.36	5.97	0.90
TGW	390.84	0.55	0.20	0.81	0.90	0.44	9.24	6.32	1.46
GNDVI	0.00	0.36	0.15	0.72	0.85	0.24	5.60	6.57	0.85
CVI	0.03	0.01	0.62	0.03	0.16	0.62	1.12	6.89	0.16
MGRVI	0.00	0.47	0.09	0.83	0.91	0.16	7.42	7.26	1.02
EVI2	0.02	0.48	0.00	0.88	0.94	0.00	7.16	7.39	0.97
NDRE	0.00	0.42	0.08	0.80	0.90	0.13	6.74	7.41	0.91
NDVI_G	0.00	0.31	0.00	0.78	0.88	0.00	5.24	7.80	0.67

CHL_total	596.62	0.12	0.51	0.29	0.54	0.58	4.59	8.03	0.57
HEI_o	114.19	0.46	0.30	0.72	0.85	0.56	11.2	8.09	1.39
GRVI	0.00	0.47	0.09	0.82	0.91	0.17	8.88	8.60	1.03
BNDVI	0.01	0.42	0.04	0.83	0.91	0.07	7.81	8.81	0.89
CIRE	0.00	0.39	0.12	0.76	0.87	0.20	8.16	9.16	0.89
Leaf N	0.25	0.18	0.27	0.48	0.69	0.33	5.53	9.53	0.58
GVI	0.34	0.24	0.36	0.51	0.71	0.47	7.93	10.3	0.77
DVI	209268.2	0.39	0.12	0.76	0.87	0.20	9.97	11.1	0.90
RGBindex	0.00	0.52	0.03	0.88	0.94	0.05	12.9	11.9	1.07
SFDVI	29135.1	0.29	0.29	0.59	0.77	0.41	10.2	12.3	0.83
EXGRaw	10778.9	0.31	0.25	0.63	0.79	0.37	10.5	12.6	0.84
GDVI	315643.7	0.27	0.30	0.58	0.76	0.41	10.9	13.6	0.80
RVI	2.05	0.40	0.17	0.74	0.86	0.29	13.7	14.1	0.97
TGI	2990.40	0.33	0.22	0.67	0.82	0.33	12.2	14.2	0.86
CIG	0.34	0.24	0.36	0.51	0.71	0.47	11.0	14.3	0.77
EXG	0.00	0.50	0.06	0.85	0.92	0.12	15.7	14.7	1.07
Plants_L	434.08	0.09	0.54	0.23	0.48	0.59	8.76	17.5	0.50
NDB	0.00	0.49	0.07	0.84	0.92	0.14	20.9	19.6	1.06
HEI_e	130.23	0.35	0.30	0.64	0.80	0.45	19.6	19.9	0.99
Plants_M	225.59	0.00	0.72	0.00	0.01	0.72	0.20	23.1	0.01
Biomass	699549.4	0.32	0.11	0.72	0.85	0.15	19.9	26.8	0.74
GY	501504.2	0.27	0.06	0.70	0.84	0.08	16.8	26.9	0.63
PanNDVI	0.01	0.40	0.11	0.77	0.88	0.18	28.1	31.1	0.90

σ^2 P: Phenotypic variance; H^2: broad heritability; $GEIr^2$: genotype x environment interaction; h_2mg: mean heritability of genotypes; Ac: accuracy; rgloc: genotypic relationship between environments; Cvg: genetic coefficient of variation; CVe: error coefficient of variation.

Considering h_2mg for the analyzed variables, high magnitude values (>80%) were found for the vegetation indices MSAVI, NDVI, OSAVI, SAVI, VEG, NDVIRE, MGRVI, EVI2, NDRE, GRVI, BNDVI, RGBindex, EXG, and NDB, which also showed a lower effect of the genotype–environment interaction ($GEIr^2$), high accuracy (Ac) (>70%), and a ratio of the genotypic coefficient of variation and error (CVg/CVe) close to or greater than 1. These factors indicate high reliability in the selection of genotypes based on these evaluated characteristics.

Biometric variables such as HEI_o, HEI_e, biomass, thousand grain weight (TGW), and grain yield (GY) presented intermediate values regarding the heritability of the characteristics (64% < h_2mg < 80%). In this scenario, a greater contribution of the G × E interaction to the expression of the characteristic was also observed (6% < $GEIr^2$ < 30%). However, the accuracy and CVg/CVe ratio maintained satisfactory values.

Low percentages of heritability and accuracy (<60%) were observed for the vegetation indices SRNIRRE, VARI, CVI, GVI, SFDVI, GDVI, and CIG, with a higher percentage of the G × E interaction and coefficient of variation of the experimental error in the respective variables. Such results were also observed for the relative content of total chlorophyll (CHLT), leaf nitrogen content (Leaf N), plants with pods at harvest (Plants_L), and dead plants (Plants_M). This implies low reliability in the use of such characteristics for the selection of soybean genotypes in the field.

3.3.2 Best Linear Unbiased Prediction (BLUP) Analysis

Considering the need to quickly evaluate a large number of cultivars based on spectral characteristics, a BLUP analysis was carried out for the vegetation indices (VIs) that presented the best values of h2mg, CVg, and CVg/CVr ratio, and also for HEI_o, biomass, and grain yield (Figures 5–11).

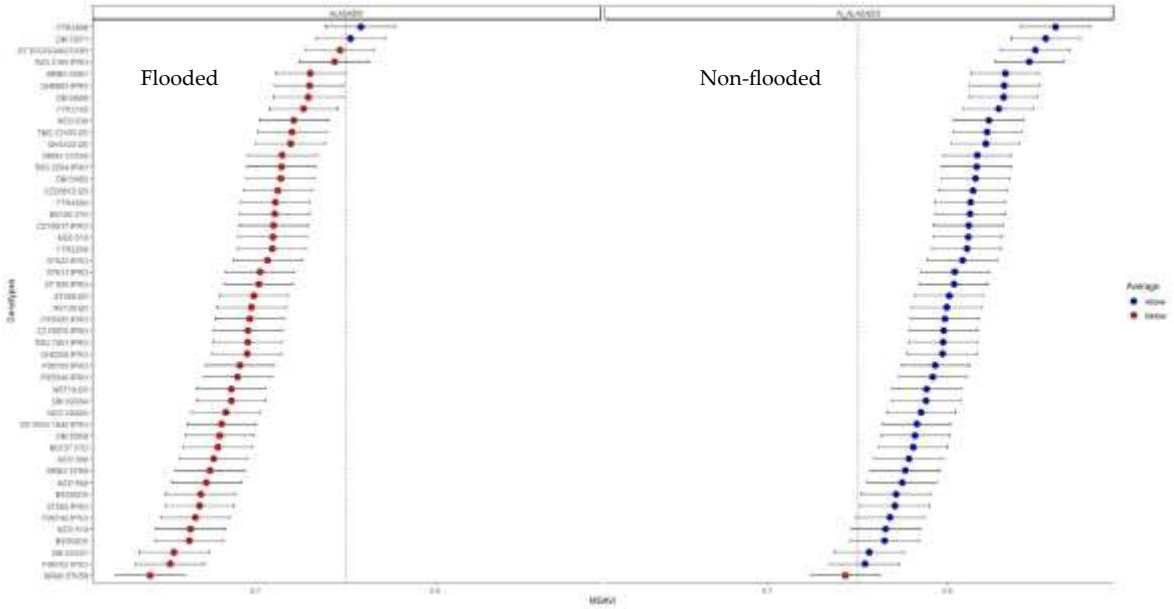


Figure 5. BLUP analysis with predicted genetic data for the MSAVI index.

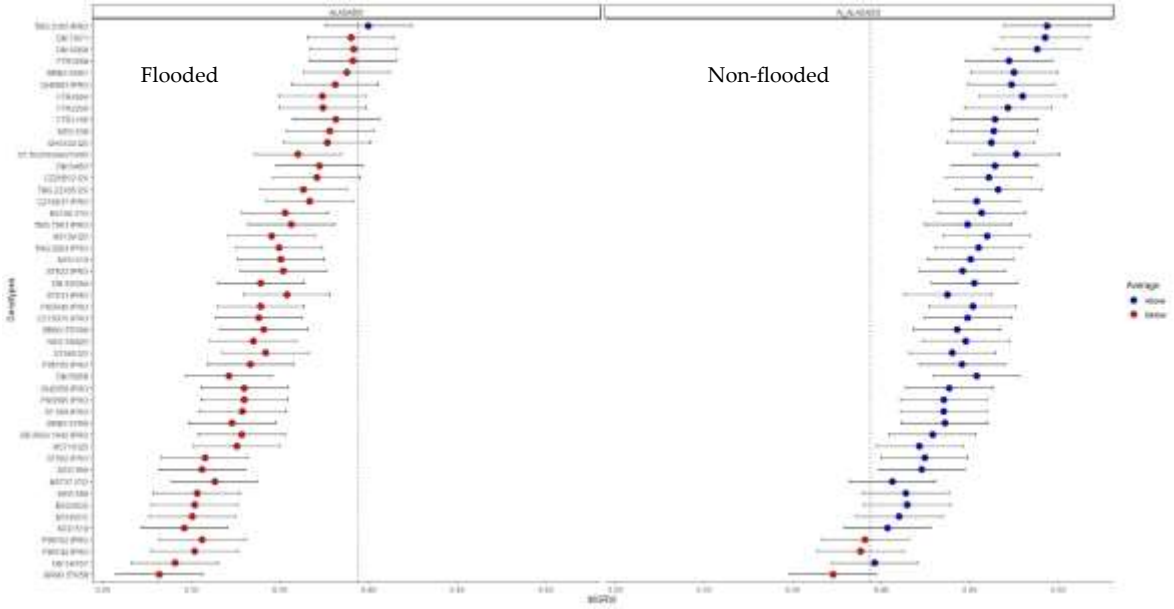


Figure 6. BLUP analysis with predicted genetic data for the MGRVI index.

It was evidenced by the BLUP analysis that the cultivars DM66I68, TMG2165, CZ26B12, FTR3165, BRMX64I61, and GH5993 IPRO presented the highest values for the vegetation indices MSAVI, MGRVI, RGBindex, and EXG under flooding conditions. These genotypes also presented higher average values for plant height, plant shoot biomass, and grain yield (60 cm, 2000 kg ha^{-1}, and 1000 kg ha^{-1}, respectively).

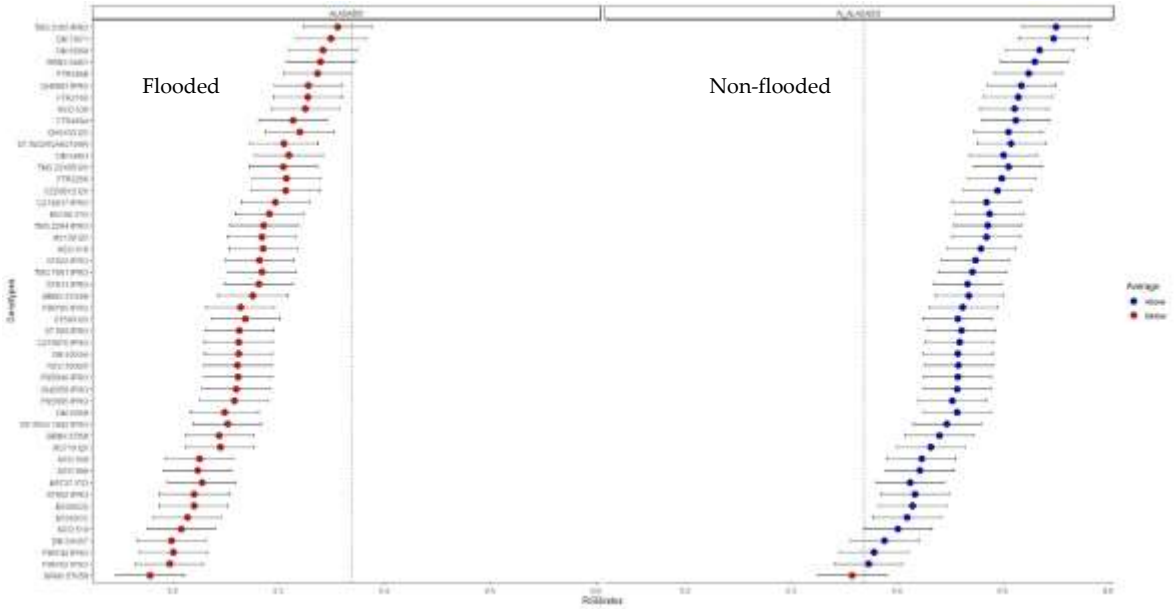


Figure 7. BLUP with the predicted genetic data for the RGB index.

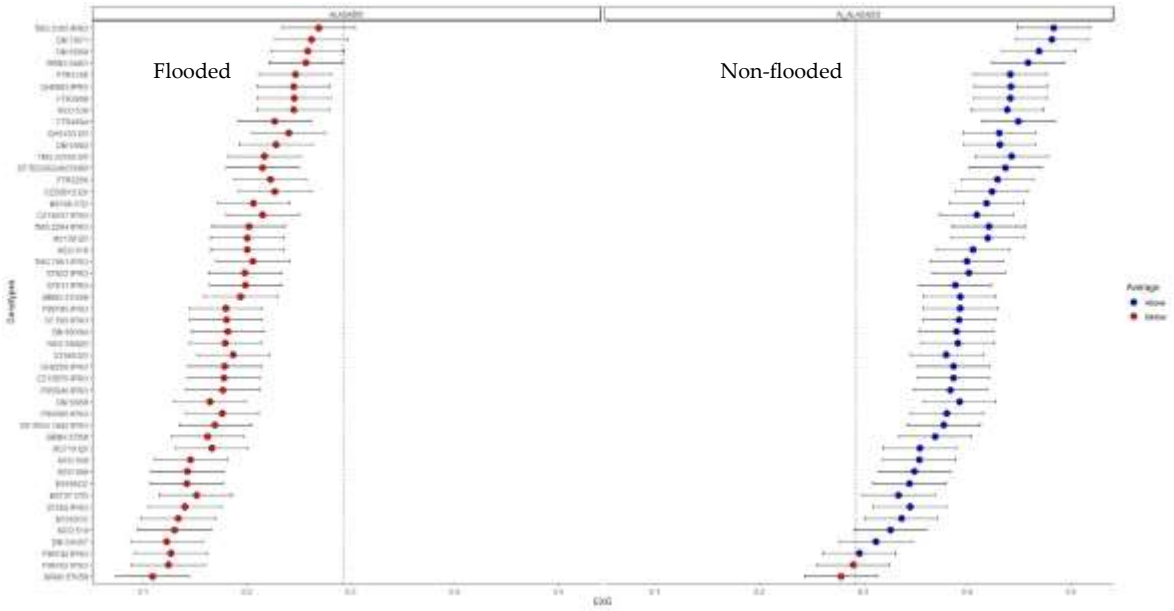


Figure 8. BLUP with the predicted genetic data for the EXG index.

Cultivars that presented low values for the MSAVI, MGRVI, RGBindex, and EXG indices in the flooded environment (DM54IX57, P95Y42 IPRO, B5560CE, ST TECIRGA6070, P95Y02 IPRO, and BRMX 57K58) also demonstrated a reduction of 30% in plant height, and 60% in plant shoot biomass and grain yield, in relation to the best genotypes. This ended up penalizing grain yield, meaning that these cultivars achieved grain yield below 200 kg ha^{-1}.

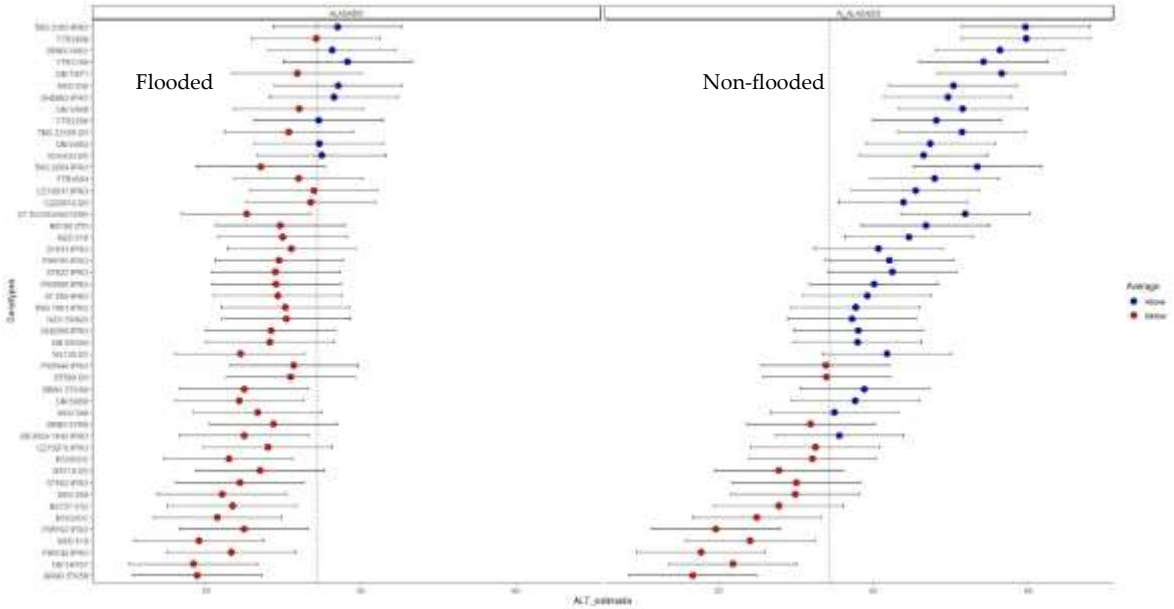


Figure 9. BLUP with estimated genetic data for plant height (cm).

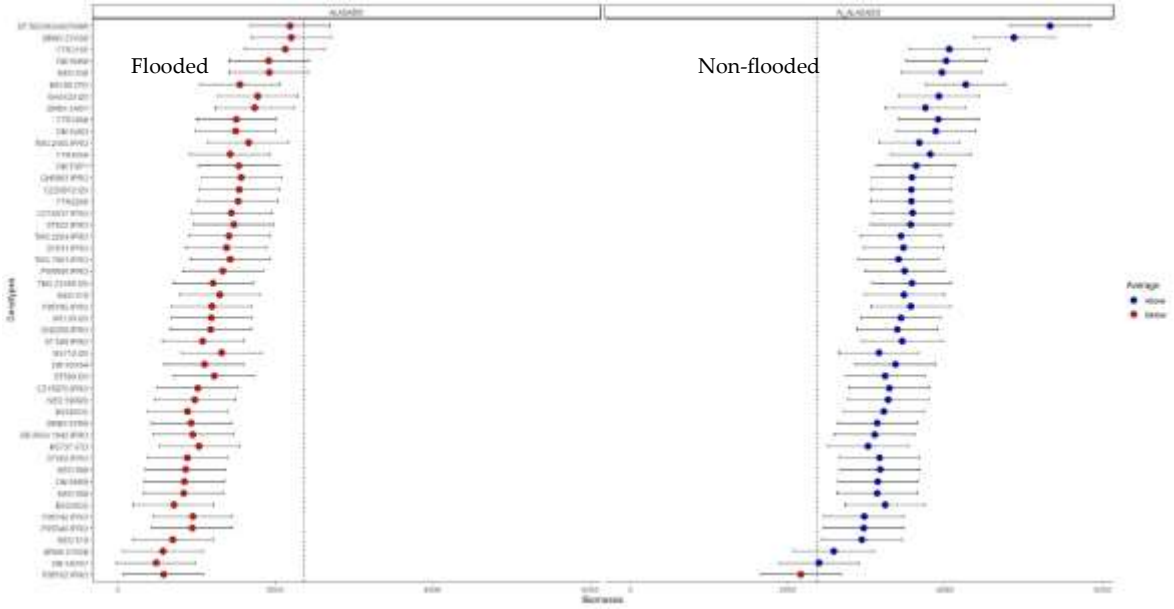


Figure 10. BLUP with genetic data estimated for shoot biomass (kg ha^{-1}).

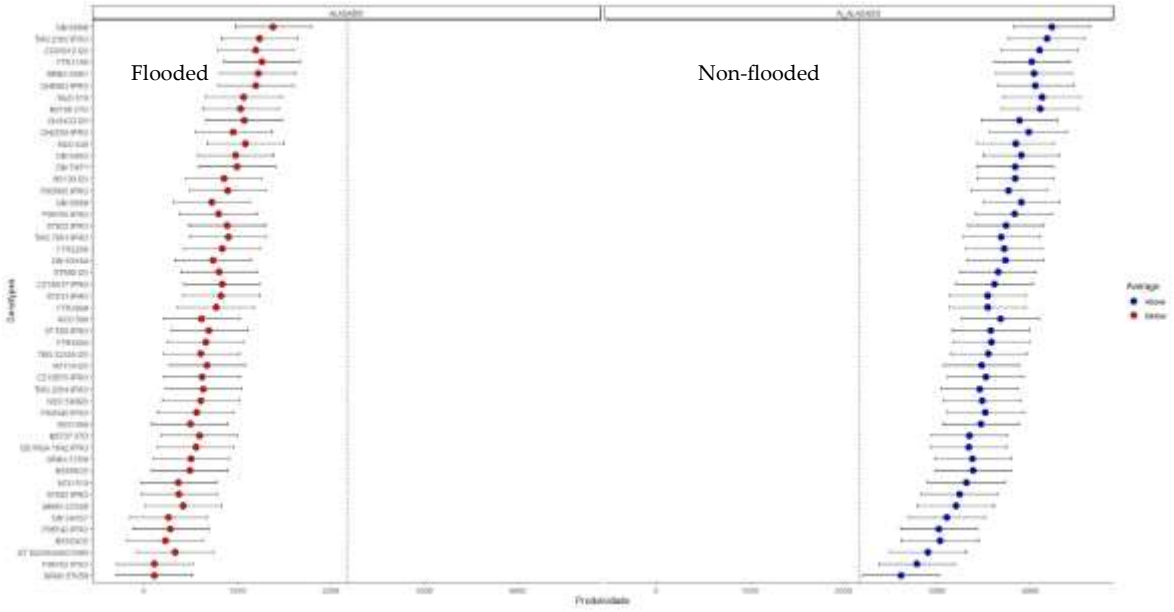


Figure 11. BLUP with predicted genetic data for grain yield (kg ha^{-1}).

In the environment without excess water (non-flooded), there was a general increase in the magnitude of the values observed for the vegetation indices and biometric variables. However, the most productive genotypes maintained the same behavior, obtaining higher values for the MGRVI and RGBindex indices, mainly. The absence of flooding allowed average values to be obtained of 80 cm, 4000 kg ha−1, and 3500 kg ha−1 for HEI_o, shoot biomass, and grain yield, respectively (Figures 8–10).

When the flooding-sensitive cultivarsDM54IX57, P95Y42 IPRO, B5560CE, ST TECIRGA6070, P95Y02 IPRO, and BRMX 57K58 were evaluated in an environment without flooding, it was found that they also presented lower values for the vegetation indices of greater genetic heritability SAVI, OSAVI, NDVI, VEG, RGBindex, and EXG (Figures 5–8). Therefore, these cultivars presented HEI_o, shoot biomass, and grain yield close to the population average of 65 cm, 2500, and 2200 kg ha−1, respectively (Figures 9–11).

The general average grain yield of the genotypes in the environments was 2200 kg ha^{-1}. Therefore, a reduction of up to 80% in productivity was observed when the cultivars were subjected to flooding (Figure 11). Additionally, it was found that cultivars with low grain yield potential in the stress-free (non-flooded) environment (P95Y02, P95Y04, and BRMX 57K58) maintained the same behavior when exposed to flooding, presenting the greatest grain yield losses.

The prediction of important agronomic traits in the evaluation of soybean cultivars subjected to flooding (Table 4), and the relationship between observed and predicted genetic data (RELM-BLUP analysis) using linear models for tolerance score (FTS), shoot biomass, and grain yield, were also analyzed (Figure 12). In this sense, it was found that the coefficient of determination for predicting the flooding tolerance score (FTS) was one of the lowest among the predicted traits (0.78). In this way, it was possible to obtain 11 significant variables by stepwise regression. On the other hand, shoot biomass and grain yield demonstrated a coefficient of determination above 0.9, with variations depending on the data used (genetic estimated via RELM-BLUP) and phenotypic value (collected directly from the field).

Table 4. Variable prediction from multiple linear models (stepwise).

Predicted Variable	r^2	Indices Selected via Stepwise ($p < 0.05$)
Flooding tolerance score (FTS)	0.78	CHLT, CIRE, EXGRaw, GVI, NDRE, NDVIRE, PanNDVI, RVI, TGI, VARI, VEG
Relative maturity group (RMG)	0.57	BNDVI, CIRE, DVI, EXG, GLI, GNDVI, GVI, MSAVI, NDB, NDVI, NDVIRe, OSAVI, PanNDVI, TGI, VEG
Shoot biomass (phenotypic values)	0.91	CHLT, CIG, CVI, EVI2, EXGraw, GDVI, GNDVI, MSAVI, PanNDVI, SAVI, TGI, VARI
Shoot biomass (genotypic values)	0.95	EVI2, NDRE, NDVI, NDVIRE
Grain yield (phenotypic values)	0.94	CIG, CIRE, EXG, EXGRaw, GDVI, NDRE, SFDVI, SRNIRRE
Grain yield (genotypic values)	0.99	CHLT, CIRE, GLI, MGRVI, OSAVI, RGBindex, RVI

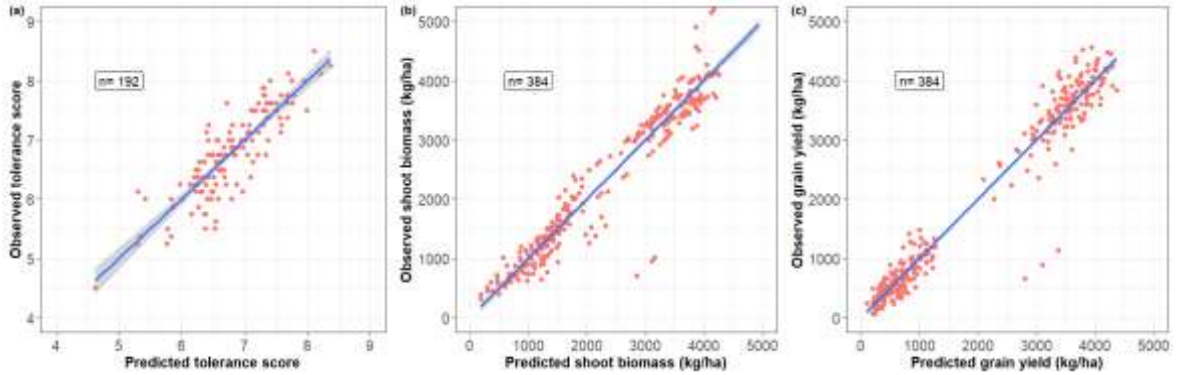


Figure 12. Relationship between observed and predicted genetic data (RELM-BLUP analysis) using linear models for flooding tolerance score—FTS (a), shoot biomass (b), and grain yield (c).

The coefficient of determination for shoot biomass and grain yield with phenotypic values was 0.91 and 0.94, respectively. However, it was found that the prediction based on genetic values tends to better estimate the behavior of biomass and productivity, with r2 of 0.95 and 0.99, respectively. Additionally, it was found that the prediction based on estimated genetic values allowed the reduction in the number of variables used within the model, making it more parsimonious.

The most important vegetation indices for predicting plant shoot biomass were EVI2, NDRE, NDVI, and NDVIRE, which were completely different from the indices selected for predicting grain yield, namely, CIRE, GLI, MGRVI, OSAVI, RGBindex, and RVI (Table 4).

The relative maturity group (RMG) of the cultivars was also predicted, as an indirect measure of the duration of the growth cycle of the tested materials (Table 4). It was observed that the prediction of RMG from vegetation indices obtained a coefficient of determination close to 0.60, requiring 14 predictors through stepwise regression, similar to the condition observed for predicting flooding tolerance, which demonstrates the greater difficulty of estimating categorical variables via machine learning.

3.4 Discussion

Under flooding stress conditions, soybean cultivars tend to exhibit distinct morphological, physiological, and spectral behaviors [24,25]. This trend was also verified in the presente study, as all genotypes showed a reduction in plant height, shoot biomass, grain yield, and magnitude of vegetation indices. However, some VIs maintained a genotype-dependent response, with high heritability regardless of the cultivation environment.

Heritability in the broad sense (H2) is defined as the sum of dominance variance, epistatic variance, and additive variance [26] The latter is the only fraction capable of being passed on in plant crossings, which can be evaluated by quantitative genetics through strict sense heritability (h2mg)

[27]. It is relevant to verify which parameters of the present study have a greater or lesser genetic contribution.

Vegetation indices, such as MSAVI, NDVI, VEG, OSAVI, SAVI, MGRVI, EVI2, NDRE, RGBindex, EXG, and NDB, showed h2mg > 80%, Ac > 90%, and a CVg/CVe ratio close to 1 (Table 3). In this sense, ref. [28] postulated that heritability values (>80%), accuracy (>70%), and Cvg/Cve ratio equal to or greater than 1 indicate data reliability and genetic variation for the trait, allowing their use for the indirect selection of genotypes due to less environmental influence. Furthermore, it indicates that fewer genes may control the expression of the parameter and that Cvg is not dependent on the G × E interaction [29,30]. These factors end up increasing the efficiency of breeding programs by inserting secondary characteristics such as VIs [31].

Recently, ref. [32] evaluated the heritability of vegetation indices in 28 soybean genotypes. These authors observed that the SAVI and EVI indices have heritability of 79% and 82%, respectively, which reported gains with indirect selection of up to 20% when plants were selected at the V8 phenological stage based on the vegetation indices. Additionally, ref. [33] evaluated the behavior of 456 wheat cultivars regarding the NDVI, NDRE, and RVI indices in four environments. The authors found that the estimated genetic values of the indices based on the RELM-BLUP methodology made it possible to accurately select 66% of the most productive genotypes, with NDVI and NDRE being the indices with the highest genetic heritability and high correlation with grain yield, similar to the data obtained in the present study. Therefore, genetic values estimated for VIs via mixed models from soybean cultivars in different environments (flooded or non-flooded) can be used as secondary selection variables. This is due to the removal of effects from the growing environment [34,35].

According to the RELM-BLUP methodology, variables that demonstrated a high percentagem of G × E and CVe interaction (CHLT, N_leaf, Plants_L, GLI, SRNIRRE, VARI, CVI, GVI, SFDVI, EXGRaw, GDVI, and CIG), did not demonstrate consistent results in the evaluation of genotypes between environments (Table 3). This may be associated with significant changes that excess water can cause in the leaf area, number of pods plant^{-1}, and photosynthetic pigments, in addition to modifying radiation reflectance at wavelengths of the visible (400–700 nm), near-infrared (760–900 nm), and short-wave infrared (1600–1850 nm) regions of the electromagnetic spectrum [25]. Previous studies [36,37] reported a better characterization of plants under stress when using the red, red-edge, and infrared spectral bands.

Due to the ability of water stress to mainly affect photosynthetic pigments and relative water content in the leaf, reflectance in the blue, red, and infrared regions of the electromagnetic spectrum is significantly higher under stress conditions [38]. Therefore, indices such as MSAVI, SAVI, OSAVI, NDRE, NDVI, EXG, VEG, MGRVI, and RGBindex can provide better characterization of plants in different environments, since they integrate spectral bands sensitive to photosynthetic changes and water content in the leaf [39,40].

From the stepwise analysis for character prediction, it was evident that RMG was the variable with the lowest fit in the linear model (0.57), requiring 14 predictors in theanalysis. In this sense, ref. [13] also found the greater complexity of the correlation between VIs and the duration of soybean crop cycle, which obtained an r2 = 0.70, 30% residual effect, and a significant contribution only from the NDVI, SAVI, GNDVI, and NDRE indices. Additionally, FTS was the variable that also presented the lowest model fit (0.78). This fact can be considered acceptable due to the impact of flooding time (DAF) and flight height on image collection. From this, it is possible to obtain better results with 6 to 12 DAF and a flight altitude of 20 m [24,41]. This was also followed in the present study, except for the flight height (30 m), in addition to the factor associated with the recovery time of the cultivars, which can change the FTS throughout the cycle.

The selection of estimated phenotypic or genetic values for predicting shoot biomass and grain yield showed similar behavior (Table 4). Both values presented a coefficient of determination higher than 90%. However, the number of variables necessary to estimate the behavior was different; a reduced model was obtained with the use of genetic valuesestimated via RELM-BLUP, with reduced processing time and complexity of the analysis.

Additionally, the comparison of predicted versus observed data (Figure 12) demonstrated that the values were adjusted by the linear model, even with a smaller number of variables in the

model with genetic data (RELM-BLUP). Furthermore, more robust prediction models could be applied as a strategy to evaluate parameters with high variability, such as shoot biomass and grain yield.

Efficiency in predicting variables within any model is essential, as it reduces data collection time and avoids using parameters with high collinearity. Therefore, using the RELM-BLUP methodology on spectral variables, the effect of the environment is removed and only the genetic weight is attributed to the variable [20]. This allows the maximization of selection accuracy and identification of variables with a greater additive genetic effect [34]. Moreover, it enables the use of VIs that have stability between environments and high genetic heritability. However, there are still few studies on this topic, which justifies the relevance of the study for high-throughput soybean phenotyping based on vegetation indices and RELM-BLUP methodology.

Thus, high-throughput phenotyping using multispectral sensors embedded in unmanned aerial vehicles (UAVs) can be applied, through the use of vegetation indices with greater genetic heritability and lower environmental effect (as e.g., MSAVI, NDVI, SAVI, OSAVI, VEG, and MGRVI). This enables a faster and more accurate selection of soybean genotypes with greater tolerance to flooding, since the usual methods used in this selection, such as tolerance scores or destructive shoot biomass samples, are time-consuming and laborious. In this sense, the tools and VIs shown in our study can be used in a complementary way in a plant breeding program, both for predicting variables as well as for genotype selection.

One of the main limitations relates to the compilation of data on a larger scale, which could be minimized by creating a phenotyping package to automate data collection on a greater number of genotypes and, especially, different sites. To minimize the effect of the environment on the methodology proposed in the present study, it is crucial to standardize the procedures for acquiring and processing images obtained by a multispectral UAVbased sensor, such as the radiometric correction by the irradiance sensor, the geometric correction using ground control points (GCPs), and time of flight. This standardization was undertaken in our study and must be observed in subsequent studies.

3.5 Conclusions

1. The environmental factor exerts a significant influence on vegetation indices, which limits their large-scale use in characterizing soybean genotypes with differential tolerance to flooding using multispectral sensors embedded on unmanned aerial vehicles.
2. The phenomic analysis was efficient for identifying vegetation indices with greater heritability, accuracy, and genetic variation, namely, MSAVI, NDVI, SAVI, OSAVI, VEG, MGRVI, EVI2, GRVI, RGBindex, EXG, NDB, and HEI_e. These variables can be used in subsequent studies to develop predictive models of agronomic variables linked to the response of soybeans to flooding with high accuracy.
3. The methodology based on RELM-BLUP for characterizing the behavior of each spectral variable depending on the environment and evaluated genotypes allows the identification of predictors (IVs) with greater genetic heritability and their use in the selection of soybean genotypes tolerant to flooding.
4. Variables predicted based on the use of genetic data estimated via phenomics presented a coefficient of determination above 0.90 and allow the reduction in the number of important variables within the linear model of prediction.

3.6 References

1. Montoya, F.; García, C.; Pintos, F.; Otero, A. Effects of irrigation regime on the growth and yield of irrigated soybean in temperate humid climatic conditions. Agric. Water Manag. **2017**, 193, 30–45. [CrossRef]
2. Sun, J.; Mooneyc, H.; Hu,W.; Tang, H.; Tong, Y.; Xu, Z.; Huang, B.; Cheng, Y.; Yang, X.;Wei, D.; et al. Importing food damages domestic environment: Evidence from global soybean trade. Proc. Natl. Acad. Sci. USA **2018**, 115, 5414–5419. [CrossRef] [PubMed]

3. Song, X.P.; Hansen, M.C.; Potapov, P.; Adusei, B.; Pickering, J.; Adami, M.; Lima, A.; Zalles, V.; Stehman, S.V.; Di Bella, C.M.; et al. Massive soybean expansion in South America since 2000 and implications for conservation. Nat. Sustain. **2021**, 4, 784–792. [CrossRef] [PubMed]
4. Finoto, E.L.; Soares, M.B.B.; Correia, A.N.; Albuquerque, J.A.A.; Silva, E.S. Sowing times in adaptation, stability, yield, and oil and protein contents of soybean genotypes. Rev. Caatinga **2021**, 34, 799–812. [CrossRef]
5. Zanon, A.J.; Silva, M.R.; Tagliapietra, E.L.; Cera, J.C.; Bexaira, K.P.; Richter, G.L.; Duarte, A.J.; Rocha, T.S.M.; Weber, P.S.; Streck, N.A. Ecofisiologia da Soja: Visando Altas Produtividades, 1st ed.; Palloti: Santa Maria, Brasil, 2018; pp. 1–136.
6. Ye, H.; Song, L.; Chen, H.; Valliyodan, B.; Chen, P.; Ali, L.; Vuong, T.; Wu, C.; Orlowski, J.; Buckley, B.; et al. A major natural genetic variation associated with root system architecture and plasticity improves waterlogging tolerance and yield in soybean. Plant Cell Environ. **2018**, 41, 2169–2182. [CrossRef]
7. Fletcher, E.; Patterson, R.; Dunne, J.; Saski, C.; Fallen, B. Evaluating the effects of flooding stress during multiple growth stages in soybean. Agronomy **2023**, 13, 1243. [CrossRef]
8. Reynolds, M.; Chapman, S.; Crespo-Herrera, L.; Molero, G.; Mondal, S.; Pequeno, D.N.L.; Pinto, F.; Pinera-Chavez, F.J.; Poland, J.; Rivera-Amado, C.; et al. Breeder friendly phenotyping. Plant Sci. **2020**, 295, 110396. [CrossRef]
9. Xie, C.; Yang, C. A review on plant high-throughput phenotyping traits using UAV-based sensors. Comp. Electron. Agric. **2020**, 178, 105731. [CrossRef]
10. Gill, T.; Gill, S.K.; Saini, D.K.; Chopra, Y.; Koff, J.P.; Sandhu, K.S. A comprehensive review of high throughput phenotyping and machine learning for plant stress phenotyping. Phenomics **2022**, 2, 156–183. [CrossRef]
11. Bannari, A.; Morin, D.; Bonn, F. A review of vegetation indices. Remote Sens. Rev. **1995**, 13, 95–120. [CrossRef]
12. Khan, Z.; Rahimi-Eichi, V.; Haefele, S.; Garnett, T.; Miklavcic, S.J. Estimation of vegetation indices for high throughput phenotyping of wheat using aerial imaging. Plant Methods **2018**, 14, 20. [CrossRef] [PubMed]
13. Santana, D.D.; Cunha, M.P.O.; Santos, R.G.; Cotrim, M.F.; Teodoro, L.P.R.; Júnior, C.A.S.; Baio, F.H.R.; Teodoro, P.E. High throughput phenotyping allows the selection of soybean genotypes for earliness and high grain yield. Plant Methods **2022**, 18, 13. [CrossRef] [PubMed]
14. Bai, D.; Li, D.; Zhao, C.;Wang, Z.; Shao, M.; Guo, B.; Liu, Y.;Wang, Q.; Li, J.; Guo, S.; et al. Estimation of soybean yield parameters under lodging conditions using RGB information from unmanned aerial vehicles. Front. Plant Sci. **2022**, 13, 1012293. [CrossRef] [PubMed]
15. Randelovic, P.; Dordevic, V.;Miladinovic, J.; Prodanivic, S.; Ceran,M.; Vollmann, J. High-throughput phenotyping for non-destructive estimation of soybean fresh biomass using a machine learning model and temporal UAV data. PlantMethods **2023**, 19, 89. [CrossRef] [PubMed]
16. Olivoto, T.; Lúcio, A.D.C.; Silva, J.A.G.; Sari, B.G.; Diel, M.I. Mean performance and stability in multi-environment trials ii: Selection based on multiple traits. Agronomy J. **2019**, 111, 2961–2969. [CrossRef]
17. Loro, M.V.; Carvalho, I.R.; Filho, A.C.; Hoffmann, J.F.; Kehl, K. Wheat grain biofortification for essential amino acids. Pesq. Agropec. Bras. **2023**, 58, e02860. [CrossRef]
18. Rutkoski, J.; Poland, J.; Mondal, S.; Autrique, E.; Pérez, L.G. Canopy temperature and vegetation indices from high-throughput phenotyping improve accuracy of pedigree and genomic selection for grain yield in wheat. G3 Genes **2016**, 6, 2799–2808. [CrossRef]
19. Kehl, K.; Carvalho, I.R.; Sacon, D.; Rizzardi, M.A.; Langaro, N.A.; Loro, M.V.; Moura, N.B.; Lautenchleger, F. Strategic positioning of soybean based on the agronomic ideotype and on fixed and mixed multivariate models. Pesq. Agropec. Bras. **2022**, 57, e02702. [CrossRef]
20. Carvalho, I.R.; Szareski, V.J.; Mambrin, R.B.; Ferrari, M.; Pelegrin, A.J.; Rosa, T.C.; Peter, M.; Silveira, D.C.; Conte, G.G.; Barbosa, M.H.; et al. Biometric models and maize genetic breeding: A review. Aust. J. Crop Sci. **2018**, 11, 1796–1805. [CrossRef]

21. Nguyen, T.V.; Vuong, T.D.; Vantoai, T.; Lee, J.D.; Wu, X.; Mian, M.A.R.; Dorrance, A.E.; Shannon, J.G.; Nguyen, H.T. Mapping of quantitative trait loci associated with resistance to Phytophthora sojae and flooding tolerance in soybean. Crop Sci. 2012, 52, 2481–2493. [CrossRef]
22. Pradebon, L.C.; Carvalho, I.R.; Da Silva, J.A.G.; Loro, M.V.; Pettenon, A.L.; Roza, J.P.D.; Da Silva, T.B. Selection based on the phenomenic approach and agronomic ideotic of white oat. Agronomy J. 2024, 116, 1275–1289. [CrossRef]
23. Olivoto, T.; Lúcio, A.D. Metan: An R package for multi-environment trial analysis. Methods Ecol. Evol. 2020, 11, 783–789. [CrossRef]
24. Zhou, J.; Mou, H.; Zhou, J.; Ali, M.L.; Ye, H.; Chen, P.; Nguyen, H.T. Qualification of soybean responses to flooding stress using uav-based imagery and deep learning. Plant Phenomics 2021, 2021, 9892570. [CrossRef] [PubMed]
25. Adegoye, G.A.; Olorunwa, O.J.; Alsajri, F.A.;Walne, C.H.;Wijewandana, C.; Kethireddy, S.R.; Reddy, K.N.; Reddy, K.R.Waterlogging effects on soybean physiology and hyperspectral reflectance during the reproductive stage. Agriculture 2023, 13, 844. [CrossRef]
26. Bernardo, R. Reinventing quantitative genetics for plant breeding: Something old, something new, something borrowed, something BLUE. Heredity 2020, 125, 375–385. [CrossRef]
27. Wang, Y.; Vik, J.O.; Omholt, S.W.; Gjuvsland, A.B. Effect of regulatory architecture on broad versus narrow sense heritability. PLoS Comput. Biol. 2013, 9, e1003053. [CrossRef]
28. Resende,M.D.V.; Duarte, J.B. Precision and quality control in cultivar evaluation experiments. Pesq. Agropec. Trop. 2007, 37, 182–194.
29. Flint-Garcia, S.A.; Thuillet, A.C.; Yu, J.; Pressoir, G.; Romero, S.M.; Mitchell, S.E.; Doebley, J.; Kresovich, S.; Goodman, M.M.; Buckler, E.S. Maize association population: A high-resolution platform for quantitative trait locus dissection. Plant J. 2005, 44, 1054–1064. [CrossRef]
30. Olivoto, T.; Nardino, M.; Carvalho, I.R.; Follman, D.N.; Ferrari, M.; Szareski, V.J.; Pelegrin, A.J.; Souza, V.Q. REML/BLUP and sequential path analysis in estimating genotypic values and interrelationships among simple maize grain yield-related traits. Genet. Mol. Res. 2018, 16, gmr16019525. [CrossRef]
31. Alcântara, J.F.; Santos, R.G.; Baio, F.H.R.; Júnior, C.A.S.; Teodoro, P.E.; Teodoro, L.P.R. High-throughput phenotyping as an auxiliary tool in the selection of corn hybrids for agronomic traits. Rev. Ceres 2023, 70, 106–113. [CrossRef]
32. Oliveira, J.F.; Alcântara, J.F.; Santana, D.C.; Teodoro, L.P.R.; Baio, F.H.R.; Coradi, P.C.; Junior, C.A.d.S.; Teodoro, P.E. Spectral variables as criteria for selection of soybean genotypes at different vegetative stages. Remote Sens. Appl. Soc. Environ. 2023, 32, 101026. [CrossRef]
33. Lozada, D.N.; Godoy, J.V.; Ward, B.P.; Carter, A.H. Genomic prediction and indirect selection for grain yield in us pacific northwestwinter wheat using spectral reflectance indices from high-throughput phenotyping. Int. J. Mol. Sci. 2020, 21, 165. [CrossRef]
34. Resende, M.D.V. Software Selegen-REML/BLUP: A useful tool for plant breeding. Crop Breed. Appl. Biotechnol. 2016, 6, 330–339. [CrossRef]
35. Carvalho, I.R.; Silva, J.A.G.; Ferreira, L.L.; Szareski, V.J.; Demari, G.H.; Lautenchleger, F.; Meneghello, G.E.; Matter, E.M.; Magano, D.A.; De Souza, V.Q. REML/BLUP applied to characterize important agronomic traits in segregating generations of bean (Phaseolus vulgaris L.). Aust. J. Crop Sci. 2020, 14, 391–399. [CrossRef]
36. Kovar, M.; Brestic, M.; Sytar, O.; Barek, V.; Hauptvogel, P.; Zivcak, M. Evaluation of hyperspectral reflectance parameters to assess the leaf water content in soybean. Water 2019, 11, 443. [CrossRef]
37. Yang, F.; Liu, S.;Wang, Q.; Liu, T.; Li, S. Assessing waterlogging stress level of winter wheat from hyperspectral imagery based on harmonic analysis. Remote Sens. 2022, 14, 122. [CrossRef]
38. Ihuoma, S.O.; Madramootoo, C.A. Sensitivity of spectral vegetation indices for monitoring water stress in tomato plants. Comp. Electron. Agric. 2019, 163, 104860. [CrossRef]
39. Yang, F.; Liu, T.; Wang, Q.; Du, M.; Yang, T.; Liu, D.; Li, S.; Liu, S. Rapid determination of leaf water content for monitoring waterlogging in winter wheat based on hyperspectral parameters. J. Integr. Agric. 2021, 20, 2613–2626. [CrossRef]

40. Tavares, C.J.; Junior, W.Q.R.; Ramos, M.L.G.; Pereira, L.F.; Casari, R.A.C.; Pereira, A.F.; de Sousa, C.A.F.; da Silva, A.R.; Neto, S.P.d.S.; Mertz-Henning, L.M. Water stress alters morphophysiological, grain quality and vegetation indices of soybean cultivars. Plants 2022, 11, 559. [CrossRef]
41. Wu, C.; Zeng, A.; Chen, P.; Florez-Palacios, L.; Hummer, W.; Mokua, J.; Klepadlo, M.; Yan, L.; Ma, Q.; Cheng, Y. An effective field screening method for flood tolerance in soybean. Plant Breed. 2017, 136, 710–719. [CrossRef]

4 ARTIGO II

Methodology for selecting stable UAV-based vegetation indices for prediction of agronomic variables in maize using a multi-spectral sensor

*Artigo formatado e submetido conforme as normas da Revista Plants 2026, 15, x, edição especial "Remote Sensing Technologies in Crop Monitoring and Plant Phenotyping".

Methodology for selecting stable UAV-based vegetation indices for prediction of agronomic variables in maize using a multi-spectral sensor

Charleston dos Santos Lima[1]*, Ana Júlia Teixeira Soares[1], Bárbara da Silva Nogueira[1], André Luis Vian[1], Ivan Ricardo Carvalho[2], Christian Bredemeier[1,3].

[1] Department of Crop Science, Federal University of Rio Grande do Sul (UFRGS), Brazil; charlescep009@gmail.com, anajuliatex3@gmail.com, barbaranogueira012@gmail.com, andre.vian@ufrgs.br, bredemeier@ufrgs.br
[2] Department of Genetic Improvement, Universidade Regional do Noroeste do Estado do Rio Grande do Sul, (UNIJUI), Brazil; Ivan.carvalho@unijui.edu.br
[3] EMBRAPII Center for Embedded Devices and Research in Digital Agriculture - Senai-RS, Brazil.
* Correspondence: charlescep009@gmail.com; Tel.: +55 55 99138-8111

4.1 Abstract

The phenotyping of plants based on unmanned aerial vehicles still faces challenges regarding the direct correlation of spectral information with field-collected variables, due to the influence of environmental factors and the significative variation between the phenological stages of the maize crop. Therefore, the objective of this research was: I) to evaluate the interaction of nitrogen doses x scenarios (flights: phenological stage x growing season) and variance components for field variables and vegetation indices, II) to identify the best indices depending on the evaluated scenario, III) to predict field variables based on relevant vegetation indices found through the methodology. The study was conducted using a randomized block experimental design with 4 repetitions, where the treatments consisted of 6 nitrogen (N) side-dress doses (0, 50, 100, 200, 300, and 400 kg ha^{-1}) during the 22/23 and 23/24 season. Field variables evaluations and image acquisition were carried out in 5 distinct phenological stages throughout the maize crop cycle. The data were subjected to deviance analysis and variance components, principal component analysis, and multivariate linear modeling for the prediction of field variables. Our results demonstrated that all indices showed an effect of the interaction doses x scenarios (flights: phenological stages x growing season). Additionally, the indices with the highest reliability were EXGRaw, TGI, GNDVI, NDRE, CIRE, GVI, CVI, BNDVI, PanNDVI, SRNIRRe, SFDVI, RGBindex, NDVI, SAVI, MSAVI, and OSAVI, resulting in a clustering of indices according to the season condition and analyzed phenological stage. Finally, the field variables predicted based on the methodology presented a determination coefficient above 0.80, except for biomass and the weight of one hundred grains. Therefore, it is concluded that vegetation indices are affected according to the tested scenario, however, the methodology based on the deduction of fixed and random effects allows for the prediction of field variables with high accuracy using less complex models.

Keywords: Maize; Plant Phenotyping; Environment; Remote sensing

4.2 Introduction

Plant phenotyping based on spectral information has become one of the most studied areas in recent years, aiming to quickly and non-destructively assess the morpho-physiological condition of vegetation by capturing plant reflectance of plants in the visible and infrared regions of the electromagnetic spectrum [1-3]. In this way, plant phenomics has surpassed classical methods based on visual scoring, sampling, and weighing, which are time-consuming, resource-intensive, and do not meet the need to accelerate the release of new, more productive, and stable maize cultivars to address the global demand for food by 2050, especially in cereal production [4,5]. In this sense, maize

characteristics directly associated with grain yield, such as number of grains per ear, weight of 1000 grains and plant height are very important and notoriously labor-intensive to measure [6].

Using multispectral or hyper-spectral sensors, it has become possible to capture the energy of the electromagnetic spectrum reflected after interacting with the plant surface at wavelengths in the visible (400 to 700 nm) and infrared ranges (750 to 2000 nm). This allows the early detection of physiological changes in vegetation due to nutritional deficiency, water shortage, or genotypic differences via spectral information [7-9]. Additionally, after obtaining the digital number of the image for each wavelength, different vegetation indices can be calculated and correlated with plant growth, leaf area index, and chlorophyll levels with high accuracy (r^2>0.70) [10,11]. In this regard, Zhou et al. [12] reported that spectral bands in the visible and near-infrared regions showed better correlation with plant nitrogen concentration (r^2>0.80), enabling the use of lower-cost multispectral sensors for predicting nutritional status of several grain crops .

Recently, plant phenomics has advanced into high-throughput phenotyping, proposing the use of multispectral sensors embedded in unmanned aerial vehicles (UAVs) to achieve greater spatial, spectral, radiometric and temporal resolution. This enables faster data collection and high image definition due to smaller pixels [13]. Furthermore, research has been conducted to adapt field data collection using UAVs for plant counting, inflorescence detection, delineation of crop growth curves, and genotype tolerance assessment to stresses, allowing rapid evaluations throughout the entire crop cycle [14-16]. However, UAV-based phenotyping can be affected by temperature, light conditions, flight altitude above ground level, crop biomass accumulation, and treatment discrepancies, which may influence the correlation between spectral information and field variables and often reduce the prediction coefficient of determination below 60% [17-20, 8]. The most effective vegetation indices for predicting field variables vary depending on the scenario, including genotypes, phenological stages, and growing season [21].

Temporal analyses of vegetation indices can reveal patterns of plant growth and development, which allows for an understanding of the vegetation's response to environmental changes [22]. In this sense, the methodology of mixed models enables an analysis of fixed and random effects that may influence data collection in experiments with different genotypes and evaluations in different phenological stages and growth seasons (years), based on restricted maximum likelihood (REML) and best linear unbiased predictor (BLUP) [23]. In this way, it becomes possible to isolate effects, to determine the heritability of parameters, and to estimate the coefficient of error for each vegetation index in multiple scenarios [24,25]. Additionally, the interaction between flight moment (phenological stage) and years (growth season) is crucial to assess the reliability of data in characterizing plants and selecting groups of better vegetation indices [21], aiming to utilize stable indices for predicting field variables. Therefore, the objective of the present research was: I) to evaluate the interaction of nitrogen doses and scenarios (phenological stages and growth seasons) and variance components for field variables and vegetation indices, II) to identify the best vegetation indices depending on the evaluated scenario, III) to predict field variables based on relevant vegetation indices selected by the methodology proposed in our study.

4.3 Materials and Methods

4.3.1 Field experiments and experimental design

The study was conducted during the 2022/2023 (S1) and 2023/2024 (S2) growth seasons at the Agricultural Experimental Station of the Federal University of Rio Grande do Sul (UFRGS), located in Eldorado do Sul, Rio Grande do Sul State, southern Brazil (Fig. 1A, B). The climate of the region is classified as Cfa (humid subtropical), with an average temperature of 25 °C during the summer and regular rainfall occurrences (Fig. 2) [26-27].

The experimental design of randomized blocks was used with four repetitions, with treatments consisting of six nitrogen (N) top dressing doses (0, 50, 100, 200, 300, and 400 kg ha^{-1}) applied at the phenological stage of four fully developed leaves (V4) (Fig. 1C, Fig. 3).

In both years, previous crop was oat (*Avena sativa*), which was terminated at flowering phenological stage by applying Glyphosate (3 L ha^{-1}) and Atrazine (4 L ha^{-1}). Subsequently, the

hybrid maize P3016 VYHR was sown in no-tillage system at a density of 8 plants per m² in the second half of October in both years. The experimental plots consisted of five rows, each five meters long, with a row spacing of 0.50 m. At sowing, 20 kg ha^{-1} of N, 120 kg ha^{-1} of P_2O_5, and 60 kg ha^{-1} of K_2O were applied via the sowing furrow. Other agronomic practices were carried out according to the technical recommendations for maize cultivation.

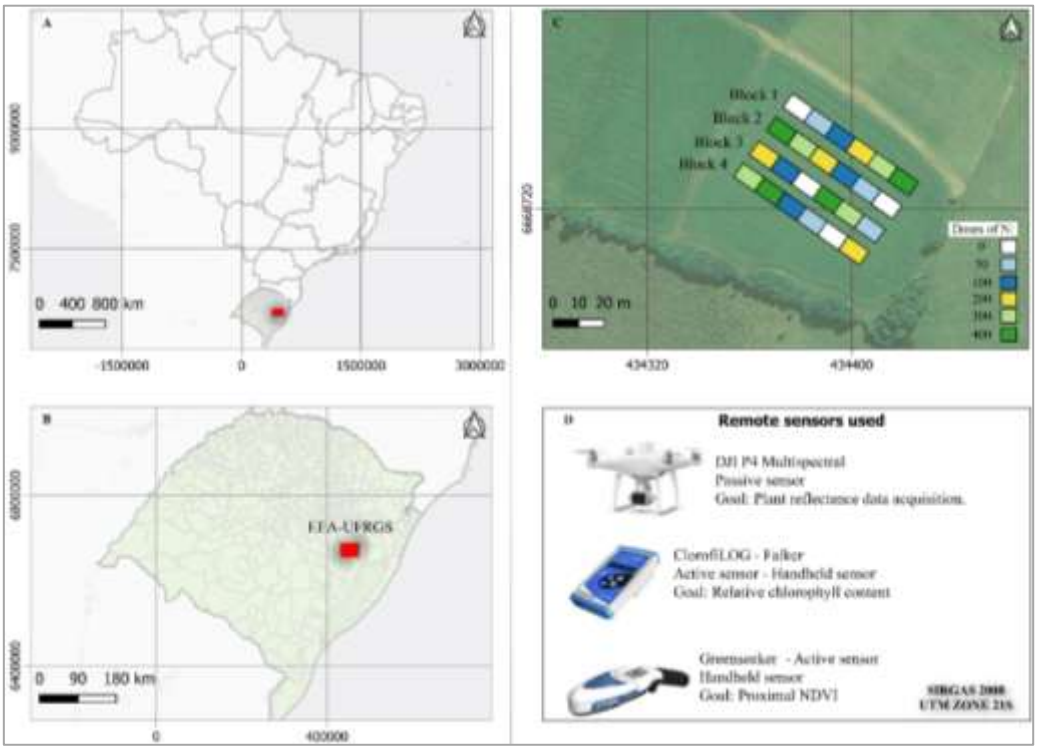


Figure 1. Localization of the experimental area (A and B), experimental design (C) and remote sensing platforms used (D).

4.3.2 Field variables evaluated

Field evaluations were conducted at phenological stages V8 (eight fully developed leaves), V11, V18, R2 (onset of grain filling), and R5 (full dent stage) during the 2022/2023 season and at growth stages V6, V8, V13, R2, and R5 during the 2023/2024 season. In each evaluation, the height of 10 plants from each plot was measured directly from the ground surface to the last expanded leaf using a graduated ruler, with values expressed in meters per plant. Simultaneously, three plants from each plot were cut, dried in a forced air oven at 60°C for later determination of plant shoot biomass, with values expressed in kilograms of dry matter per hectare. After weighting the plants, the material was ground and the percentage of nitrogen in the tissue (PNC) was determined by Kjeldahl method.

Portable proximal sensors were also used. The relative chlorophyll content (RCC) was measured at each phenological stage using a portable chlorophyll meter (Figure 1D). Measurements were taken on 10 plants per plot at the last fully developed leaf during the vegetative stage (season 22/23: V8, V12, V18; season 23/24: V6, V8, V13), and on the ear leaf during the reproductive stages (R2 and R5) in both seasons [28]. Additionally, proximal NDVI readings were conducted using the hand-held Greenseeker sensor (Trimble), equipped with an active light source that emits radiation in the red wavelength (660 nm) and near-infrared (790 nm) and calculates the reflected radiation in these regions (Figure 1D). Furthermore, at the R6 phenological stage (maturity), plants were harvested and the number of grains per ear (NGE), weight of one hundred grains (W100G), and grain yield were determined. Yield was converted to kilograms per hectare, and the grain moisture was standardized at 13%.

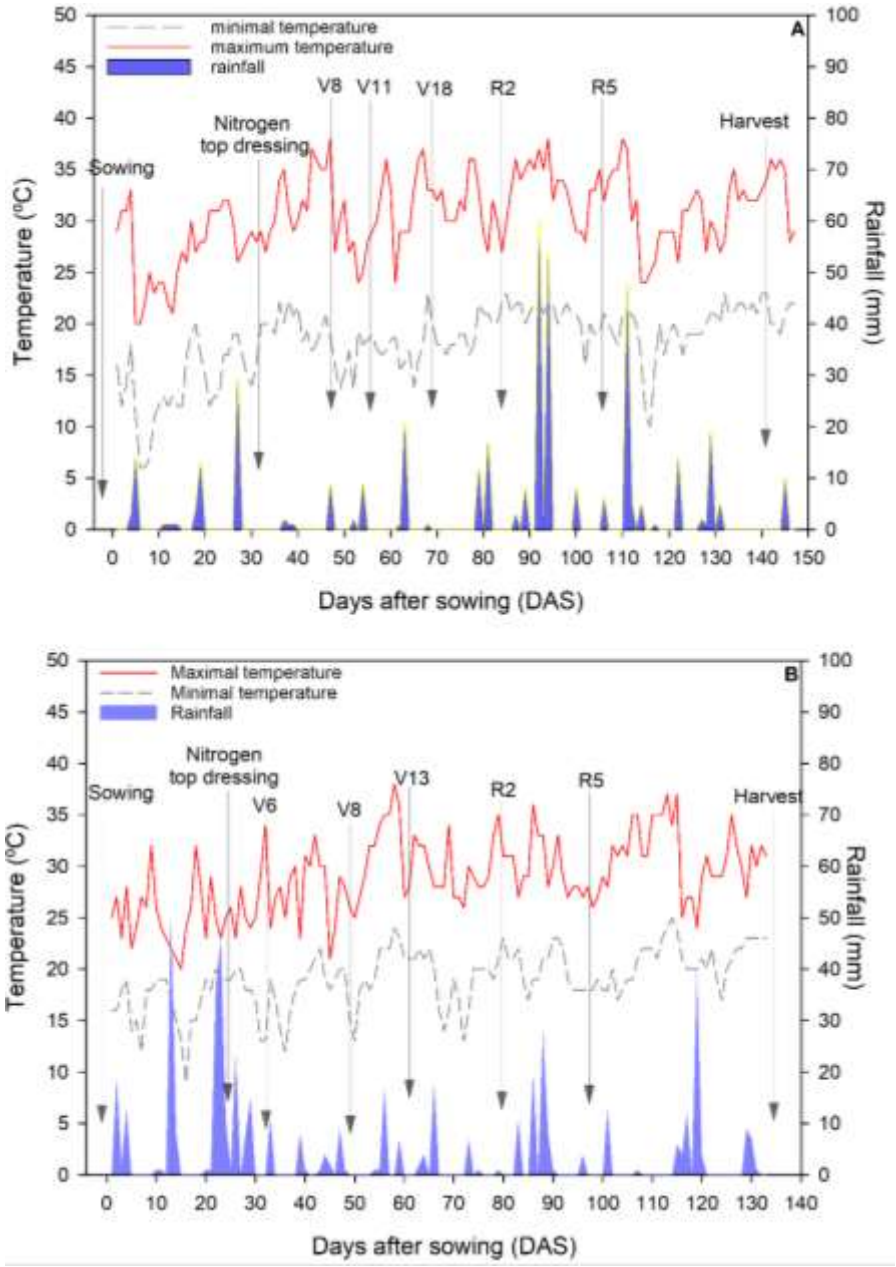


Figure 2. Temperature and precipitation data during the 2022/23 (A) and 2023/24 (B) growth seasons.

4.3.3 UAV-based image acquisition and vegetation indices

The collection of images for spectral evaluation of the plots subjected to different N doses was carried out on the same day as the assessment of field variables, with the assistance of a DJI Phantom 4 Multispectral RTK drone (Fig. 1D), using a flight plan and autonomous control via the Mobile app GS pro (Figure 3). The multispectral sensor allowed for the acquisition of plant reflectance at the wavelengths of red (R: 660 nm ± 16 nm), green (G: 550 nm ± 16 nm), blue (B: 450 nm ± 16 nm), Red-Edge (RE: 730 nm ± 16 nm), and near infrared (NIR: 840 nm ± 26 nm) (Fig. 3). The general flight configurations consisted of 75% frontal and lateral overlap, a flight height of 30 meters above ground level and a camera angle of 90º (Nadir). The time for image collection was the same for all flights, which were executed between 11:00 AM and 2:00 PM. Additionally, a irradiance sensor (sunshine sensor) was used, embedded at the upper surface of the drone, for radiometric correction of the images. This configuration resulted in a resolution of 5 cm per pixel.

The image processing was performed using Agisoft Metashape software to construct the orthomosaics. These orthomosaics were associated with information from seven georeferenced ground control points using GNSS-RTK for geometric correction of the photos. Subsequently, spectral information was extracted from the orthomosaics using QGIS software, utilizing the raster

calculator plugin to separate the wavelengths present in each image. Based on this, three central lines, each 4 meters long, were delineated for each plot by adding a shapefile vector layer to extract digital numbers at the wavelengths in red, green, blue, red-edge, and infrared regions. Finally, different vegetation indices were calculated using the visible and near-infrared bands (Fig. 3, Table 1).

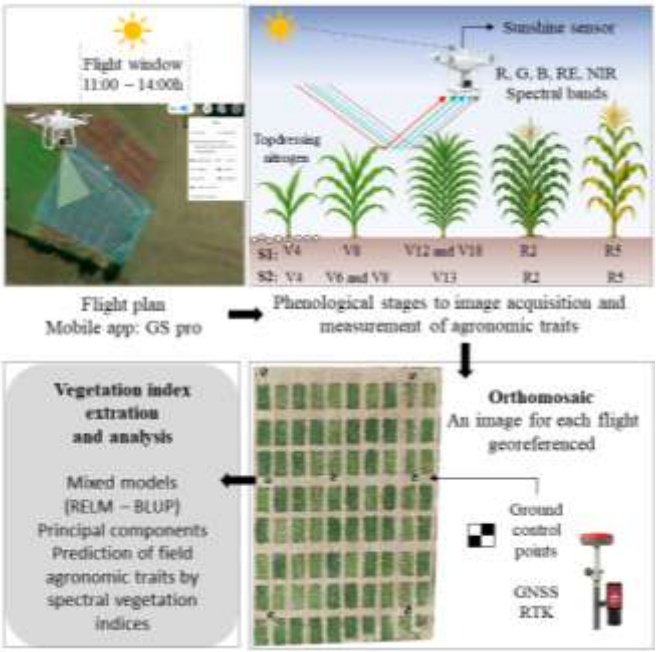


Figure 3. Workflow for data acquisition and analysis during the growing season maize 2022/2023 (S1) and 2023/2024 (S2) in different phenological stages.

Table 1. List of spectral vegetation indices calculated in out study.

Type	Vegetation indices	Equation
RGB	Excess of green (EXG)	2*(G(R+G+B))-(R/(R+G+B))-B/(R+G+B))
	Excess of green raw (EXGRaw)	2*G-R-B
	Excess of red (EXR)	(1.4*R-G)/(R+G+B)
	Excess of red raw (ExRRaw)	1.4*R-G
	Vegetation extraction color index (CIVE)	(0.44*R-0.81*G+0.39*B)/(R+G+B)+ 18.79
	Normalized green-red index (GRVI)	(G – R) / (G + R)
	Modified excess of red (ExRM)	(2*R-G-B) / (R+G+B)
	Vegetative index (VEG)	g/((r^a)*(b^(1-a))) a=0.667, r=R/(R+G+B), g=G/(G+R+B), b=B/(R+G+B)
	Excess of blue (ExB)	(1.4*B-G)/(R+G+B)
	Normalized difference of blue (NDB)	(G-B)/(G+B)
	Atmospheric resistant index in the visible (VARI)	(G–R)/(G+R+B)
	Green leaf index GLI	((G-R)+(G-B))/(2*G+R+B)
	Triangular green index (TGI)	(-0.5)*[(190)*(R-G)-(120)*(R-B)]/(R+G+B)
	Red-Blue index (RBI)	(R-B)/(R+B)
	Modified green-red index (MGRVI)	$(G^2–R^2)/(G^2+R^2)$
	RGB index RGBindex	$(G^2-B*R)/ (G^2+B*R)$
MULTI	- Normalized Difference (NDVI)	(NIR - R) / (NIR + R)

- Red Edge (NDRE)	(NIR – RE) / (NIR + RE)
- Soil Adjusted Index (SAVI)	(1 + 0.5) * [(NIR – R)/(NIR + R + 0.5)]
- Modified Soil Adjusted Index (MSAVI)	(2*NIR+1−sqrt((2*NIR+1)*2−8* (NIR−R)))/2
- Optimized Soil Adjusted Index (OSAVI)	(1+0.5)*((NIR-R)/(NIR+R+0.5))
- Enhanced Vegetation Index (EVI)	2.5*(NIR-R)/(NIR+6*R -7.5*B+1)
- Normalized Difference of Green (GNDVI)	((NIR-G)/(NIR+G))
- Green Chlorophyll Index (CIG)	NIR/G-1
- Rededge Chlorophyll Index (CIRE)	NIR/RE-1
- Simple Ratio Index (RVI)	NIR/R
- Vegetation Difference Index (DVI)	NIR-R
- Green Vegetation Difference Index (GDVI)	NIR-G
- Green Ratio Vegetation Index (GVI)	NIR/G
- Vegetation-Chlorophyll Index (CVI)	$NIR*(R/G^2)$
- Enhanced Vegetation Index 2 (EVI2)	2.5*(NIR-R)/(NIR+2.4*R+1)
- Normalized Difference of Blue (BNDVI)	(NIR-B)/(NIR+B)
- Normalized Difference R-Re (NDVIRE)	(RE-R)/(RE+R)
- PanNDVI (PanNDVI)	NIR-(G+R+B)/ NIR+(G+R+B)
- Simple Ratio NIR/RE (SRNIRRe)	NIR/RE
- Spectral Feature Depth (SFDVI)	((NIR+G)/2)-((R+NIR)/2)

4.3.4 Statistical analysis

To verify the effect of N doses, scenarios (phenological stages and growing seasons), and the interaction among them, the restricted maximum likelihood test (RELM) was applied to obtain the analysis of variance components and estimated values for each field variable. In this sense, the significance of the interaction between the factors was evaluated through deviance analysis ($p<0.05$) (RLT test), and subsequently, the variance components were assessed: phenotypic variance, heritability (H2), accuracy, and the coefficient of variation of the error (CVr). This procedure is based on the statistical model: $Yij = \mu + Bj + Gi + Ej + \varepsilon ij$, where: Yij is the measured value for each variable in each plot, Bj is the block effect (fixed), Gj indicates the effect attributed to the fixed effects (Nitrogen doses), Ej represents the environmental effect or evaluated scenarios (phenological stages x growing season), and εij is the effect associated with experimental error.

Starting from the separation and quantification of associated effects, new values were estimated using the best linear unbiased predictor (BLUP). Thus, a new mean was obtained for each analyzed variable, without the influence of environmental factors (scenarios). Additionally, after determining which vegetation indices showed better quality higher H^2 and lower CVr, a principal component analysis was conducted with the BLUP values for each index. The indices grouped for each scenario were considered in the discussion of the results.

After identifying the indices with better reliability and stability for predicting field variables of mayze, a multivariate analysis was performed to assess the prediction of these variables: NDVI Greenseeker, RCC, shoot biomass, grain yield, NGE, W100G and plant nitrogen content (PNC) based on the selected vegetation indices via stepwise regression, ensuring that only the significant indices were retained in the model. All statistical analyses were conducted using R Studio with the EstimateBreed package [29].

4.4 Results

4.4.1 Deviance and variance components analysis

The different vegetation indices and field variables were subjected to deviance analysis to evaluate the statistical influence of the factors: nitrogen doses and scenarios (phenological stage and growing season), on the response of all variables analyzed in this study (Table 2). The deviance analysis via the RTL test demonstrated a significant effect for the interaction Doses x Scenarios for all indices ($p<0.05$), without distinction between RGB and multispectral indices (Table 2). This result was also observed for the field variables, except for the weight of a hundred grains (W100G), which showed a significant effect only for the applied nitrogen dose, without influence from the scenarios (phenological stage and growing season), indicating the stability of the variable even under contrasting environmental conditions.

Table 2. Deviance analysis by maximum likelihood test (RLT) $p<0.05$.

Model	**EXG**	**EXGRaw**	**EXR**	**EXRRaw**	**CIVE**	**GRVI**	**EXRM**
Doses of N	5.24E-07	2.21E-09	0.00253	0.00057	2.46E-09	0.00389	0.24621
Doses*Scenarios	9.09E-05	1.72E-19	2.9E-11	1.62E-16	5.50E-19	1.31E-14	2.54E-21
Model	**VEG**	**EXB**	**NDB**	**VARI**	**GLI**	**TGI**	**RBI**
Doses of N	5.36E-06	0.00262	0.01216	0.00969	0.06862	2.43E-09	1,00000
Doses*Scenarios	4.60E-12	6.69E-19	2.9E-28	3.62E-24	5.35E-16	9.89E-21	1.73E-48
Model	**MGRVI**	**RGBindex**	**NDVI**	**SAVI**	**MSAVI**	**OSAVI**	**EVI**
Dose of N	0.00514	4.18E-08	2.3E-07	2.19E-07	9.61E-07	2.32E-07	0.56113
Doses*Scenarios	4.27E-08	1.71E-05	2.9E-10	2.83E-10	2.01E-08	2.96E-10	3.49E-07
Model	**GNDVI**	**CIG**	**NDRE**	**CIRE**	**RVI**	**DVI**	**GDVI**
Dose of N	2.35E-14	3.03E-12	1.6E-13	8.02E-12	1.20E-10	9.48E-12	6.69E-14
Doses*Scenarios	4.86E-06	3.88E-10	1.5E-27	5.06E-31	5.99E-06	3.65E-03	4.34E-02
Model	**GVI**	**CVI**	**EVI2**	**BNDVI**	**NDVIRe**	**PanNDVI**	**SRNIRRe**
Dose of N	3.03E-12	1.76E-12	5.8E-08	2.62E-11	8.48E-02	1.58E-13	1.58E-12
Doses*Scenarios	3.88E-10	6.33E-14	9.4E-11	1.11E-05	8.08E-06	2.85E-05	2.50E-19
Model	**SFDVI**	**NDVIG**	**RCC**	**Plant Height**	**Biomass**	**NGE**	**W100G**
Dose of N	3.15E-14	5.7E-08	1.3E-09	9.4E-11	2.41E- 6	0.11902	0.04193
Doses*Scenarios	2.43E-03	4.3E-07	1.7E-22	3.8E-27	5.22E-29	1.5E-08	0.24488
Model	**Grain Yield**	**Plant Nitrogen Content**					
Doses of N	0.13656	1.59E-12					
Doses*Scenarios	1.9E-08	6.50e-13					

*Doses x Scenarios (interaction between phenological stage of flight and season growing (season 2022/2023 and season 2023/2024)). NDVIG: NDVI greenseeker, CHLT: Total chlorophylls, Biomass: Biomass per hectare, NGE: number of grains per ear, W100G: weight of one hundred grains, Plant nitrogen content: % of nitrogen in plant.

The vegetation indices that showed adequate data quality were evaluated for heritability (H2) and residual coefficient of variation (CVr) (Table 3). It was found that the vegetation indices EXGRaw, TGI, GNDVI, NDRE, CIRE, GVI, CVI, BNDVI, PanNDVI, SRNIRRe, and SFDVI presented high heritability (>50%) and an intermediate residual coefficient of variation (≤10%). On the other hand, the indices RGBindex, NDVI, SAVI, MSAVI, and OSAVI demonstrated lower heritability values (<40%), however, the residual coefficient of variation remained below 5%. Therefore, these indices have a high potential for use in predicting field variables due of maize to the greater stability of the data under different scenarios. Additionally, the indices EXRRaw, RBI, and EVI were discarded due to low data quality due to H_2 <10% and CVr >50%. These indices were not considered in subsequent analyses.

It was observed that RCC, plant height, and plant nitrogen concentration presented high heritability values and low residual coefficient, 60% and 5%, respectively (Table 3). Additionally, NDVI Greenseeker, NGE, W100G and grain yield maintained intermediate heritability values (40 to 50%), with a greater contribution from the error variation coefficient compared to the previous variables. On the other hand, plant biomass showed low heritability (43%) and high contribution

from the residual factor (18%), due to the variation of the scenarios tested in the experiment. Furthermore, the accuracy of all analyzed variables remained above 70% (Table 3). However, it is noted that the indices with higher heritability and lower residual variation coefficient demonstrated accuracy above 95%. This suggests that the experimental control was adequate, with a minor contribution of experimental error to the dataset.

Table 3. Estimates of variance components by restricted maximum likelihood (REML) for the vegetation indices and field variables analyzed in different phenological stages and two growing seasons in maize.

Variables	Phenotypic variance	Heritability	Accuracy	CVr
EXG	0.002160972	0.298322576	0.9565	7.72687
EXGRaw	34022.94092	0.502042235	0.9707	10.4995
EXR	0.001367014	0.173048153	0.89522	24.022
CIVE	5511.530079	0.498192153	0.9705	11.5138
GRVI	0.001771366	0.174529284	0.8885	9.49921
EXRM	0.002733207	0.060379092	0.70918	16.0389
VEG	0.02571401	0.31587324	0.94709	5.1861
EXB	0.000701777	0.197243604	0.89478	12.7299
NDB	0.000946425	0.170802888	0.86545	5.14314
VARI	0.005576628	0.171254055	0.87066	9.03051
GLI	0.000652438	0.097034947	0.80576	2.64288
TGI	8538.502439	0.505190614	0.97052	10.0706
MGRVI	0.003257385	0.142385462	0.88354	8.40255
RGBindex	0.001616469	0.35254211	0.9641	5.14621
NDVI	0.002306615	0.420698934	0.96702	3.86299
SAVI	0.004774655	0.367891171	0.95936	3.87187
MSAVI	0.001138486	0.325164107	0.95431	2.67695
OSAVI	0.002306721	0.420699554	0.96702	3.86297
GNDVI	0.005282602	0.690480478	0.99009	5.2412
CIG	1.464103084	0.660117711	0.98657	13.223
NDRE	0.003147606	0.668118211	0.9834	7.02357
CIRE	0.054607787	0.623926922	0.97931	10.1084
RVI	3.132649066	0.456132875	0.97568	11.9591
DVI	279301.621	0.448005783	0.97911	9.33951
GDVI	400991.2332	0.599258444	0.98944	10.0743
GVI	1.464103083	0.660117711	0.98657	10.5603
CVI	0.53109168	0.690550917	0.98703	10.8016
EVI2	0.017953289	0.396504174	0.96324	5.01772
BNDVI	0.001351255	0.581385526	0.98453	2.43715
NDVIRe	0.001910347	0.087256701	0.82652	5.34105
PanNDVI	0.009213034	0.654627705	0.98886	12.2851
SRNIRRe	0.065328767	0.713469828	0.98712	4.52934
SFDVI	56236.84554	0.644381308	0.98991	9.72557
NDVIG	0.002567746	0.455806328	0.97299	4.62018
RCC	55.0014609	0.620730963	0.9797	5.87724
Plant height	361.608103	0.625459854	0.9796	4.24519
Shoot biomass	1045457500	0.435000000	0.9530	18.0000
Number of grains ear^{-1}	10553.18567	0.588555621	0.9733	8.31013
Weight 100 grains	16.06307227	0.551315445	0.9852	8.26493

Grain yield	10186376.14	0.565259238	0.9708	11.42764
Plant nitrogen content	0.3180	0.6910	0.9870	12.00

σ^2 P: Phenotypic variance, H2: Heritability, GEIr2: Genotype x environment interaction, Ac: Accuracy, CVr: coefficient of variation of the residual.

After obtaining the BLUP values for each vegetation index (Supplement 1), a principal component analysis (PCA) was conducted with these values, which allowed for the identification of clusters associated with different nitrogen doses, phenological stages and growing seasons. Thus, 88.3% of the variance was explained by the two-plotted principal components (Fig. 4). It was found that the best indices for characterizing the initial stages of corn (V5 and V8) in the 2022/2023 crop season were the CIVE and EXB indices, even under conditions of lower biomass and vegetation cover, which may facilitate modeling due to the smaller number of indices in the model. Additionally, it was evidenced that the GRVI, MGRVI, VARI, GLI, DVI, MSAVI, SAVI, NDRE, NDVI, OSAVI, CIRE, EVI 2, and RVI indices exhibited a consistent relationship with advanced phenological stages (V12, V18, R2, and R5), regardless of the nitrogen dose applied (Fig. 4).

Similar to the behavior observed previously, there was a distinction in indices regarding the phenological stage in the second growing season. Thus, the indices grouped in 2023/2024 were entirely different from those in 2022/23. In this sense, the PCA analysis showed that the indices EXRM and EXR demonstrated a behavior similar to the variance observed only at the V6 growth stage. On the other hand, NDB, TGI, EXGRaw, RGBindex, EXG, and VEG were grouped at the phenological stages V8, V13, R2, and R5, regardless of the nitrogen dose applied (Fig. 4). Therefore, it is evident that the specificity of the spectral parameters varies with phenological stage and growing season, which may increase the complexity of the generic use of phenotypic indices.

Field variables subjected to BLUP analysis showed that biometric parameters also exhibited differences for nitrogen doses and evaluated scenarios (Supplementary 1). From the V12-V13 stage onwards, treatments which received higher N doses (200, 300, and 400 kg ha-1) showed greater plant height, shoot biomass, relative chlorophyll content, and plant nitrogen concentration. This response was also observed for the yield components, achieving 475 grains per ear in 2022/23 and 392 grains per ear in 2023/24 with doses of 300 and 200 kg ha-1, respectively. Additionally, the higher grain yield was also observed in these N doses, with 13,700 kg ha-1 and 8,540 kg ha-1, respectively (Fig. 5). Such results support the higher heritability and lower residual coefficient observed in the variance component analysis for these parameters (Table 3), which was not clearly observed for NDVI Greenseeker and shoot biomass (Supplementary material 1). Due to the specific moment of sampling (phenological stage) or growing season variation, data showed CVr >10% or low H_2 and had less characterization of the tested scenarios. The weight of a hundred grains was not affected by the interaction of phenological stage and season growing with variations only associated with the nitrogen dose, achieving greater grain weight when plants received 400 kg N ha-1 (Supplementary 1).

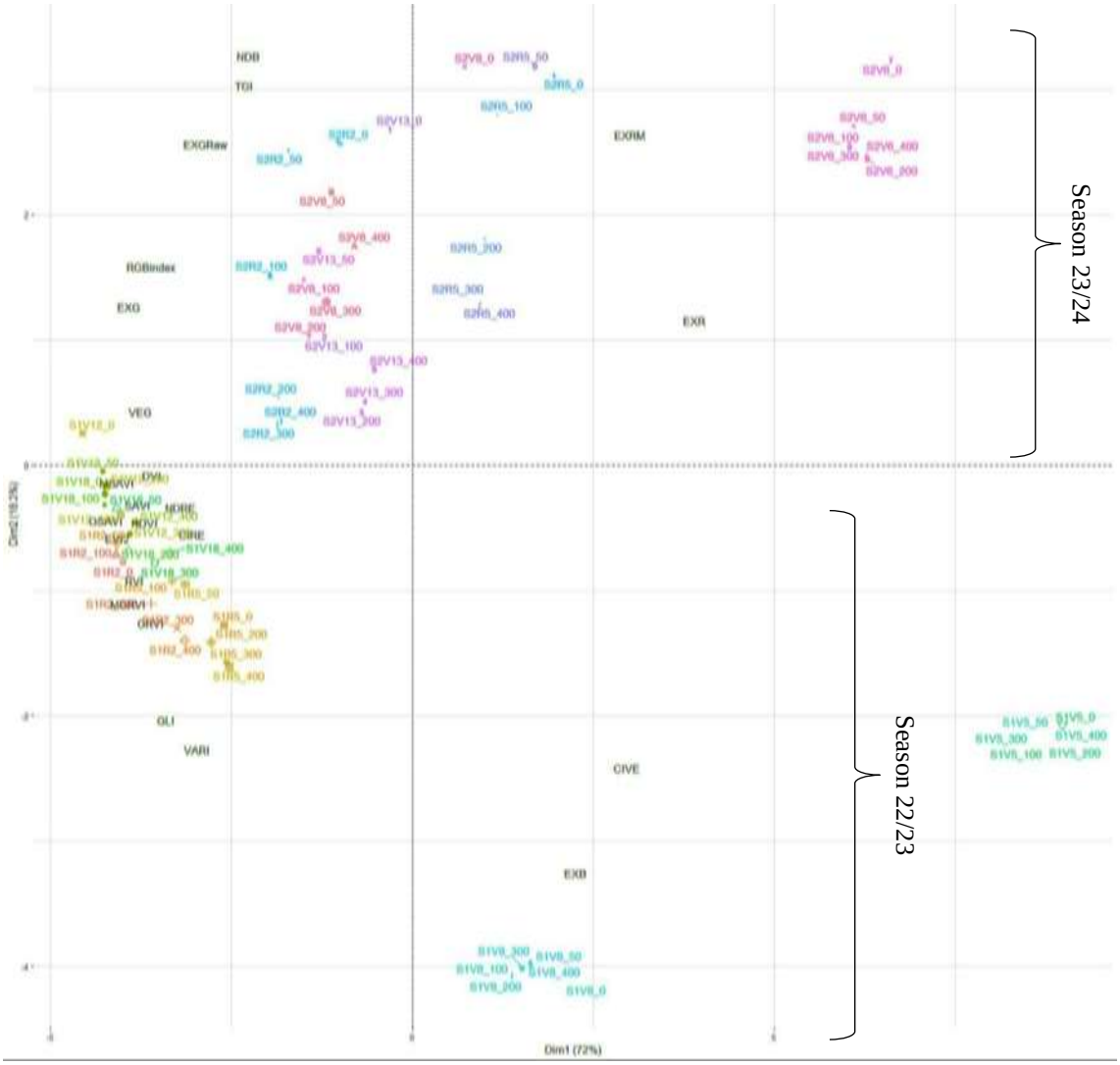


Figure 4. Principal components analysis of the BLUP values for each vegetation indices.

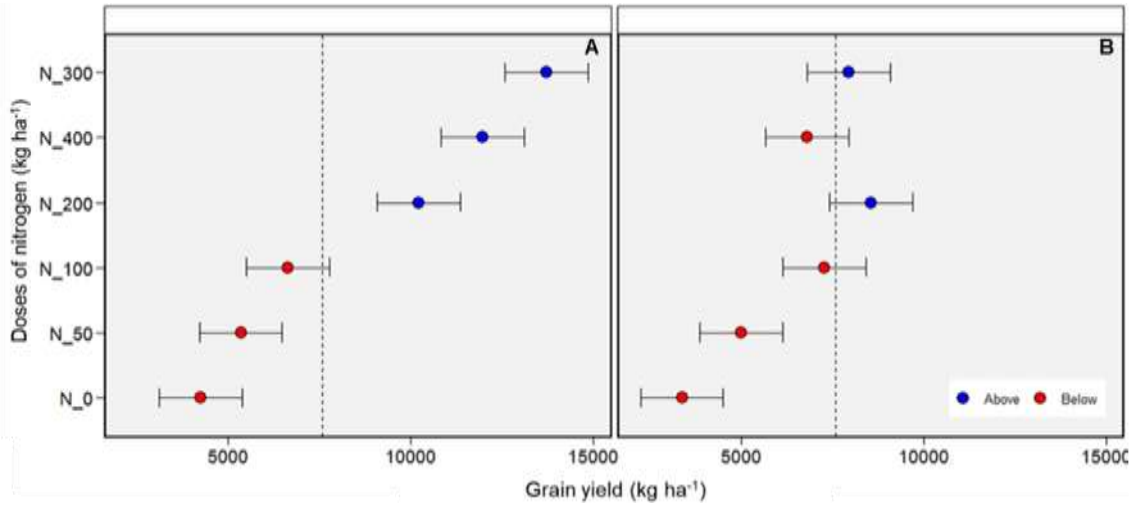


Figure 5. BLUP of maize yield data subjected to nitrogen doses and different phenological stages in the season growing 2022/2023 (A) and 2023/2024 (B).

Based on the observed response for the different vegetation indices and field variables, an effort was made to establish a prediction model for field variables based on relevant spectral information through stepwise regression, presenting the intercept of the multivariate linear model and the

angular coefficient of each index (Table 4). It was found that the methodology adopted in this study allowed for prediction with high accuracy for most field variables ($R^2 > 0.80$), except for shoot biomass and W100G, which showed lower coefficients of determination of 0.71 and 0.65, respectively. Additionally, it was noted that variables NDVI Greenseeker, relative chlorophyll content, plant height, biomass, plant nitrogen concentration, and number grains ear^{-1} required an average of 15 vegetation indices within the prediction model (Table 4 and Fig. 6). On the other hand, W100G and grain yield required up to 10 predictors, highlighting the inherent complexity of each field variable and the need to find relevant spectral vegetation indices even under different scenarios.

Starting from the summarization of the different indices used (Fig. 6), it was identified that the indices CIG, GLI, NDB, and RGBindex can predict 6 of the 8 field variables studied. Additionally, the indices BNDVI, CVI, EVI2, EXR, EXRM, MGRVI, NDVIRe, PanNDVI, RBI, RVI, and VEG are necessary to predict up to 5 field variables. However, CIRE, CIVE, DVI, EVI, EXB, EXRRaw, GNDVI, GVI, NDRE, NDVI, OSAVI, RVI, SAVI, SFDVI, SRNIRRe, TGI, and VARI can be used to predict 3 or fewer field variables. Thus, this demonstrates the existence of more generalist indices and others with a higher level of specificity depending on the field variable considered.

Table 4. Multivariate models for each field variable from vegetation indices in maize.

Predicted variable	Selected vegetation indices	R^2 adjusted	p<0,05
NDVI Greenseeker *****(Intercepto:6,38)	******(0,003) EXRRaw, (-0,03) CIVE, (-3,0) VEG, (17,36) EXB, (59,65) NDB, (-0,02) TGI, (-19,69) RBI, (3,94) MGRVI, (-24,47) RGBindex, (3730) NDVI, (-2481) SAVI, (-11,65) GNDVI, (0,0003) DVI, (-2,83) EVI2, (-3,30) NDVIRe, (9,73) PanNDVI, (-0,001) SFDVI	0,93	2e-16
Relative chlorophyll content (Intercepto:1450)	(5757) EXR, (-0,07) EXRRaw, (0,04) CIVE, (-4421) EXRM, (4529) NDB, (-4299) GLI, (-1189) RBI, (1473) MGRVI, (-1987) RGBindex, (-15,71) CIRE, (2,20) GVI, (84,64) EVI2, (-194) NDVIRe	0,86	2e-16
Plant height (Intercepto: -60910)	(117800) EXR, (1,68) CIVE, (74660) GRVI, (37530) NDB, (-6745) VARI, (92030) GLI, (0,97) TGI, (-26700) RGBindex, (-268,60) CIG, (2008) NDRE, (70,05) RVI, (191,60) CVI, (-3249) BNDVI, (2095) NDVIRe	0,89	2e-16
Shoot biomass (Intercepto: -28000000)	(25860000) EXR, (21930000) GRVI, (21510000) EXRM, (-503500) VEG, (19100000) NDB, (50270000) GLI, (-6657000) RBI, (1308000) MGRVI, (-15950000) RGBindex, (204500000) NDVI, (-136300000) SAVI, (-1122) EVI, (-2947) CIG, (44410) NDRE, (-285500) BNDVI, (158100) PanNDVI	0,71	2e-16
Plant nitrogen concentration (Intercepto:1667)	(-2975) EXR, (-1502) GRVI, (40,29) VEG, (-1683) NDB, (76,47) VARI, (-2635) GLI, (0,005) TGI, (344,10) RBI, (959) RGBindex, (28,50) OSAVI, (0,43) CIG, (-1,41) CIRE, (-17,94) EVI2, (24,63) BNDVI	0,87	2e-16
Number grains ear^{-1} (Intercepto:95389)	(-300483) EXR, (231189) EXB, (-118205) MGRVI, (50691) RGBindex, (65919) SAVI, (6727) CIG, (-2683) CIRE, (-2773) RVI, (-4105) CVI, (-101759) EVI2, (-47033) BNDVI, (-17368) NDVIRe, (142005) PanNDVI, (125000) NDB	0,80	4e-10
Weight 100 grains (Intercepto: -7230)	(6518) EXRM, (-280) VARI, (13488) GLI, (-1478) RGBindex, (-118) CIG, (50) RVI, (84) CVI, (609) EVI2, (168) NDVIRe, (-1238) PanNDVI	0,65	1e-07
Grain yield (Intercepto: -4217772)	(4862062) EXRM, (320572) VEG, (-1559654) NDB, (8022900) GLI, (22051) GNDVI, (14563) CIG, (307968) NDRE, (-26282) CVI, (-70675) SRNIRRe	0,85	1e-14

* Value of intercept of the equation for each model, ** Angular coefficient for each vegetation index within the model.

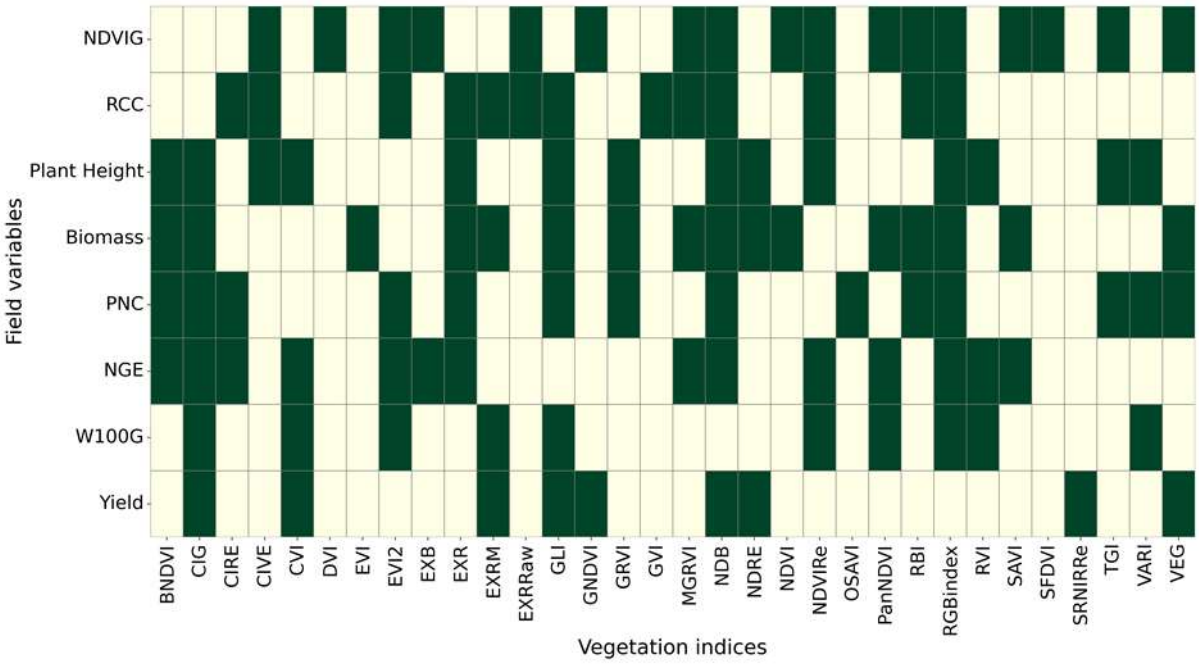


Figure 6. Map with the frequency and number of predictor indices for each field variable in maize. *Yellow and green rectangles represent the absence or presence of the vegetation index in the prediction model for each field variable, respectively.

4.5 Discussion

The modulation of maize response to nitrogen fertilization is linked to the influence of environmental factors such as the phenological stage at which the application occurred, climatic conditions during the growing season, genotype, and the type of fertilizer applied [30,31]. Among these factors, the variation between years (growing season) can affect up to 50% of the response of the evaluated parameters in the field, due to changes in rainfall availability and temperature range [32]. This result was also observed in the present study, as a variation between seasons was noted in plant height, biomass, and productivity from 10 up to 30% (Supplementary 1, Fig. 5). Such effects also altered the magnitude and behavior of vegetation indices, reinforcing the need to use big spectral dataset with more temporal and spatial information to identify indices that are less susceptible to environmental variations [33].

The deviance analysis demonstrated that all vegetation indices can be affected by the interaction between N doses and scenarios (phenological stage and growing season) (Table 2). In this sense, [21] found that the variation in vegetation indices collected on different flight dates can be explained by the physiological and morphological modifications that plants express throughout their development. This is related to changes in leaf structure, chemical composition, and interaction with the environment, which tend to alter how plants reflect light and consequently, the dynamics of the vegetation indices [16]. On the other hand, the weight of 100 grains was not influenced by the interaction nitrogen doses x scenarios, which can be explained by the greater genetic contribution, lesser environmental effect, and interaction between management and environment in the expression of this yield component, ensuring greater stability of the variable independent of the scenario and reliability in productivity prediction [34-36]. Additionally, the data collection for the W100G occurred only after harvest, which reduces the contribution of phenological stages to the variance of this field variable.

The restricted maximum likelihood analysis (RELM) is a method for estimating the variance components and heritability parameters of a dataset, which allows for the identification of significant variables with high heritability, lower influence of experimental error, and reliability in prediction models [23,24].

Heritability of a variable can be defined by its ability to be transferred among plants or quantified independently of the environmental conditions of the experiment, yielding relevant

variables when they present H^2>50% and low experimental error (CVr<10%) [37,38]. Thus, it was found that the indices EXGRaw, TGI, GNDVI, NDRE, CIRE, GVI, CVI, BNDVI, PanNDVI, SRNIRRe, and SFDVI exhibited high heritability (>50%) and an intermediate coefficient of residual variation (≤10%). These data corroborate the results obtained by Lima et al. [39], from the evaluation of the variance components of 40 vegetation indices in soybean cultivars subjected to flooding evaluated with data from UAV-based RGB and multispectral sensors, which identified H^2>60% and low CVe for the indices EXGRaw, GNDVI, NDRE, CIRE, BNDVI, and SFDVI. Additionally, [33] emphasized that most vegetation indices are influenced by the flight moment and experimental condition, obtaining greater contributions from scenarios and lower heritability for the indices EXG, GLI, MGRVI, RGBindex, and VARI. Like the results obtained in the present study (Table 3), these indices were still considered important within phenotyping due to the low coefficient of experimental error. These data corroborate Pradebon et al. [40], which identified that the indices EXG, GLI, and VARI were important for the characterization of ideotypes of white oats based on a spectral approach for resistance to lodging, suggesting the specificity of vegetation index concerning the type of plant and experimental condition. This may be associated with the predominant wavelength type at the time of flight, as the availability of radiation, temperature, and flight time can affect the index's ability to adequately distinguish differences among treatments [8]. Therefore, in the present study, the methodology of flights close to noon and preferably in sunny day conditions was adopted, due to the influence of lighting variation on vegetation indices, which can significantly increase the standard deviation and absolute error in predictions based on spectral information [19].

The PCA analysis with the BLUP values demonstrated a clustering of vegetation indices depending on the flight timing and growing season (Fig. 4). This environmental effect on the expression of the indices corroborates results obtained by Shrestha et al. [18], who found that during three years of study in maize, the best index was dependent on the phenological stage and climatic conditions of the season, with no stable index to accurately predict grain productivity independent of the evaluated scenario. Additionally, in both seasons in our study, the highest number of indices with similar behavior was identified at late phenological stages (V12, V18, R2) (Fig. 4). Such dynamics are expected due to the low differences between plants in shoot biomass and cover soil in the initial stages and the reduced influence of the soil background in the imagery starting from V12. Yang et al. [3] studied the efficiency of predicting maize productivity throughout the crop cycle based on spectral data collected with UAV, with flights conducted from V2 (two fully developed leaves) up to physiological maturity (R6). These authors identified that productivity prediction exhibited higher accuracy (r^2>0.80) starting from the growth stage V14 (fourteen fully developed leaves), achieving greater accuracy in the results when data from the phenological stages of tasseling, full flowering, milky grain, and farinaceous grain were grouped (r^2>0.93).

The analyzed scenarios also influenced the type of grouped indices. It was found that scenarios with lower plant biomass, plant height, relative chlorophyll content, number of grains per ear, and grain yeld (Supplement 1 and Fig. 5) were grouped with indices solely from the visible spectrum (CIVE, EXB, EXRM, EXR, NDB, TGI, EXGRaw, RGBindex, EXG, VEG). This was especially evident in season 2023/24, which experienced a high volume of rainfall and a greater number of cloudy days, resulting in lower grain yield (<9,000 kg ha-1) (Fig. 2 and Fig. 5). On the other hand, the multispectral indices NDRE, CIRE, NDVI, SAVI, MSAVI, OSAVI, RVI, DVI, and EVI2 were grouped in season 2022/23, which had a higher shoot biomass, plant height, and grain yield (>14,000 kg ha-1) due to better distribution of rainfall, temperatures near 30 ºC, and fewer cloud days (Fig. 2). Research comparing RGB and multispectral indices has shown that under contrasting conditions of fertilizer doses and canopy cover, visible indices perform better in scenarios with lower biomass and leaf area, achieving a high correlation with grain yield [41,42]. Thus, greater soil exposure at the beginning of the cycle may limit the use of multispectral indices, so that a better characterization of maize development up to 60 days after plant emergence using indices that utilize visible bands (as e.g. EXG, CIVE, GRVI, EXGRaw, and NDB) was achieved [43,44]. On the other hand, multispectral indices that use the near-infrared band in their equations, such as EVI, SAVI, OSAVI, GNDVI, NDVI, and NDRE, can characterize shoot biomass differences even at conditions of fully canopy cover. [45,46]. Therefore, the type of clustered index is correlated with the scenario obtained for each

growing season, with a predominance of multispectral indices in 2022/23 and visible indices in 2023/24.

The collection of biometric data in the field is still a common practice that characterizes the classical plant phenotyping, both for analyzing genotypic differences and for evaluating crop response to specific management practices [47]. Although this methodology is efficient in assessing crop responses, it constitutes a bottleneck for plant breeding and experimental evaluation due to low operational capacity and labor costs, which calls for new approaches to accelerate these processes [48]. Thus, field variables with high heritability and low residual variance coefficients, such as plant height and relative chlorophyll content (Table 2), can be important predictors in plant phenotyping, since these variables have a direct relationship with biomass increase, leaf nitrogen concentration, lodging resistance, and grain yield [49,50].

The prediction of maize yield and other attributes from vegetation indices has been widely studied in recent years due to the need to monitor crop growth and development in response to different factors such as environment, genotypes, nutritional management, and irrigation [51,19]. Such research highlights the absence of linearity between spectral variables and grain yield, indicating the need to use unconventional analyses to evaluate the correlation of parameters and achieve greater prediction accuracy. Additionally, the overfitting of complex prediction models trained from spectral data with low temporal and spatial repetition can limit their applicability.

According to the methodology proposed in our study, it was possible to achieve a satisfactory prediction accuracy ($r^2 > 0.80$) for most field variables, using only the relevant vegetation indices identified by the multivariate regression model (Table 4). Thus, the methodology allowed the creation of a function for each field variable considering all flight data and different growing seasons after applying RELM-BLUP techniques and identifying significant vegetation indices within the prediction model via stepwise regression. This procedure is essential to reduce the variation factors associated with experimental error, identify reliable variables, avoid multicollinearity, reduce the dimensionality of independent variables, and identify relevant predictors to compose the function [54,33,25]. Furthermore, although more general indices such as CIG, GLI, NDB, and RGBindex were identified, which were used to predict most of the analyzed variables, more specific indices like NDVI, SAVI, GNDVI, CIG, NDRE, CIRE, GVI, CVI, PanNDVI, SRNIRRe, and SFDVI showed a high angular coefficient within the prediction models (Table 4), highlighting the strong relationship of these vegetation indices with the response field variable [55]. Thus, this response supports the higher heritability and lower experimental error identified by the analysis of variance components (Table 3).

Various prediction models have been tested over time, with variations in the type of model (linear or nonlinear) as well as the complexity established for each tool. In this sense, Random Forest and Support Vector Machine models have been validated by research as the main prediction tools for variables related to grain yield, nutrient concentration, and biomass production due to their high prediction accuracy ($r^2>0.70$) [56,57]. However, training these models with multicollinear data, significant residual effects, low reliability, and greater complexity in processing may explain their limited use in plant phenotyping.

Multiple linear regression models are widely used in agricultural remote sensing; however, they tend to exhibit low prediction accuracy when working with large volumes of spectral data [58]. Nevertheless, tools for feature selection, dimensionality reduction, and multicollinearity can significantly improve the performance of these simple models, achieving better characterization of the physiological state of plants from a regression model based on a few predictors [59-61]. Thus, this study highlights the relevance of the proposed methodology to create the ideal model according to the study scenarios, using vegetation indices with relevant spectral information and easy application of the collected values in a response equation.

4.6 Conclusions

This study aimed to understanding the effect of fixed factors and environmental conditions in dynamic of vegetation indices in prediction of field variables in maize, emphasizing the need to consider these factors for the correct selection of predictor vegetation indices in modeling. Thus, it

was concluded that: All vegetation indices are influenced by nitrogen doses and scenarios (phenological stages and growing season), achieving greater heritability and lower coefficient of variation of error for the indices: EXGRaw, TGI, GNDVI, NDRE, CIRE, GVI, CVI, BNDVI, PanNDVI, SRNIRRe, and SFDVI. Furthermore, there is specificity between vegetation indices and phenological stages, with the grouping of multispectral indices under conditions of greater plant height, shoot biomass, and grain productivity (as e.g. V12, V13, V18, R2 and R5). RGB indices, on the other hand, were preferentially grouped in scenarios of lower shoot biomass at initial growth stages (as e.g. V6 and V8), and in growing seasons with lower grain productivity. Finally, the prediction of variables using the methodology proposed in this study allowed for the identification of the best indices to estimate maize field variables, with high accuracy and based on a multivariate linear model.

Supplementary Materials: The following supporting information can be downloaded at: https://www.mdpi.com/article/doi/s1, Table S1: title: Table_Supplementary_1

Author Contributions: Charleston S Lima: Conceptualization, methodology, validation, visualization, writing—original draft, writing—review and editing. Ana J Teixeira: Data collection and investigation. Barbara Nogueira: Data collection and investigation. André L Vian: Conceptualization, review and supervision. Ivan R Carvalho: editing, software, formal analysis and methodology. Christian Bredemeier: Supervisor, review, writing, funding acquisition and project administration.

Funding: This research received funding from the National Council for Scientific and Technological Development of Brazil (CNPq), for the Ph.D. scholarship of the first author, process number: 140742/2021-2, and from EMBRAPII Center for Embedded Devices and Research in Digital Agriculture (CEDRA) of SENAI-RS, with financial resources from the PPI IoT/Manufatura 4.0 / PPI HardwareBR of the MCTI, grant number 056/2023, signed with EMBRAPII.

Data Availability Statement: The data supporting the study findings are available on request from the corresponding author. The data are not publicly available due to the authors' plan to conduct a series of follow-up studies based on this dataset.

Conflicts of Interest: The authors declare no competing financial interests or personal relationships that could have influenced the work in the paper.

4.7 References

1. Xie, C.; Yang, C. A review on plant high-throughput phenotyping traits using UAV-based sensors. *Computers and Electronics in Agriculture*. **2020**, 178, 1-14. https://doi.org/10.1016/j.compag.2020.105731
2. Chivasa, W.; Mutanga, O.; Burgueno, J. UAV-based high-throughput phenotyping to increase prediction and selection accuracy in maize varieties under artificial MSV inoculation. *Computers and Electronics in Agriculture*. **2021**, 184, 1-14. https://doi.org/10.1016/j.compag.2021.106128
3. Yang, B., Zhu, W., Rezaei, E. E., Li, J., Sun, Z., Zhang, J. (2022). Optimal Phenological Phase of Maize for Yield Prediction with High Frequency UAV Remote Sensing. Remote Sensing, v. 14, p. 1-18. https://doi.org/10.3390/rs14071559
4. Banerjee, B. P.; Joshi, S.; Thoday-Kennedy, E.; Pasam, R. K.; Tibbits, J.; Hayden, M.; Spangenberg, G.; Kant, S. High-throughput phenotyping using digital and hyperspectral imaging-derived biomarkers for genotypic nitrogen response. *Journal of Experimental Botany*. **2020**, 71, 4604-4615. https://doi.org/10.1093/jxb/eraa143
5. Roy, A.; Moradkhani, H.; Mekonnen, M.; Moftakhari, H.; Magliocca, N. Towards strategic interventions for global food security in 2050. *Science of the Total Environment*. **2024**, 954, 1-15. https://doi.org/10.1016/j.scitotenv.2024.176811
6. Cui, J.; Cui, Z.; Lu, Y.; Lv, X.; Cao, Q.; Hou, Y.; Yang, X.; Gu, Y. Maize grain yield enhancement in modern hybrids associated with greater stalk lodging resistance at a high planting density: a case study in northeast China. *Scientific Reports*. **2022**, 12, 14647, 1-12. https://doi.org/10.1038/s41598-022-18908-z
7. Cotrozzi, L.; Peron, R.; Tuinstra, M. R.; Mickelbart, M. V.; Couture, J. J. Spectral phenotyping of physiological and anatomical leaf traits related with maize water status. *Plant Physiology*. **2020**, 184, 1363-1377. https://doi.org/10.1104/pp.20.00577

8. Li, C.; Czyz, E. A.; Halitschke, R.; Baldwin, I. T.; Schaepman, M. E.; Schuman, M. C. Evaluating potential of leaf reflectance spectra to monitor plant genetic variation. *Plant Methods*. **2023**, 19, 1-28. https://doi.org/10.1186/s13007-023-01089-9
9. Pereira, H. D.; Nonato, J. V. A.; Duarte, R. C. R. M.; Gerhardt, I. R.; Dante, R. A.; Arruda, P.; Yassitepe, J. E. C. T. Temporal field phenomics of transgenic maize events subjected to drought stress: Cross-validation scenarios and machine learning models. *The Plant Phenome Journal*. **2025**, 8, 1-16. https://doi.org/10.1002/ppj2.70015
10. Ma, H.; Li, X.; Ji, J.; Cui, H.; Shi, Y.; Li, N.; Yang, C. Monitoring indicators for comprehensive growth of summer maize based on uav remote sensing. *Agronomy*. **2023**, 13, 1-17. https://doi.org/10.3390/agronomy13122888
11. Sun, X.; yang, Z.; Su, P.; Wei, K.; Wang, Z.; Yang, C.; Wang, C.; Qin, M.; Xiao, L.; Yang, W.; Zhang, M.; Song, X.; Feng, M. Nondestructive monitoring of maize LAI by fusing UAV spectral and textural features. *Frontiers in Plant Science*. **2023**, 14, 1-11. https://doi.org/10.3389/fpls.2023.1158837
12. Zhou, J.; Wang, B.; Fan, J.; Ma, Y.; Wang, Y.; Zhang, Z. A systematic study of estimating potato n concentrations using uav-based hyper- and multi-spectral imagery. *Agronomy*. **2022**, 12, 1-16. https://doi.org/10.3390/agronomy12102533
13. Tayade, R.; Yoon, J.; Lay, L.; Khan, A. L.; Yoon, Y.; Kim, Y. Utilization of spectral indices for high-throughput phenotyping. *Plants*. **2022**, 11, 1-20. https://doi.org/10.3390/plants11131712
14. Haghighattalab, A.; Pérez, L. G.; Mondal, S.; Singh, D.; Schinstock, D.; Rutkoski, J.; Ortiz-monasterio, I.; Singh, R. P.; Goodin, D.; Poland, J. Application of unmanned aerial systems for high throughput phenotyping of large wheat breeding nurseries. *Plant Methods*. **2016**, 12, 1-15. https://doi.org/10.1186/s13007-016-0134-6
15. Zhao, Y.; Zheng, B.; Chapman, S. C.; Laws, K.; George-jaeggli, B.; Hammer, G. L.; Jordan, D. R.; Potgieter, A. B. Detecting sorghum plant and head features from multispectral UAV imagery. *Plant Phenomics*. **2021**, 2021, 1-14. https://doi.org/10.34133/2021/9874650
16. Feng, L.; Chen, S.; Shang, C.; Zhang, Y.; He, Y. A comprehensive review on recent applications of unmanned aerial vehicle remote sensing with various sensors for high-throughput plant phenotyping. *Computers and Electronics in Agriculture*. **2021**, 182, 1-19. https://doi.org/10.1016/j.compag.2021.106033
17. Chen, D.; Shi, R.; Pape, J.; Neumann, K.; Arend, D.; Graner, A.; Chen, M.; Klukas, C. Predicting plant biomass accumulation from image-derived parameters. *GigaScience*. **2018**, 7, 1-13. https://doi.org/10.1093/gigascience/giy001
18. Shrestha, A.; Bheemanahalli, R.; Adeli, A.; Samiappan, S.; Czarnecki, J. M. P.; Mccraine, C. D.; Reddy, K. R.; Moorhead, R. Phenological stage and vegetation index for predicting corn yield under rainfed environments. *Frontiers in Plant Science*. **2023**, 14, 1-12. https://doi.org/10.3389/fpls.2023.1168732
19. Wang, Z.; Chen, J.; Zhang, J.; Fan, Y.; Cheng, Y.; Wang, B.; Wu, X.; Tan, X.; Tan, T.; Li, S.; Raza, M. A.; Wang, X.; Yong, T.; Liu, W.; Liu, J.; Du, J.; Wu, Y.; Yang, W.; Yang, F. Predicting grain yield and protein content using canopy reflectance in maize grown under different water and nitrogen levels. *Field Crops Research*. **2021**, 260, 1-15. https://doi.org/10.1016/j.fcr.2020.107988
20. Njane, S. N.; Tsuda, S.; Marrewijk, B. M. V.; Gerrit, P.; Katayama, K.; Tsuji, H. Effect of varying UAV height on the precise estimation of potato crop growth. *Frontiers in Plant Science*. **2023**, 14, 1-14. https://doi.org/10.3389/fpls.2023.1233349
21. Alves, A. K. S.; Araújo, M. S.; Chaves, S. F. S.; Dias, L. A. S.; Corredo, L. P.; Pessoa, G. G. F. A.; Bezerra, A. R. G. High throughput phenotyping in soybean breeding using RGB image vegetation indices based on drone. *Scientific Reports*. **2024**, 14, 1-11. https://doi.org/10.1038/s41598-024-83807-4
22. Silva, C. M.; Mezzomo, H. C.; Ribeiro, J. P. O.; Signorini, V. S.; Lima, G. W.; Vieira, E. F. T.; Portes, M. F.; Morota, G.; Corredo, L. P.; Nardino, M. Insights on multi-spectral vegetation indices derived from UAV-based high-throughput phenotyping for indirect selection in tropical wheat breeding. *Euphytica*. **2024**, *35*, 1-16. https://doi.org/10.1007/s10681-024-03299-1
23. Carvalho, I. R.; Silva, J. A. G.; Ferreira, L. L.; Szareski, V. J.; Demari, G. H.; Lautenchleger, F.; Meneghello, G. E.; Matter, E. M.; Magano, D. A.; Souza, V. Q. REML/BLUP applied to characterize important agronomic

traits in segregating generations of bean (Phaseolus vulgaris L.). *Australian Journal of Crop Science*. **2020**, 14, 391 – 399. DOI: 10.21475/ajcs.20.14.03.p1520

24. Resende, M. D. V. Software Selegen-REML/BLUP: a useful tool for plant breeding. *Crop Breeding and Applied Biotechnology*. **2016**, 6, 330-339. https://doi.org/10.1590/1984-70332016v16n4a49
25. Oliveira, J. F.; Alcântara, J. F.; Santana, D. C.; Teodoro, L. P. R.; Baio, F. H. R.; Coradi, P. C.; Junior, C. A. S.; Teodoro, P. E. Spectral variables as criteria for selection of soybean genotypes at different vegetative stages. *Remote Sensing Applications: Society and Environment*. **2023**, 32, 1-8. https://doi.org/10.1016/j.rsase.2023.101026
26. Kuinchtner, A.; Buriol, G. A. Clima do estado do Rio Grande do Sul segundo a classificação climática de Köppen e Thornthwaite. *Disciplinarum Scientia, Série: Ciências Exatas*. **2001**, 2, 171-182.
27. Bergamaschi, H.; Dalmago, G. A.; Bergonci, J. I.; Bianchi, C. A. M.; Muller, A. G.; Comiran, F.; Heckler, B. M. M. Distribuição hídrica no período crítico do milho e produção de grãos. *Pesquisa Agropecuária Brasileira*. **2004**, 39, 831-839.
28. Argenta, G.; Silva, P. R. F.; Sangoi, L. Leaf relative chlorophyll content as an indicator parameter to predict nitrogen fertilization in maize. *Ciência Rural*. **2004**, 34, 1379-1387.
29. Bandeira, W. J. A.; Carvalho, I. R.; Loro, M. V.; Pradebon, L. C.; Silva, J. A. G. EstimateBreed: Estimation of Environmental Variables and Genetic Parameters. Available at:<https://cran.r-project.org/web/packages/EstimateBreed/index. html>. Accessed on: Apr. 25 2025.
30. Gheith, E. M. S.; El-badry, O. Z.; Lamlom, S. F.; Ali, H. M.; Siddiqui, M. H.; Ghareeb, R. Y.; El-sheikh, M. H.; Jebril, J.; Abdelsalam, N. R.; Kandil, E. E. Maize (Zea mays L.) Productivity and nitrogen use efficiency in response to nitrogen application levels and time. *Frontiers in Plant Science*. **2022**, 13, 1-12. https://doi.org/10.3389/fpls.2022.941343
31. Wang, J.; Guo, J.; Li, G.; Lu, W.; Lu, D. Effects of different fertilizer combinations on the yield and nitrogen use efficiency of summer maize in Jiangsu Province, China. *Scientific reports*. **2025**, 15, 1-16. https://doi.org/10.1038/s41598-025-89918-w
32. Su, Y.; Sun, P.; Dai, H.; Kuo, B. Evaluating the impact of weather variability on maize yield fluctuation for different sowing dates. *Agricultural and Forest Meteorology*. **2025**, 371, 1-16. https://doi.org/10.1016/j.agrformet.2025.110625
33. Adak, A.; Murray, S. C.; Bozinovic, S.; Lindsey, R.; Nakasagga, S.; Chatterjee, S.; Anderson S. L.; Wilde, S. Temporal vegetation indices and plant height from remotely sensed imagery can predict grain yield and flowering time breeding value in maize via machine learning regression. *Remote sensing*. **2021**, 13, 1-21. https://doi.org/10.3390/rs13112141
34. Olivoto, T.; Nardino, M.; Carvalho, I. R.; Follmann, D. N.; Ferrari, M.; Szareski, V. J.; Pelegrin, A. J.; Souza, V. Q. REML/BLUP and sequential path analysis in estimating genotypic values and interrelationships among simple maize grain yield-related traits. *Genetics and Molecular Research*. **2018**, 16, 1-19. http://dx.doi.org/10.4238/gmr16019525
35. Olivoto, T.; Lúcio, A. D. C.; Silva, J. A. G.; Sari, B. G. S.; Diel, M. I. Performance and Stability in Multi-Environment Trials II: Selection Based on Multiple Traits. *Agronomy Journal*. **2019**, 111, 2961-2969. https://doi.org/10.2134/agronj2019.03.0221
36. Berlezi, J. D.; Carvalho, I. R.; Silva, J. A. G.; Loro, M. V.; Sfalcin, I. C.; Pradebon, L. C.; Port, E. D.; Ourique, R. S.; Roza, J. P. D. Selection of white oat genotypes for contrasting fungicide management conditions. *Pesquisa Agropecuária Brasileira*. **2023**, 58, 1-13. https://doi.org/10.1590/S1678-3921.pab2023.v58.03084
37. Resende, M. D. V.; Duarte, J. B. Precisão e controle de qualidade em experimentos de avaliação de cultivares. *Pesquisa Agropecuária Tropical*. **2007**, 37, 182 – 194.
38. Bernardo, R. Reinventing quantitative genetics for plant breeding: something old, something new, something borrowed, something BLUE. *Heredity*. **2020**, 125, 375 – 385. https://doi.org/10.1038/s41437-020-0312-1
39. Lima, c. S.; Junior, D. F. U.; Carvalho, I. R.; Bredemeier, C. Use of phenomics in the selection of uav-based vegetation indices and prediction of agronomic traits in soybean subjected to flooding. *AgriEngineering*. **2024**, 6, 3261-3278. https://doi.org/10.3390/agriengineering6030186

40. Pradebon, L. C.; Carvalho, Ivan R.; Silva, J. A. G.; Loro, M. V.; Pettenon, A. L.; Roza, J. P. D.; Schulz, A. D.; Silva, T. B. Selection based on the phenomenic approach and agronomic ideotype of white oat. *Agronomy journal*. **2024**, 116, 1275-1289. https://doi.org/10.1002/agj2.21569
41. Yang, B.; Zhu, W.; Rezaei, E. E.; Li, J.; Sun, Z.; Zhang, J. Optimal Phenological Phase of Maize for Yield Prediction with High Frequency UAV Remote Sensing. *Remote Sensing*. **2022**, 14, 1-18. https://doi.org/10.3390/rs14071559
42. Vergara-diaz, O.; Zaman-allah, M. A.; Masuka, B.; Hornero, A.; Zarco-tejada, P.; Prasana, B. M.; Cairns, J. E.; Araus, J. L. A novel remote sensing approach for prediction of maize yield under different conditions of nitrogen fertilization. *Frontiers in Plant Science*. **2016**, 7, 1-13. https://doi.org/10.3389/fpls.2016.00666
43. Gracia-romero, A.; Kefauver, S. C.; Vergara-díaz, O.; Zaman-allah, M. A.; Prasanna, B. M.; Cairns, J. E.; Araus, J. L. Comparative performance of ground vs. aerially assessed RGB and multispectral indices for early-growth evaluation of maize performance under phosphorus fertilization. *Frontiers in Plant Science*. **2017**, 8, 1-13. https://doi.org/10.3389/fpls.2017.02004
44. Marcial-pablo, M. J.; Gonzalez-sanchez, A.; Jimenez-jimenez, S. I.; Ontiveros-capurata, R. E.; Bustamante, W. O. Estimation of vegetation fraction using RGB and multispectral images from UAV. *International Journal of Remote Sensing*. **2019**, 1-20. https://doi.org/10.1080/01431161.2018.1528017
45. Ashapure, A.; Jung, J.; Chang, A.; Oh, S.; Maeda, M.; Landivar, J. A comparative study of RGB and multispectral sensor-based cotton canopy cover modelling using multi-temporal UAS data. *Remote Sensing*. **2019**, 11, 1-18. https://doi.org/10.3390/rs11232757
46. Venancio, L. P.; Mantovani, E. C.; Amaral, C. H.; Neale, C. M. U.; Gonçalves, I. Z.; Filgueiras, R.; Eugenio, F. C. Potential of using spectral vegetation indices for corn green biomass estimation based on their relationship with the photosynthetic vegetation sub-pixel fraction. *Agricultural Water Management*. **2020**, 236, 1-14. https://doi.org/10.1016/j.agwat.2020.106155
47. Liu, S.; Zeng, W.; Wu, L.; Lei, G.; Chen, H.; Srivastava, A. K. Simulating the leaf area index of rice from multispectral images. *Remote Sensing*. **2021**, 13, 1-22. https://doi.org/10.3390/rs13183663
48. Rui, Z.; Zhang, Z.; Zhang, M.; Azizi, A.; Igathinathane, C.; Cen, H.; Vougioukas, S.; Li, H.; Zhang, J.; Jiang, Y.; Jiao, X.; Wang, M.; Ampatzidis, Y.; Oladele, O. I.; Varnamkhasti, M.; Radi, R. High-throughput proximal ground crop phenotyping systems – A comprehensive review. *Computers and Electronics in Agriculture*. **2024**, 224, 1-22. https://doi.org/10.1016/j.compag.2024.109108
49. Araus, J. L.; Cairns, J. E. Field high-throughput phenotyping: the new crop breeding frontier. *Trends in Plant Science*. **2014**, 19, 52-61. http://dx.doi.org/10.1016/j.tplants.2013.09.008
50. Prey, L.; Hu, Y.; Schmidhalter, U. High-throughput field phenotyping traits of grain yield formation and nitrogen use efficiency: optimizing the selection of vegetation indices and growth stages. *Frontiers in Plant Science*. **2020**, 10, 1-20. https://doi.org/10.3389/fpls.2019.01672
51. Stubbs, C. J.; Kunduru, B.; Bokros, N.; Verges, V.; Porter, J.; Cook, D. D.; Debolt, S.; Memahan, C.; Sekhon, R. S.; Robertson, D. J. Moving toward short stature maize: The effect of plant height on maize stalk lodging resistance *Field Crops Research*. **2023**, 300, 1-13. https://doi.org/10.1016/j.fcr.2023.109008
52. Baio, F. H. R.; Santana, D. C.; Teodoro, L. P. R.; Oliveira, I. C.; Gava, R.; Oliveira, J. L. G.; Junior, C. A. S.; Teodoro, P. E.; Shiratsuchi, L. S. Maize yield prediction with machine learning, spectral variables and irrigation management. *Remote Sensing*. **2023**, 15, 1-13. https://doi.org/10.3390/rs15010079
53. Meyer, H.; Reudenbach, C.; Hengi, T.; Katurji, M.; Nauss, T. Improving performance of spatio-temporal machine learning models using forward feature selection and target-oriented validation. *Environmental Modelling & Software*. **2018**, 101, 1-9. https://doi.org/10.1016/j.envsoft.2017.12.001
54. Yu, H.; Wu, Y.; Niu, L.; Chai, Y.; Feng, Q.; Wang, W.; Liang, T. A method to avoid spatial overfitting in estimation of grassland above-ground biomass on the Tibetan Plateau. *Ecological Indicators*. **2021**, 125, 1-8. https://doi.org/10.1016/j.ecolind.2021.107450
55. Abbasi, M.; Verrelst, J.; Mizaei, M.; Marofi, S.; Bakhtiari, H. R. R. Optimal spectral wavelengths for discriminating orchard species using multivariate statistical techniques. *Remote Sensing*. **2020**, 12, 1-16. https://doi.org/10.3390/rs12010063

56. Barboza, T. O. C.; Ardigueri, M.; Souza, G. F. C.; Ferraz, M. A. J.; Gaudencio, J. R. F.; Santos, A. F. Performance of vegetation indices to estimate green biomass accumulation in common bean. *AgriEngineering*. **2023**, 5, 840–854. https://doi.org/10.3390/agriengineering5020052
57. Lee, H.; Wang, J.; Leblon, B. Using linear regression, random forests, and support vector machine with unmanned aerial vehicle multispectral images to predict canopy nitrogen weight in corn. *Remote Sensing*. **2020**, 12, 1-20. https://doi.org/10.3390/rs12132071
58. Ge, H.; Zhang, Q.; Shen, M.; Qin, Y.; Wang, L.; Yuan, C. Enhancing yield prediction in maize breeding using UAV derived RGB imagery: a novel classification-integrated regression approach. *Frontiers in Plant Science*. **2025**, 16, 1-13. https://doi.org/10.3389/fpls.2025.1511871
59. Fei, S.; Xu, D.; Chen, Z.; Xiao, Y.; Ma, Y. MLR-based feature splitting regression for estimating plant traits using high-dimensional hyperspectral reflectance data. *Field Crops Research*. **2023**, 293, 1-12. https://doi.org/10.1016/j.fcr.2023.108855
60. Krishna, G.; Sahoo, R. N.; Singh, P.; Bajpai, V.; Patra, H.; Kumar, S.; Dandapani, R.; Gupta, V. K.; Viswanathan, C.; Ahmad, T.; Sahoo, P. M. Comparison of various modelling approaches for water deficit stress monitoring in rice crop through hyperspectral remote sensing. *Agricultural Water Management*. **2019**, 213, 231-244. https://doi.org/10.1016/j.agwat.2018.08.029
61. Zhang, L.; Han, W.; Niu, Y.; Chávez, J. L.; Shao, G.; Zhang, H. Evaluating the sensitivity of water stressed maize chlorophyll and structure based on UAV derived vegetation indices. *Computers and Electronics in Agriculture*. **2021**, 185, 1-9. https://doi.org/10.1016/j.compag.2021.106174
62. Nagy, A.; Szabó, A.; Elbeltagi, A.; Nxumalo, G. S.; Bódi, E. B.; Tamás, J. Hyperspectral indices data fusion-based machine learning enhanced by MRMR algorithm for estimating maize chlorophyll content. *Frontiers in Plant Science*. **2024**, 15, 1-18. https://doi.org/10.3389/fpls.2024.1419316

Disclaimer/Publisher's Note: The statements, opinions and data contained in all publications are solely those of the individual author(s) and contributor(s) and not of MDPI and/or the editor(s). MDPI and/or the editor(s) disclaim responsibility for any injury to people or property resulting from any ideas, methods, instructions or products referred to in the content.

Dados Suplementares

Supplement 1. Blups of field variables in maize crop.

SCENARIO	NDVIG	CHLT	PH	Biomass	NCP	NGE	W100G	YIELD
S1R2_0	0.60	36	191	6324	0.59			
S1R2_50	0.65	43	218	8813	0.65			
S1R2_100	0.67	45	232	10195	0.72			
S1R2_200	0.70	53	234	12993	0.98			
S1R2_300	0.72	58	242	13698	1.21			
S1R2_400	0.72	59	244	15445	1.36			
S1R5_0	0.49	34	189	10554	0.46	214	31	4239
S1R5_50	0.56	39	221	13406	0.50	251	27	5338
S1R5_100	0.56	41	230	15182	0.52	309	27	6641
S1R5_200	0.59	47	234	23117	0.61	405	29	10200
S1R5_300	0.63	54	243	22326	0.80	475	33	13709
S1R5_400	0.63	53	245	24383	0.98	434	33	11970
S1V12_0	0.72	37	98	2535	1.20			
S1V12_50	0.78	48	129	2745	1.53			
S1V12_100	0.79	50	134	3237	1.66			
S1V12_200	0.80	51	138	3608	2.06			
S1V12_300	0.81	54	143	5229	2.25			
S1V12_400	0.80	57	143	6046	2.34			
S1V18_0	0.71	35	152	4516	0.74			
S1V18_50	0.77	42	204	5829	0.88			
S1V18_100	0.78	44	215	6381	0.96			
S1V18_200	0.79	48	220	8004	1.27			
S1V18_300	0.79	52	234	9006	1.64			
S1V18_400	0.80	52	240	9651	1.71			
S1V5_0	0.34							
S1V5_50	0.35							
S1V5_100	0.36							
S1V5_200	0.32							
S1V5_300	0.36							
S1V5_400	0.36							
S1V8_0	0.60	39	76	1493	1.1			
S1V8_50	0.67	44	89	1403	1.7			
S1V8_100	0.69	44	97	1866	1.9			
S1V8_200	0.71	46	96	1977	2.5			
S1V8_300	0.71	47	101	2408	2.7			
S1V8_400	0.72	49	104	2790	2.5			
S2R2_0			155	4852	1.1			
S2R2_50			180	6828	1.0			
S2R2_100			184	9104	1.1			
S2R2_200			183	10170	1.8			
S2R2_300			178	10554	2.1			
S2R2_400			176	10448	2.0			
S2R5_0		33	159	6835		150	30	3374
S2R5_50		34	178	11480		275	23	4987
S2R5_100		39	185	15243		350	25	7284
S2R5_200		50	183	19895		392	26	8541

S2R5_300		53	177	17589		370	29	7952
S2R5_400		56	177	17277		257	32	6812
S2V13_0	0.69	37	106	2116	1.3			
S2V13_50	0.76	40	148	3078	1.2			
S2V13_100	0.78	47	160	5248	1.4			
S2V13_200	0.78	49	170	6223	2.1			
S2V13_300	0.78	49	162	5928	2.3			
S2V13_400	0.78	49	151	5640	2.5			
S2V6_0	0.44	32	35	84	2.4			
S2V6_50	0.48	39	45	343	3.0			
S2V6_100	0.51	41	46	527	3.4			
S2V6_200	0.49	40	48	768	3.8			
S2V6_300	0.50	40	47	747	4.0			
S2V6_400	0.50	39	47	781	4.4			
S2V8_0	0.64	31	58	867	2.1			
S2V8_50	0.73	40	78	1359	2.1			
S2V8_100	0.76	44	88	2174	2.2			
S2V8_200	0.76	45	90	2611	2.9			
S2V8_300	0.75	41	87	2857	3.1			
S2V8_400	0.74	38	82	2614	3.5			

*Scenario: interaction flight x season; NDVIG: NDVI greenseeker; CHLT: Total chlorophyll; PH: Plant height; NCP: Nitrogen concentration in the plant; NGE: Number of grains per ear; W100G: Weight 100 grains; Yield: Yield grains.

5 CONSIDERAÇÕES FINAIS

A partir dos dados espectrais coletados com o uso de VANT foi possível identificar e avaliar a tolerância de cultivares de soja ao alagamento, bem como predizer variáveis de campo na cultura do milho em dois anos de cultivo. A metodologia baseada na utilização de modelos mistos (RELM-BLUP) para a dedução dos efeitos genéticos, manejos, estádio fenológico e ambiente permitiu a dedução dos fatores e limpeza dos dados para o modelo de predição linear misto posteriormente.

A partir da decomposição dos componentes de variância, foram obtidos os índices com maior herdabilidade, menor efeito do ambiente e do erro experimental para os diferentes genótipos de soja submetidos ao alagamento, os quais foram: MSAVI, NDVI, OSAVI, SAVI, VEG, MGRVI, EVI2, NDRE, GRVI, BNDVI, RGBindex. Obtendo-se maior coeficiente de determinação na predição das variáveis de campo com a utilização da metodologia.

Na cultura do milho, os índices de vegetação que apresentaram maior confiabilidade foram: EXGRaw, TGI, GNDVI, NDRE, CIRE, GVI, CVI, BNDVI, PanNDVI, SRNIRRe, SFDVI, RGBindex, NDVI, SAVI, MSAVI e OSAVI. Além disso, a maioria das variáveis de campo foram preditas com coeficiente de determinação elevado (>0,70), apenas com o uso de dados espectrais e modelo misto multivariado.